

**SPECTROSCOPIC AND THERMAL ANALYSIS OF EXPLOSIVE AND  
RELATED COMPOUNDS VIA GAS CHROMATOGRAPHY/VACUUM  
ULTRAVIOLET SPECTROSCOPY (GC/VUV)**

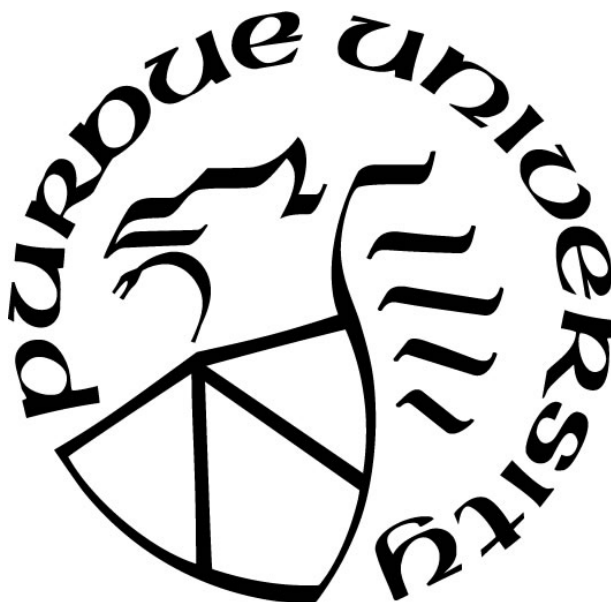
by  
**Courtney Cruse**

**A Dissertation**

*Submitted to the Faculty of Purdue University*

*In Partial Fulfillment of the Requirements for the degree of*

**Doctor of Philosophy**



Department of Chemistry and Chemical Biology at IUPUI

Indianapolis, Indiana

December 2021

**THE PURDUE UNIVERSITY GRADUATE SCHOOL  
STATEMENT OF COMMITTEE APPROVAL**

**Dr. John V. Goodpaster, Chair**

School of Science

**Dr. Nicholas Manicke**

School of Science

**Dr. Robert Minto**

School of Science

**Dr. Sébastien Laulhé**

School of Science

**Approved by:**

Dr. Eric Long

*To God, my family, and friends  
for your unconditional love.*

## ACKNOWLEDGMENTS

*And whatever you do, whether in word or deed, do it all in the name of the Lord Jesus, giving thanks to God the Father through him. Colossians 3:17*

I am thankful for everything and everyone that has led me to where I am today.

To start at the beginning, I first want to thank Mr. Minarik for introducing me to forensic science my Junior year of high school. This is where I first learned the love of forensic science and where the desire to pursue a career in forensic chemistry first began.

To Dr. Cobane and the Honors College at Western Kentucky University for the incredible academic opportunities and support I had during my undergraduate career. To Dr. Jennings and Dr. Grimsley in the Office of Scholar Development for your assistance and knowledge in fellowship applications that has been invaluable to my success thus far. Also, to the WKU Department of Chemistry and my academic advisor Dr. Burris for four great years in undergraduate chemistry, and to Dr. Dahl for instilling in me a love for analytical chemistry.

I am also thankful for the research opportunities while at WKU that have helped to define and direct my career path. To Dr. Conte, thank you for taking me into your lab and introducing me to research. The opportunity to work with you and the other students in lab was significant in defining my undergraduate experience and decision to continue to a doctoral program. To The Washington Center Summer Internship Program and the research opportunity with Dr. Brown at the US Food and Drug Administration in 2015. Also, to the Homeland Security STEM Summer Internship Program at the Customs and Border Protection lab in Springfield, VA and the research with Dr. Gerde and Dr. Bondoc in 2016. These research experiences have helped develop the chemist I am today.

To the Department of Chemistry and Chemical Biology at IUPUI for the hard work and support shown to me during my graduate career. To Dr. Goodpaster for this life changing research and graduate experience. Thank you for sharing your love of explosive analysis, for your support and encouragement. It is truly an honor to learn from you and work with you. Also, to my lab mates: Madi, Ashur, Kymeri, Alex, Zack, Jackie, and Logan. Thank you for your comradery, advice, and encouragement.

For their overwhelming support through everything, I want to thank my family. Thank you mom and dad for your unfailing support and love. Thank you for always supporting me and encouraging me in everything I do. Thank you Kristen for being the best twin sister. Even though we live in separate states, you are never far from my heart.

Thank you Anna, Lindsey and Rachel, for your friendship and support.

And above all else, God for blessing me with this experience and every single one of these people and experiences. Thank you for your unconditional and unfailing love.

## DISCLAIMER

Portions of this dissertation have been reproduced with permissions from published journals.

Chapter 2. Generating Highly Specific Spectra and Identifying Thermal Decomposition Products via Gas Chromatography / Vacuum Ultraviolet Spectroscopy (GC/VUV): Application to Nitrate Ester Explosives is reproduced from *Talanta*, 2019, 195:p. 580-586, Cruse, C. A. and Goodpaster, J. V.

Chapter 3. Identifying Thermal Decomposition Products of Nitrate Ester Explosives Using Gas Chromatography/Vacuum Ultraviolet Spectroscopy: An Experimental and Computational Study is reproduced from *Applied Spectroscopy*, 2020 74(12):1486-1495, Cruse et al.

Chapter 4. Thermal and Spectroscopic Analysis of Nitrated Compounds and their Break-Down Products Using Gas Chromatography/Vacuum UV Spectroscopy (GC/VUV) is reproduced from *Analytica Chimica Acta*, 2021, 1143:p.117-123, Cruse, C. A. and Goodpaster, J. V.

Chapter 5. A systematic study of the absorbance of the nitro functional group in the vacuum UV region is reproduced from *Analytica Chimica Acta*

Chapter 6. Optimization of Gas Chromatography/Vacuum Ultraviolet (GC/VUV) Spectroscopy for Explosive Compounds and Application to Post-Blast Debris is reproduced from *Forensic Chemistry*

## TABLE OF CONTENTS

LIST OF TABLES.....	11
LIST OF FIGURES .....	13
LIST OF ABBREVIATIONS.....	16
ABSTRACT.....	19
CHAPTER 1. INTRODUCTION .....	20
1.1 Explosive Analysis .....	20
1.2 Vacuum Ultraviolet Spectroscopy.....	22
1.3 References .....	24
CHAPTER 2. GENERATING HIGHLY SPECIFIC SPECTRA AND IDENTIFYING THERMAL DECOMPOSITION PRODUCTS VIA GAS CHROMATOGRAPHY / VACUUM ULTRAVIOLET SPECTROSCOPY (GC/VUV): APPLICATION TO NITRATE ESTER EXPLOSIVES .....	30
2.1 Abstract.....	30
2.2 Introduction .....	31
2.3 Materials and Methods .....	32
2.3.1 Chemicals .....	32
2.3.2 Sample Preparation .....	33
2.3.3 Gas Chromatography.....	33
2.3.4 Vacuum Ultraviolet Spectroscopy .....	34
2.3.5 Ultraviolet/Visible Spectroscopy .....	34
2.3.6 Spectral Math .....	34
2.3.7 Calculations.....	35
2.4 Results and Discussion.....	35
2.4.1 GC/VUV Analysis of EGDN, ETN, NG, and PETN.....	35
2.4.2 Temperature Effects and Thermal Degradation .....	37
2.4.3 Identification of Thermal Decomposition .....	40
2.4.4 Effect of Thermal Degradation on Sensitivity .....	43
2.4.5 Analysis of Intact and Burned Double-Base Smokeless Powders .....	44
2.5 Conclusions .....	46

2.6	Acknowledgements .....	47
2.7	References .....	47
CHAPTER 3. IDENTIFYING THERMAL DECOMPOSITION PRODUCTS OF NITRATE ESTER EXPLOSIVES USING GAS CHROMATOGRAPHY/VACUUM ULTRAVIOLET SPECTROSCOPY: AN EXPERIMENTAL AND COMPUTATIONAL STUDY .....		
3.1	Abstract.....	50
3.2	Introduction .....	50
3.3	Materials and Methods .....	52
3.3.1	Chemicals .....	52
3.3.2	Gas Chromatography.....	52
3.3.3	Vacuum Ultraviolet Spectroscopy .....	53
3.3.4	Theoretical Calculations.....	53
3.4	Results and Discussion.....	54
3.4.1	Nitric Oxide.....	57
3.4.2	Water .....	62
3.4.3	Carbon Monoxide.....	65
3.4.4	Oxygen .....	67
3.4.5	Formaldehyde.....	70
3.5	Conclusions .....	74
3.6	Acknowledgements .....	74
3.7	References .....	75
CHAPTER 4. THERMAL AND SPECTROSCOPIC ANALYSIS OF NITRATED COMPOUNDS AND THEIR BREAK-DOWN PRODUCTS USING GAS CHROMATOGRAPHY/VACUUM UV SPECTROSCOPY (GC/VUV).....		
4.1	Abstract.....	84
4.2	Introduction .....	85
4.3	Materials and Methods .....	86
4.3.1	Chemicals .....	86
4.3.2	Sample Preparation .....	86
4.3.3	Gas Chromatography.....	87
4.3.4	Vacuum Ultraviolet Spectroscopy .....	87

4.3.5	JMP Analysis.....	87
4.4	Results and Discussion.....	88
4.4.1	VUV Spectra of Nitrate Esters and Nitramines .....	88
4.4.2	Effect of GC Flow Rate on Decomposition Temperature.....	89
4.4.3	Determination of Decomposition Temperatures of Nitrated Compounds .....	93
4.5	Conclusions .....	97
4.6	Acknowledgements .....	98
4.7	References .....	98
CHAPTER 5. A SYSTEMATIC STUDY OF THE ABSORBANCE OF THE NITRO FUNCTIONAL GROUP IN THE VACUUM UV REGION.....		105
5.1	Abstract.....	105
5.2	Introduction .....	105
5.3	Materials and Methods .....	107
5.3.1	Chemicals .....	107
5.3.2	Sample Preparation .....	108
5.3.3	Gas Chromatography.....	108
5.3.4	Vacuum Ultraviolet Spectroscopy .....	108
5.3.5	Principal Component Analysis and Discriminant Analysis .....	109
5.4	Results and Discussion.....	109
5.4.1	Nitroalkanes .....	109
5.4.2	Nitroaromatics.....	110
5.4.3	Nitrate Esters and Nitramines .....	113
5.4.4	PCA and DA.....	114
5.4.5	Nitro Group Absorption Classification .....	117
5.5	Conclusions .....	117
5.6	Acknowledgements .....	118
5.7	References .....	118
CHAPTER 6. OPTIMIZATION OF GAS CHROMATOGRAPHY/VACUUM ULTRAVIOLET (GC/VUV) SPECTROSCOPY FOR EXPLOSIVE COMPOUNDS AND APPLICATION TO POST-BLAST DEBRIS.....		123
6.1	Abstract.....	123

6.2	Introduction .....	123
6.3	Materials and Methods .....	125
6.3.1	Chemicals .....	125
6.3.2	Sample Preparation .....	125
6.3.3	Gas Chromatography/Vacuum Ultraviolet Spectroscopy .....	125
6.3.4	DOE.....	126
6.4	Results and Discussion.....	126
6.4.1	GC/VUV Analysis of Explosives.....	126
6.4.2	Optimization Results .....	128
6.4.3	Figures of Merit.....	130
6.4.4	Application to Post-Blast Debris.....	131
6.5	Conclusions .....	132
6.6	Acknowledgements .....	133
6.7	References .....	133
CHAPTER 7. FUTURE DIRECTIONS .....		135
7.1	Solid Phase Microextraction (SPME) GC/VUV .....	135
7.2	Total Vaporization-SPME GC/VUV.....	136
7.3	Analysis of High Explosives in Soil.....	137
7.4	Analysis of Inorganic Explosives by GC/VUV.....	138
7.5	References .....	140
VITA.....		143

## LIST OF TABLES

Table 2.1. Experimentally determined wavelengths of maximum absorbance ( $\lambda_{\max} \pm 95\%$ confidence interval) of EGDN, ETN, EGDN, and PETN in the VUV at 190 °C (n = 3). In methanol, the $\lambda_{\max}$ of these compounds are found at 278 - 280 nm (data not shown). .....	36
Table 2.2. Linearity, linear range, limit of detection and sensitivity of GC/VUV for EGDN, ETN, EGDN, and PETN.....	37
Table 2.3. Relative percent composition of each decomposition product for EGDN, ETN, NG, and PETN at 280 °C and the squared correlation coefficients ( $r^2$ ) and the sum of squares residual (SSR) between the summed components and the experimental spectra.....	43
Table 3.1. Comparison of VGA101 VUV vibronic transitions in nitric oxide to previously reported values. (Sync= Synchrotron, FTS= Fourier transform spectrometer, and PA= Photoabsorption). .....	60
Table 3.2. Computationally predicted vibrational frequencies ( <i>vvibcalc</i> ) and calculated energy differences between the vibronic transitions ( $\Delta E$ ) for the first four excited state of nitric oxide compared to experimental data. *Approximated B $^2\Pi \leftarrow X \ ^2\Pi$ (0,0) energy using the known distances between the second excited state vibrational transitions.....	62
Table 3.3. Comparison of the VGA101 VUV absorption maxima of the first and second excited state electronic transitions of water to previously reported experimental values. (PA= Photoabsorption).....	64
Table 3.4. Comparison of VGA101 VUV vibrational transitions in the second excited state of water to previously reported experimental values. *Shoulder approximation. (PA= Photoabsorption).....	64
Table 3.5. Computationally predicted vibrational frequency ( <i>vvibcalc</i> ) and calculated energy difference between the vibronic transitions ( $\Delta E$ ) for the second excited state of water compared to experimental data.....	65
Table 3.6. Comparison of VGA101 VUV vibronic transitions of the first excited state in carbon monoxide to previously reported values. (PA= Photoabsorption).....	67
Table 3.7. Comparison of the continuum maxima and dissociation peaks of the VGA101 VUV transitions in oxygen to previously reported experimental values. *Shoulder approximation (Sync= Synchrotron and PA= Photoabsorption). .....	70
Table 3.8. Comparison of VGA101 VUV transitions in formaldehyde to previously reported experimental values. *Shoulder approximation (Sync= Synchrotron and PA= Photoabsorption). .....	72
Table 3.9. Comparison of B3LYP computational transitions in formaldehyde to previously reported computational values. ....	74

Table 4.1. Inflection points determined by a 3-parameter logistic function for 50% decomposition of NG and 50% formation of the decomposition products H <sub>2</sub> CO, NO, and CO across four flow rates and the corresponding residence time in the transfer line/flow cell.....	92
Table 4.2. JMP curve fitting results (plus or minus standard error). Literature values for reported decomposition temperatures via DSC and TGA reported at various temperature programs (DSC and TGA decomposition temperatures reported as peak temperature of decomposition).....	96
Table 4.3. Correlation analysis between the 50% decomposition temperature of nitrated compounds and reported thermodynamic properties (decomposition temperature, oxygen balance, melting point, heat of explosion and heat of detonation). The standard deviation is included for averaged values. ....	97
Table 5.1 Summary of previously analyzed compounds via GC/VUV.....	107
Table 6.1 JMP summary of variables and variable interaction p-values for all compounds and for each individual compound where flow rate=FR, make-up gas pressure=MGP. Underlined values are p-values >0.05, indicating variable/variable interactions are not statistically significant. ...	129
Table 6.2 DOE Optimized parameters for all compounds and for each individual compound. *Parameter is not statistically significant. ....	130
Table 6.3 LOD, linear range, linearity (R <sup>2</sup> ), and sensitivity (slope) of GC/VUV for all compounds utilizing the optimized method. ....	131

## LIST OF FIGURES

Figure 1.1. Bombing trends from 2015 to 2020 as reported by the United States Bomb Data Center (USBDC) through the Bomb Arson Tracking System (BATS) Explosives Incident Reports (EIR).[1-6] .....	21
Figure 1.2. Schematic of the GC/VUV system.....	23
Figure 2.1. Comparison of “as is” VUV spectra at 190 °C and EI mass spectra for nitrate ester explosives.....	38
Figure 2.2. Stacked VUV spectra of (A) EGDN ( $T_{\text{dec}} = 198$ ), (B) NG ( $T_{\text{dec}} = 167$ ), (C) ETN ( $T_{\text{dec}} = 170$ ), and (D) PETN ( $T_{\text{dec}} = 157$ ) at 190 °C (bottom), 220 °C (middle), and 280 °C (top). Decomposition temperatures are derived from Differential Scanning Calorimetry (DSC).[24, 25] .....	39
Figure 2.3. Overlay of VUV spectra of EGDN, NG, ETN, and PETN at 190 °C demonstrates the subtle and reproducible differences in the spectra.....	40
Figure 2.4. VUV spectra of NG and three of its thermal decomposition products: NO, CO, and CH <sub>2</sub> O.[26] .....	41
Figure 2.5. Experimental VUV spectra of NG (top) and the calculated sum of NG thermal decomposition products (bottom) per Table 2.3 .....	42
Figure 2.6. Effect of flow cell temperature on the peak area for nitrate ester explosives using a spectral filter from 125 nm - 240 nm. ....	44
Figure 2.7. 5 mg of intact and 50 mg of burned Red Dot, Accurate No. 7, and Accurate No. 5 Double-Base Smokeless Powder with GC/VUV spectral filters (A) 175-205 nm, (B) 128-129 nm. (1) Nitroglycerine, (2) diphenylamine, (3) ethyl centralite, and (4) di-n-butyl phthalate. Each chromatogram normalized to unit absorbance. VUV spectra of smokeless powder components shown in Figure 2.8.....	45
Figure 2.8. Stacked VUV spectra of double-base smokeless powder components. ....	46
Figure 3.1. a) VUV spectra of nitrate ester explosives exhibiting fine structure at 300 °C. b) Thermal decomposition of nitroglycerine across the temperature range 200 °C (intact) to 300 °C (complete decomposition).....	55
Figure 3.2. Thermal decomposition products of nitrate ester explosives. ....	56
Figure 3.3. VUV spectra of nitric oxide (NO).....	58
Figure 3.4. Molecular orbital diagram for visualization of the first four excited states of nitric oxide. The first, third, and fourth excited states result from Rydberg transitions and the second results from a valence transition, where 8 is the HOMO and 9 is the LUMO. The HOMO (8) and LUMO (9) transitions were not involved in the first four transitions.....	59

Figure 3.5. a) VUV spectra of water (H <sub>2</sub> O) normalized to 1 and b) molecular orbital diagram for visualization of the first and second excited states of water (Rydberg transitions), where 5 is the HOMO and 6 is the LUMO. ....	63
Figure 3.6. a) VUV spectra of carbon monoxide (CO) normalized to 1 and b) molecular orbital diagram for visualization of the first excited state resulting in a valence transition of carbon monoxide, where 7 is the HOMO and 8 is the LUMO. ....	66
Figure 3.7. a) VUV spectra of Oxygen (O <sub>2</sub> ) normalized to 1 and b) Molecular orbital diagram for visualization of the second excited state (valence transition) of oxygen, where 9 is the HOMO and 10 is the LUMO. ....	69
Figure 3.8. VUV spectra of formaldehyde (H <sub>2</sub> CO) normalized to 1. ....	71
Figure 3.9. Molecular orbital diagram for visualization of the excited states in formaldehyde, where 8 is the HOMO and 9 is the LUMO. ....	73
Figure 4.1. Nitrate ester and nitramine VUV spectra A) intact at 200 °C; and B) decomposed at 300 °C measured at 3.2 mL/min. Fine structure in the spectra are labelled with corresponding decomposition product. * The minimum flow cell temperature for HMX was 240 °C due to its high elution temperature. ....	89
Figure 4.2. A. Trends in decomposition of NG at various flow rates. B. Trends in the formation of decomposition products at a 0.70 mL/min flow rate. ....	91
Figure 4.3. A) logarithmic relationship between the calculated 50% decomposition temperature for NG across the four flow rates B) logarithmic relationship between the TGA onset temperature of decomposition for NG (literature data) across four temperature ramps.[64] ....	93
Figure 4.4. Decomposition curves of nitrate ester and nitramine compounds at a flow rate of 3.2 mL/min via a 2-parameter logistic function. ....	94
Figure 5.1. Nitroalkane VUV spectra at 300 °C. ....	110
Figure 5.2. VUV spectra at 300 °C of nitroaromatic compounds. Compounds are grouped by parent structure: A) nitrobenzenes, B) mononitrotoluenes, C) di- and tri- nitrotoluenes, and D) more complex nitroaromatics, where TNT = trinitrotoluene, DNT = dinitrotoluene, NT = nitrotoluene, TNB = trinitrobenzene, DNB = dinitrobenzene, and NB = nitrobenzene. ....	112
Figure 5.3. Nitrate ester and nitramine VUV intact spectra analyzed at 200 °C. ....	114
Figure 5.4. A. Three-dimensional factor score plot for five replicates of nitroaromatic, nitrate ester, and nitramine compounds. Cross markers denote nitroaromatic compounds while circle markers denote nitrate ester and nitramine compounds. B. Three-dimensional canonical plot for LDA based upon the first four principal components with 80:20 training:validation. ....	116
Figure 5.5. Absorption bands of the nitro group characterized by chemical structure. ....	117
Figure 6.1. VUV spectra of seven explosive and explosive related compounds (TATP, DMNB, NG, diphenylamine (DPA), TNT, PETN, RDX) analyzed in DOE optimization with the following parameters: final ramped inlet temperature 200 °C, flow rate 1.9 mL/min, VUV make-up gas pressure 0.00 psi, and flow cell temperature 300 °C. ....	127

Figure 6.2. Chromatogram of stock solution with the following parameters: final ramped inlet temperature 200 °C, flow rate 1.9 mL/min, VUV make-up gas pressure 0.00 psi, and flow cell temperature 300 °C. .... 128

Figure 6.3. DMNB response surface plots for A) final ramped inlet temperature \* flow rate and B) make-up gas pressure \* flow rate..... 129

Figure 6.4. 3D chromatograms of post blast debris A) SBSP in PVC, B) SBSP in steel, C) DBSP in PVC, and D) DBSP in steel. 1) NG decomposition product, 2) NG, 3) 2,4-dinitrotoluene, 4) diphenylamine, and 5) ethyl centralite..... 132

Figure 7.1. Comparison of traditional SPME fiber and SPME Arrow fiber.[2]..... 135

Figure 7.2. Comparison of (A) headspace SPME and (B) total vaporization SPME. [13] ..... 137

## LIST OF ABBREVIATIONS

APCI	atmospheric pressure chemical ionization
BATS	Bomb Arson Tracking System
BSA	<i>N,O</i> -bis(trimethylsilyl)acetamide
BSTFA	<i>N,O</i> -bis(trimethylsilyl)trifluoroacetamide
CCD	central composite design
CCD	charged coupled device
CW	carbowax
DART	direct analysis in real time
DBSP	double base smokeless powder
DCDA	benzoic acid
DCM	dichloromethane
DESI	desorption electrospray ionization
DMNB	2,3-dimethyl-2,3-dinitrobutane
DNB	dinitrobenzene
DNT	dinitrotoluene
DPA	diphenylamine
DSC	differential scanning calorimetry
DVB	divinylbenzene
EELS	electron energy loss spectroscopy
EGDN	ethylene glycol dinitrate
EI	electron ionization
EIR	Explosive Incident Reports
ESI	electrospray ionization
ETN	erythritol tetranitrate
FC-CCD	face centered-central composite design
FTIR	Fourier transform infrared spectroscopy
FTS	Fourier transform spectrometer
GC	gas chromatography
HME	homemade explosive device

IED	improvised explosive device
ISDN	isosorbide dinitrate
ISMN	isosorbide mononitrate
LC	liquid chromatography
LDA	linear discriminant analysis
LOD	limit of detection
LTP	low-temperature plasma
MGP	make-up gas pressure
MS	mass spectrometry
NB	nitrobenzene
NCI	negative chemical ionization
NG	nitroglycerine
NT	nitrotoluene
PA	photoabsorption
PCA	principal component analysis
PDMS	polydimethylsiloxane
PEG	polyethylene glycol
PETN	pentaerythritol tetranitrate
PVC	polyvinyl chloride
RDX	cyclonite
RSM	response surface methodology
SALDI	surface-assisted laser desorption/ionization
SBSP	single base smokeless powder
SPME	solid phase microextraction
SSR	sum of square residuals
SYNC	synchrotron
TATP	triacetone triperoxide
TDDFT	time dependent density functional theory
TGA	thermal gravimetric analysis
TMCS	trimethylchlorosilane
TMS	trimethylsilyl

TNB	trinitrobenzene
TNT	2,4,6-trinitrotoluene
TV	total vaporization
TWGFEX	Technical Working Group for Fire and Explosive Analysis
USBDC	United States Bomb Data Center
VUV	vacuum ultraviolet spectroscopy

## ABSTRACT

Analysis of explosives (intact and post-blast) is of interest to the forensic science community to qualitatively identify the explosive(s) in an improvised explosive device (IED). This requires high sensitivity, selectivity, and specificity. Forensic science laboratories typically utilize visual/microscopic exams, spectroscopic analysis (e.g., Fourier Transform Infrared Spectroscopy (FTIR)) and gas chromatography/mass spectrometry (GC/MS) for explosive analysis/identification. However, GC/MS has limitations for explosive analysis due to difficulty differentiating between structural isomers (e.g., 2,4-dinitrotoluene, 2,5-dinitrotoluene and 2,6-dinitrotoluene) and thermally labile compounds (e.g., ethylene glycol dinitrate (EGDN), nitroglycerine (NG) and pentaerythritol tetranitrate (PETN)) due to mass spectra with very similar fragmentation patterns.

The development of a benchtop vacuum ultraviolet spectrometer coupled to a gas chromatography (GC/VUV) was developed in 2014 with a wavelength region of 120 nm to 430 nm. GC/VUV can overcome limitations in differentiating explosive compounds that produces similar mass spectra. This work encompasses analysis of explosive compounds via GC/VUV to establish the sensitivity, selectivity, and specificity for the potential application for forensic explosive analysis. Nitrate ester and nitramine explosive compounds thermally decompose in the VUV flow cell resulting in higher specificity due to fine structure in the VUV spectra. These fine structures originate as vibronic and Rydberg transitions in the small decomposition compounds (nitric oxide, carbon monoxide, formaldehyde, water, and oxygen) and were analyzed computationally. The thermal decomposition process was further investigated for the determination of decomposition temperatures for the nitrate ester and nitramine compounds which range between 244 °C and 277 °C. Nitrated compounds were extensively investigated to understand the absorption characteristics of the nitro functional group in the VUV region. The nitro absorption maximum appeared over a wide range (170 - 270 nm) with the wavelength and intensity being highly dependent upon the structure of the rest of the molecule. Finally, the GC/VUV system was optimized for post-blast debris analysis. Parameters optimized include the final temperature of a ramped multimode inlet program (200 °C), GC carrier gas flow rate (1.9 mL/min), and VUV make-up gas pressure (0.00 psi). The transfer line/flow cell temperature was determined not to be statistically significant.

# CHAPTER 1. INTRODUCTION

## 1.1 Explosive Analysis

Identifying the explosive component at the scene of a bombing or on post-blast debris is of importance in forensic explosive investigations. Between 2015 and 2020, there have been 2,142 bombing events in the United States as reported by United States Bomb Data Center (USBDC) through the Bomb Arson Tracking System (BATS) (Figure 1-1).[1-6] These categorized as improvised explosive devices (IEDs), non-IED (commercial, military, fireworks, homemade explosives (HMEs)), over pressure device, other, and not specified, with IED and non-IED comprising a majority of the bombing events. More generally, explosives are categorized as low or high explosives, in which low explosives deflagrate (burn rapidly with propagation slower than the speed of sound) and high explosives detonate (shock wave with a propagation faster than the speed of sound).[7, 8] Therefore, low explosives must be contained for an explosion to occur, while high explosives only use containment for generating fragmentation. A common means for this are pipe bombs, which are a type of improvised explosive device (IED) that consist of a pipe made of typically steel or polyvinyl chloride (PVC).[7] Other components include the explosive material (e.g. black powder, black powder substitute, smokeless powder, etc.) and an initiator. In regards to forensic science analysis of explosives, the pipe/endcaps, explosive component, and initiators are collected as evidence for analysis in the laboratory.[9, 10] Identifying explosive material is ideal in assisting in providing means in court.

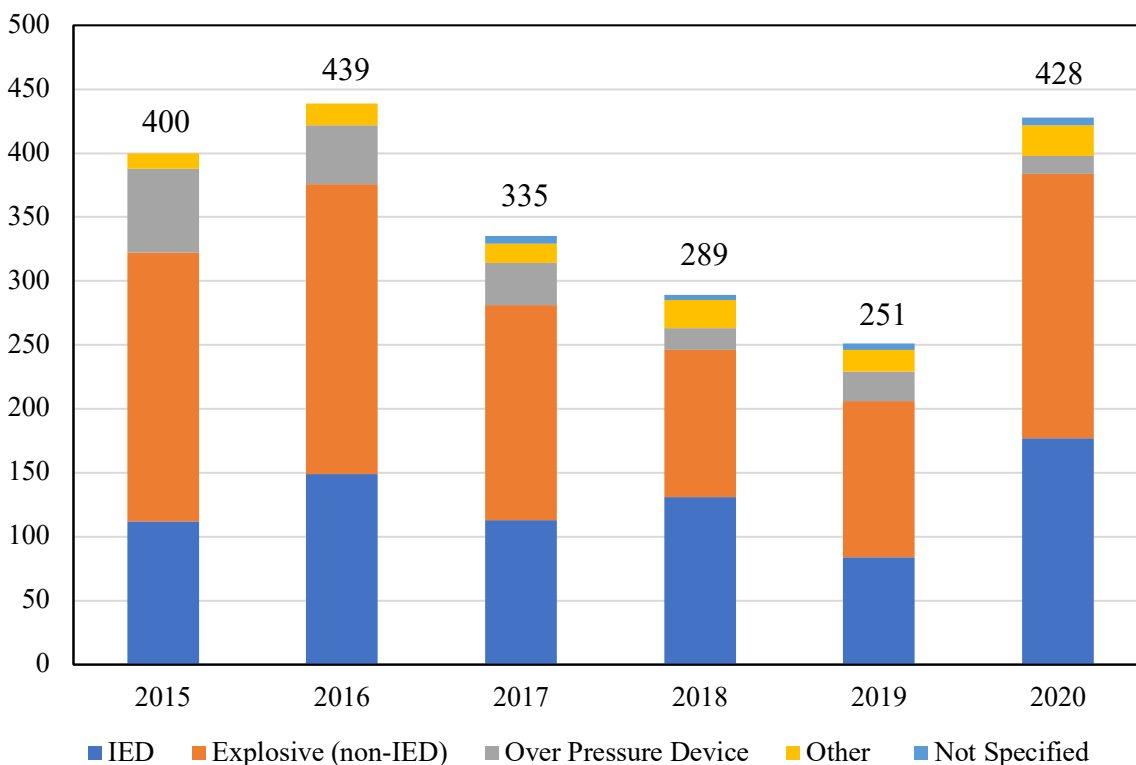


Figure 1.1. Bombing trends from 2015 to 2020 as reported by the United States Bomb Data Center (USBDC) through the Bomb Arson Tracking System (BATS) Explosives Incident Reports (EIR).[1-6]

Regarding the forensic analysis, there is more interest in qualitative (what explosive material was used) rather than quantitative (how much explosive material is present). In the absence of intact particles, post-blast fragments are analyzed by extraction with dichloromethane and/or acetone followed by visual/microscopic exams, spectroscopic analysis (e.g., Fourier Transform Infrared Spectroscopy (FTIR)) and gas chromatography/mass spectrometry (GC/MS) to identify the explosive material used. Although liquid chromatography/mass spectrometry (LC/MS) has also developed as a technique for explosives analysis, LC/MS instruments are relatively rare in state/local laboratories.

Analysis of explosive residues in post-blast debris requires high sensitivity (response of an analytical instrument to an analyte), selectivity (ability of an analytical instrument to respond to an analyte in the presence of interferences), and specificity (extent an analytical instrument can conclusively identify an analyte). Despite the power of GC/MS as an analytical technique, a precise retention time and a mass spectrum that is sufficiently specific is required to

unambiguously identifying a compound. To have a “specific” mass spectrum, a molecular ion that indicates the molecular weight of the analyte and the formation of several high mass fragments that are highly characteristic of the molecule are needed. For explosive analysis, limitations are encountered in that compounds yield similar or identical mass spectra, often with no molecular ion. This includes ethylene glycol dinitrate (EGDN), nitroglycerine (NG) and pentaerythritol tetranitrate (PETN), which yield only two major ions in electron impact (EI) ionization ( $m/z$  46 and  $m/z$  76). Additionally, 2,4-dinitrotoluene, 2,5-dinitrotoluene and 2,6-dinitrotoluene yield the same major ions in ( $m/z$  63,  $m/z$  89, and  $m/z$  165). In these cases, identification of an explosive compound relies to a much greater extent on retention time rather than on the detector providing specificity.

Conversely, the utilization of a vacuum ultraviolet spectrometer (VUV) can overcome these limitations observed in mass spectrometry for the analysis of explosives.

## 1.2 Vacuum Ultraviolet Spectroscopy

VUV has previously been limited to large synchrotron facilities to overcome background absorption. However, advancements were made in 2014 by VUV Analytics with the development of a benchtop VUV spectrometer that is coupled to a gas chromatograph.[11] VUV is a universal detector capable of both qualitative and quantitative data acquisition that has the ability to overcome limitations observed in mass spectrometry (e.g. differentiation of isomeric, isobaric, or labile compounds).[11]

As the sample is introduced into the inlet of the gas chromatograph, the sample is vaporized and a carrier gas (e.g., hydrogen or helium gas) is utilized to move the compounds along a column. Compounds of a complex mixture are then separated along the compound based on relative interaction with the stationary phase of the column. As the compounds elute from the column, they travel through a heated transfer line and into a heated flow cell (typically  $\sim 275$  °C). In the flow cell (40  $\mu$ L volume), a make-up gas (typically nitrogen) is used to assist in reducing band broadening and a deuterium lamp is used to excite the molecule and the change in energy is detected via a charged coupled device (CCD) detector. The VUV detector is capable of detecting absorption between 120 nm and 430 nm (Figure 1.2). The capability of probing into the VUV region is advantageous as energy transitions are detectable that are not in traditional ultraviolet/visible (UV/vis) spectroscopy and vibronic transitions (vibrational and electronic transitions) and Rydberg transitions (high

energy transitions beyond the valence shell) are possible. These include  $\sigma \rightarrow \sigma^*$  transitions (alkane),  $n \rightarrow \sigma^*$  transitions (alcohols, amines, alkyl halides), and higher energy  $\pi \rightarrow \pi^*$  (unsaturated alkanes and dienes).[11] Therefore, all gas phase species absorb and display characteristic spectra in the wavelength region probed in the VUV and small changes in the chemical backbone result in differences in the VUV spectrum. In this region.

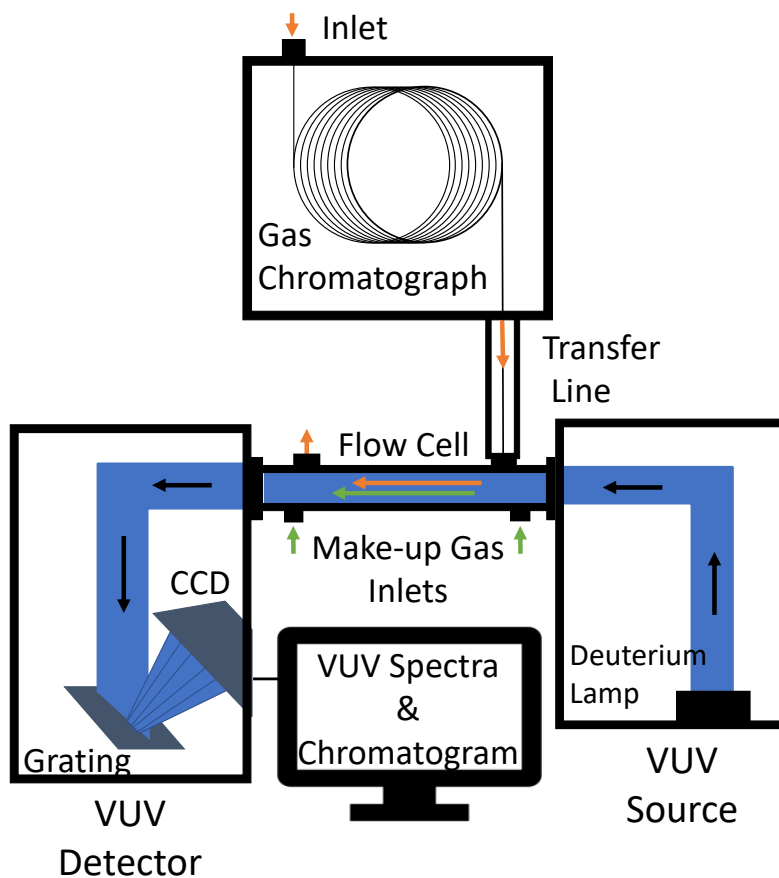


Figure 1.2. Schematic of the GC/VUV system.

To date, GC/VUV has been applied to a number of different applications including hydrocarbons [12-27], fatty acids [28-32], flavor/fragrance [33, 34], drugs [35-45], explosives [39, 46-50], environmental [33, 51-53], other volatiles organic compounds [54-56], etc.[57-59]

Research encompassed in this dissertation includes utilization of GC/VUV for:

- Analysis of nitrate ester explosives (Chapter 2).[46]
- Analysis and identification of the vibronic and Rydberg transitions via computational methods (Chapter 3).[47]

- Analysis and identification of thermal decomposition and the decomposition products in the transfer line/flow cell (Chapters 4).[48]
- Characterization of the nitro functional group in the VUV region (Chapter 5).[49]
- Optimization of the GC/VUV system for explosive analysis (Chapter 6).[50]

### 1.3 References

1. United States Bomb Data Center (USBDC) Bomb Arson Tracking System (BATS), *Explosives Incident Report (Eir)*. 2015, Bureau of Alcohol, Tobacco, Firearms and Explosives (ATF).
2. United States Bomb Data Center (USBDC) Bomb Arson Tracking System (BATS), *Explosives Incident Report (Eir)*. 2016, Bureau of Alcohol, Tobacco, Firearms and Explosives (ATF).
3. United States Bomb Data Center (USBDC) Bomb Arson Tracking System (BATS), *Explosives Incident Report (Eir)*. 2017, Bureau of Alcohol, Tobacco, Firearms and Explosives (ATF).
4. United States Bomb Data Center (USBDC) Bomb Arson Tracking System (BATS), *Explosives Incident Report (Eir)*. 2018, Bureau of Alcohol, Tobacco, Firearms and Explosives (ATF).
5. United States Bomb Data Center (USBDC) Bomb Arson Tracking System (BATS), *Explosives Incident Report (Eir)*. 2019, Bureau of Alcohol, Tobacco, Firearms and Explosives (ATF).
6. United States Bomb Data Center (USBDC) Bomb Arson Tracking System (BATS), *Explosives Incident Report (Eir)*. 2020, Bureau of Alcohol, Tobacco, Firearms and Explosives (ATF).
7. Beveridge, A., *Forensic Investigation of Explosions. Chapter 11 Investigation of Pipe Bombs*. 2011, Taylor & Francis. p. 429-491.
8. Akhavan, J., *The Chemistry of Explosives*. 2 ed. 2004: The Royal Society of Chemistry.
9. Beveridge, A., *Forensic Investigation of Explosions. Chapter 4 General Protocols at the Scene of an Explosion*. 2011, Taylor & Francis. p. 79-117.
10. Beveridge, A., *Forensic Investigation of Explosions. Chapter 5 Recovery of Material from the Scene of an Explosion*. 2011, Taylor & Francis. p. 119-157.
11. Schug, K.A., et al., *Vacuum Ultraviolet Detector for Gas Chromatography*. *Anal Chem*, 2014. **86**(16): p. 8329-35.

12. Bai, L., et al., *Permanent Gas Analysis Using Gas Chromatography with Vacuum Ultraviolet Detection*. J Chromatogr A, 2015. **1388**: p. 244-50.
13. Weber, B.M., P. Walsh, and J.J. Harynuk, *Determination of Hydrocarbon Group-Type of Diesel Fuels by Gas Chromatography with Vacuum Ultraviolet Detection*. Anal Chem, 2016. **88**(11): p. 5809-17.
14. Schenk, J., et al., *Analysis and Deconvolution of Dimethylnaphthalene Isomers Using Gas Chromatography Vacuum Ultraviolet Spectroscopy and Theoretical Computations*. Anal Chim Acta, 2016. **945**: p. 1-8.
15. Walsh, P., M. Garbalena, and K.A. Schug, *Rapid Analysis and Time Interval Deconvolution for Comprehensive Fuel Compound Group Classification and Speciation Using Gas Chromatography-Vacuum Ultraviolet Spectroscopy*. Anal Chem, 2016. **88**(22): p. 11130-11138.
16. Bai, L., et al., *Pseudo-Absolute Quantitative Analysis Using Gas Chromatography - Vacuum Ultraviolet Spectroscopy - a Tutorial*. Anal Chim Acta, 2017. **953**: p. 10-22.
17. Bai, L., et al., *Comparison of Gc-Vuv, Gc-Fid, and Comprehensive Two-Dimensional Gc-Ms for the Characterization of Weathered and Unweathered Diesel Fuels*. Fuel, 2018. **214**: p. 521-527.
18. Liu, H., et al., *Hyphenation of Short Monolithic Silica Capillary Column with Vacuum Ultraviolet Spectroscopy Detector for Light Hydrocarbons Separation*. J Chromatogr A, 2019. **1595**: p. 174-179.
19. Dunkle, M.N., et al., *Quantification of the Composition of Liquid Hydrocarbon Streams: Comparing the Gc-Vuv to Dha and Gcxgc*. J Chromatogr A, 2019. **1587**: p. 239-246.
20. Garcia-Cicourel, A.R., et al., *Comprehensive Off-Line Silver Phase Liquid Chromatography X Gas Chromatography with Flame Ionization and Vacuum Ultraviolet Detection for the Detailed Characterization of Mineral Oil Aromatic Hydrocarbons*. J Chromatogr A, 2019. **1607**: p. 460391.
21. Garcia-Cicourel, A.R. and H.G. Janssen, *Direct Analysis of Aromatic Hydrocarbons in Purified Mineral Oils for Foods and Cosmetics Applications Using Gas Chromatography with Vacuum Ultraviolet Detection*. J Chromatogr A, 2019. **1590**: p. 113-120.
22. Mao, J.X., P. Kroll, and K.A. Schug, *Vacuum Ultraviolet Absorbance of Alkanes: An Experimental and Theoretical Investigation*. Structural Chemistry, 2019. **30**(6): p. 2217-2224.
23. Groger, T., et al., *A Vacuum Ultraviolet Absorption Array Spectrometer as a Selective Detector for Comprehensive Two-Dimensional Gas Chromatography: Concept and First Results*. Anal Chem, 2016. **88**(6): p. 3031-9.

24. Mao, J.X., et al., *Simulation of Vacuum Ultraviolet Absorption Spectra: Paraffin, Isoparaffin, Olefin, Naphthene, and Aromatic Hydrocarbon Class Compounds*. Appl Spectrosc, 2020. **74**(1): p. 72-80.
25. Wang, F.C.Y., *Gc X Vuv Study of Diesel: A Two-Dimensional Separation Approach*. Energy & Fuels, 2020. **34**(2): p. 1432-1437.
26. Wang, F.C.Y., *Comprehensive Two-Dimensional Gas Chromatography Hyphenated with a Vacuum Ultraviolet Spectrometer to Analyze Diesel-a Three-Dimensional Separation (Gc X Gc X Vuv) Approach*. Energy & Fuels, 2020. **34**(7): p. 8012-8017.
27. Rael, A.S., et al., *A Critical Comparison of Vacuum Uv (Vuv) Spectrometer and Electron Ionization Single Quadrupole Mass Spectrometer Detectors for the Analysis of Alkylbenzenes in Gasoline by Gas Chromatography: Experimental and Statistical Aspects*. Talanta, 2021. **225**: p. 122081.
28. Fan, H., et al., *Gas Chromatography-Vacuum Ultraviolet Spectroscopy for Analysis of Fatty Acid Methyl Esters*. Food Chem, 2016. **194**: p. 265-71.
29. Weatherly, C.A., et al., *Analysis of Long-Chain Unsaturated Fatty Acids by Ionic Liquid Gas Chromatography*. J Agric Food Chem, 2016. **64**(6): p. 1422-32.
30. Santos, I.C., et al., *Analysis of Bacterial Fames Using Gas Chromatography - Vacuum Ultraviolet Spectroscopy for the Identification and Discrimination of Bacteria*. Talanta, 2018. **182**: p. 536-543.
31. Santos, I.C., et al., *Large-Volume Injection Gas Chromatography-Vacuum Ultraviolet Spectroscopy for the Qualitative and Quantitative Analysis of Fatty Acids in Blood Plasma*. Anal Chim Acta, 2019. **1053**: p. 169-177.
32. Zoccali, M., et al., *Flow-Modulated Comprehensive Two-Dimensional Gas Chromatography Combined with a Vacuum Ultraviolet Detector for the Analysis of Complex Mixtures*. J Chromatogr A, 2017. **1497**: p. 135-143.
33. Qiu, C., et al., *Gas Chromatography-Vacuum Ultraviolet Detection for Classification and Speciation of Polychlorinated Biphenyls in Industrial Mixtures*. J Chromatogr A, 2017. **1490**: p. 191-200.
34. Anthony, I.G.M., et al., *Improving Accuracy and Confidence of Chemical Identification by Gas Chromatography/Vacuum Ultraviolet Spectroscopy-Mass Spectrometry: Parallel Gas Chromatography, Vacuum Ultraviolet, and Mass Spectrometry Library Searches*. Anal Chem, 2018. **90**(20): p. 12307-12313.
35. Leghissa, A., et al., *Detection of Cannabinoids and Cannabinoid Metabolites Using Gas Chromatography with Vacuum Ultraviolet Spectroscopy*. Separation Science Plus, 2018. **1**(1): p. 37-42.

36. Zheng, J., C. Huang, and S. Wang, *Challenging Pharmaceutical Analyses by Gas Chromatography with Vacuum Ultraviolet Detection*. J Chromatogr A, 2018. **1567**: p. 185-190.
37. Buchalter, S., et al., *Gas Chromatography with Tandem Cold Electron Ionization Mass Spectrometric Detection and Vacuum Ultraviolet Detection for the Comprehensive Analysis of Fentanyl Analogues*. J Chromatogr A, 2019. **1596**: p. 183-193.
38. Skultety, L., et al., *Resolution of Isomeric New Designer Stimulants Using Gas Chromatography - Vacuum Ultraviolet Spectroscopy and Theoretical Computations*. Anal Chim Acta, 2017. **971**: p. 55-67.
39. Reiss, R., et al., *Evaluation and Application of Gas Chromatography - Vacuum Ultraviolet Spectroscopy for Drug- and Explosive Precursors and Examination of Non-Negative Matrix Factorization for Deconvolution*. Spectrochim Acta A Mol Biomol Spectrosc, 2019. **219**: p. 129-134.
40. Roberson, Z.R. and J.V. Goodpaster, *Differentiation of Structurally Similar Phenethylamines Via Gas Chromatography-Vacuum Ultraviolet Spectroscopy (Gc-Vuv)*. Forensic Chemistry, 2019. **15**: p. 100172.
41. Roberson, Z.R., H.C. Gordon, and J.V. Goodpaster, *Instrumental and Chemometric Analysis of Opiates Via Gas Chromatography-Vacuum Ultraviolet Spectrophotometry (Gc-Vuv)*. Anal Bioanal Chem, 2020. **412**(5): p. 1123-1128.
42. Tanen, J.L., I.S. Lurie, and I. Marginean, *Gas Chromatography with Dual Cold Electron Ionization Mass Spectrometry and Vacuum Ultraviolet Detection for the Analysis of Phenylethylamine Analogues*. Forensic Chemistry, 2020. **21**: p. 100281.
43. Roberson, Z.R. and J.V. Goodpaster, *Optimization of the Qualitative and Quantitative Analysis of Cocaine and Other Drugs of Abuse Via Gas Chromatography - Vacuum Ultraviolet Spectrophotometry (Gc - Vuv)*. Talanta, 2021. **222**: p. 121461.
44. Kranenburg, R.F., et al., *Distinguishing Drug Isomers in the Forensic Laboratory: Gc-Vuv in Addition to Gc-Ms for Orthogonal Selectivity and the Use of Library Match Scores as a New Source of Information*. Forensic Sci Int, 2019. **302**: p. 109900.
45. Kranenburg, R.F., et al., *Spotting Isomer Mixtures in Forensic Illicit Drug Casework with Gc-Vuv Using Automated Coelution Detection and Spectral Deconvolution*. Journal of Chromatography B-Analytical Technologies in the Biomedical and Life Sciences, 2021. **1173**: p. 122675.
46. Cruse, C.A. and J.V. Goodpaster, *Generating Highly Specific Spectra and Identifying Thermal Decomposition Products Via Gas Chromatography / Vacuum Ultraviolet Spectroscopy (Gc/Vuv): Application to Nitrate Ester Explosives*. Talanta, 2019. **195**: p. 580-586.

47. Cruse, C.A., J. Pu, and J.V. Goodpaster, *Identifying Thermal Decomposition Products of Nitrate Ester Explosives Using Gas Chromatography-Vacuum Ultraviolet Spectroscopy: An Experimental and Computational Study*. Appl Spectrosc, 2020. **74**(12): p. 1486-1495.
48. Cruse, C.A. and J.V. Goodpaster, *Thermal and Spectroscopic Analysis of Nitrated Compounds and Their Break-Down Products Using Gas Chromatography/Vacuum Uv Spectroscopy (Gc/Vuv)*. Anal Chim Acta, 2021. **1143**: p. 117-123.
49. Cruse, C.A. and J.V. Goodpaster, *A Systematic Study of the Absorbance of the Nitro Functional Group in the Vacuum Uv Region*. Analytica Chimica Acta, 2021. **1185**: p. 339042.
50. Cruse, C.A. and J.V. Goodpaster, *Optimization of Gas Chromatography/Vacuum Ultraviolet (Gc/Vuv) Spectroscopy for Explosive Compounds and Application to Post-Blast Debris*. Forensic Chemistry, 2021. **26**: p. 100362.
51. Pechancova, R., et al., *Comparative Study of Ink Photoinitiators in Food Packages Using Gas Chromatography with Vacuum Ultraviolet Detection and Gas Chromatography with Mass Spectrometry*. J Sep Sci, 2019. **42**(2): p. 556-565.
52. Fan, H., et al., *Gas Chromatography-Vacuum Ultraviolet Spectroscopy for Multiclass Pesticide Identification*. J Chromatogr A, 2015. **1389**: p. 120-7.
53. Schenk, J., et al., *Lab-Simulated Downhole Leaching of Formaldehyde from Proppants by High Performance Liquid Chromatography (Hplc), Headspace Gas Chromatography-Vacuum Ultraviolet (Hs-Gc-Vuv) Spectroscopy, and Headspace Gas Chromatography-Mass Spectrometry (Hs-Gc-Ms)*. Environ Sci Process Impacts, 2019. **21**(2): p. 214-223.
54. Zanella, D., et al., *Comparison of Headspace Solid-Phase Microextraction High Capacity Fiber Coatings Based on Dual Mass Spectrometric and Broadband Vacuum Ultraviolet Absorption Detection for Untargeted Analysis of Beer Volatiles Using Gas Chromatography*. Anal Chim Acta, 2021. **1141**: p. 91-99.
55. Diekmann, J.A., 3rd, et al., *Quantitation and Identification of Ethanol and Inhalant Compounds in Whole Blood Using Static Headspace Gas Chromatography Vacuum Ultraviolet Spectroscopy*. J Chromatogr A, 2020. **1611**: p. 460607.
56. Gruber, B., et al., *Vacuum Ultraviolet Absorption Spectroscopy in Combination with Comprehensive Two-Dimensional Gas Chromatography for the Monitoring of Volatile Organic Compounds in Breath Gas: A Feasibility Study*. J Chromatogr A, 2016. **1464**: p. 141-6.
57. Qiu, C., et al., *Gas Chromatography-Vacuum Ultraviolet Spectroscopic Analysis of Organosilanes*. Talanta, 2021. **223**(Pt 2): p. 121781.
58. Weston, C., et al., *Investigation of Gas Phase Absorption Spectral Similarity for Stable Isotopically Labeled Compounds in the 125-240 Nm Wavelength Range*. Talanta, 2018. **177**: p. 41-46.

59. Ponduru, T.T., et al., *Copper(I)-Based Oxidation of Polycyclic Aromatic Hydrocarbons and Product Elucidation Using Vacuum Ultraviolet Spectroscopy and Theoretical Spectral Calculations*. *New Journal of Chemistry*, 2018. **42**(24): p. 19442-19449.

## **CHAPTER 2. GENERATING HIGHLY SPECIFIC SPECTRA AND IDENTIFYING THERMAL DECOMPOSITION PRODUCTS VIA GAS CHROMATOGRAPHY / VACUUM ULTRAVIOLET SPECTROSCOPY (GC/VUV): APPLICATION TO NITRATE ESTER EXPLOSIVES**

Courtney A. Cruse, John V. Goodpaster\*

Department of Chemistry and Chemical Biology, Indiana University - Purdue University Indianapolis (IUPUI), 402 North Blackford Street LD326, Indianapolis, Indiana 46202, United States

### **2.1 Abstract**

Gas chromatography/mass spectrometry (GC/MS) is a "workhorse" instrument for chemical analysis, but it can be limited in its ability to differentiate structurally similar compounds. The coupling of GC to vacuum ultraviolet (VUV) spectroscopy is a recently developed technique with the potential for increased detection specificity. To date, GC/VUV has been demonstrated in the analysis of volatile organic compounds, petroleum products, aroma compounds, pharmaceuticals, illegal drugs, and lipids. This paper is the first to report on the utility of GC/VUV for explosives analysis in general, and the first to report on thermal degradation within the VUV cell and its analytical utility. The general figures of merit and performance of GC/VUV were evaluated with authentic standards of nitrate ester explosives (e.g., nitroglycerine (NG), ethylene glycol dinitrate (EGDN), pentaerythritol tetranitrate (PETN), and erythritol tetranitrate (ETN)). In addition, the explosive analytes were thermally degraded in the VUV cell, yielding reproducible, complex, and characteristic mixtures of gas phase products (e.g., nitric oxide, carbon monoxide, and formaldehyde). The relative amounts of the degradation products were estimated via spectral subtraction of library spectra. Lastly, GC/VUV was used to analyze milligram quantities of intact and burned samples of double-base smokeless powders containing nitroglycerine, diphenylamine, ethyl centralite, and dibutyl phthalate.

## 2.2 Introduction

A recent development with the potential to complement mass spectrometry is a benchtop vacuum ultraviolet (VUV) detector for GC (GC/VUV). The VUV (VGA101) detector acquires gas phase absorption data between 125 and 430 nm. In this region,  $\sigma$  to  $\sigma^*$ ,  $n$  to  $\pi^*$ , and high probability  $\pi$  to  $\pi^*$  transitions are evident.[1, 2] Prior to this, a bright source synchrotron facility was required to obtain absorption information in this low wavelength region.[1, 3] Prior research has shown that gas phase absorption spectra in the 125 to 240 nm range are highly informative due to the presence of  $\sigma$  to  $\sigma^*$  transitions originating primarily from C-C and C-H bonds.[4] As the spectra are acquired in the gas phase, no interactions occur between species; thus spectra will not shift like in liquid phase spectroscopy.[5] Furthermore, the molecular absorption cross section in this region allows for orders of magnitude larger sensitivity than those in the ultraviolet and infrared regions.[6] Additionally, VUV has the ability to deconvolute species in a single peak. [3, 5, 7, 8] This originates from the additive nature of the Beer Lambert Law where the total absorption is a linear combination of each, non-interacting species.[2-5, 9, 10] To date, GC/VUV has been used to analyse drugs,[2, 11] fatty acid methyl esters,[9] diesel fuel,[3, 6, 7, 10] hydrocarbons,[12] and perfume and essential oil[4, 13] from 125 to 230 nm.

Ultimately, explosives analysis requires high sensitivity, selectivity, and specificity. Towards that end, gas chromatography / mass spectrometry (GC/MS) is one of the current “gold standard” methods for the analysis of semi-volatile and volatile explosives.[1, 5, 14] That being said, the analysis of nitrate ester explosives is inherently more difficult via GC/MS. For example, nitrate ester explosives are thermally labile and are prone to decomposition in the GC inlet. This can be largely overcome by using a multi-mode inlet with a temperature program and a shorter column.[15] However, these analytes have essentially identical mass spectra by electron ionization (EI) due to extensive fragmentation into  $\text{NO}_2^+$  at  $m/z$  46 (as the base peak) and  $\text{CH}_2\text{ONO}_2^+$  at  $m/z$  76 without a molecular ion.[14-16] In negative-ion chemical ionization (NCI), fragmentation of nitrate ester explosives results in ions for  $\text{ONO}_2^-$  at  $m/z$  62 and  $\text{NO}_2^-$  at  $m/z$  46. When dichloromethane is used as the reagent gas, an  $[\text{M} + \text{Cl}]^-$  adduct is seen at  $m/z$  262/264.[1, 5, 14]

Analysis of nitrate ester explosives by liquid chromatography/mass spectrometry (LC/MS) is also possible using either electrospray ionization (ESI) or atmospheric pressure chemical ionization (APCI). LC/MS overcomes the issue of thermal decomposition in GC/MS. In some cases, post-column introduction of chemical additives are necessary for the identification of EGDN,

NG, and PETN.[15] According to the Technical Working Group for Fire and Explosive Analysis (TWGFEX), GC/MS and LC/MS are categorized as Category 1 (provide significant structural/element information) and Category 2 (provide limited structural/element information), respectively.[17] Most recently, ambient ionization using desorption electrospray ionization (DESI)[18] and low-temperature plasma (LTP)[19] have been used to identify PETN with MS/MS analysis. Direct analysis in real time (DART)/MS and surface-assisted laser desorption/ionization (SALDI)/TOF/MS analysis of explosives, including NG and PETN, has also been used.[20] In these cases, there is no chromatographic separation and these techniques have yet to become generally available to and accepted by forensic scientists.

Andrasko et al. were the first to demonstrate that thermal decomposition of explosives can occur in GC with a UV detector with a spectral range of 178 - 330 nm.[21] In particular, they observed that at higher transfer line temperatures, nitrate ester explosives such as ethylene glycol dinitrate (EGDN), nitroglycerine (NG), and pentaerythritol tetranitrate (PETN) decomposed into nitric oxide, which was easily detectable in their spectral range. This has informed our approach, but due to a wider spectral range (125 - 430 nm) and other factors, we have identified several additional thermal degradation products of this class of explosives as well as estimates of their relative concentrations.

The aim of this work is to use GC/VUV to generate spectra at different transfer line and flow cell temperatures to investigate the thermal decomposition of analytes. Our application of interest has not been previously explored using GC/VUV, and that is the identification of explosives in intact, post-burn and post-blast samples. Hence, realistic samples of unburned and burned double-base smokeless powders have been analysed to demonstrate the application of GC/VUV to forensic explosives analysis. To the best of our knowledge, this is the first published application of GC/VUV to the analysis of explosives.

## **2.3 Materials and Methods**

### **2.3.1 Chemicals**

Pentane (pesticide grade), methanol (optima LC/MS), and dichloromethane (stabilized HPLC grade) were purchased from Fisher Scientific. Nitroglycerine (1000 µg/mL in methanol), erythritol tetranitrate (1000 µg/mL in acetonitrile), ethylene glycol dinitrate (1000 µg/mL in

methanol), and pentaerythritol tetranitrate (1000 µg/mL in methanol) were purchased from Restek as single-component standards. Ethyl centralite was purchased from Aldrich Chemistry, diphenylamine was purchased from Acros Organics, and dibutyl phthalate was purchased from Supelco. Double-base smokeless powders (Alliant Red Dot, Accurate No. 7, and Accurate No. 5) were purchased locally. All 9 mm screw thread liquid injection vials were purchased from Fisher Scientific.

### **2.3.2 Sample Preparation**

A mixture of nitroglycerine (NG), erythritol tetranitrate (ETN), ethylene glycol dinitrate (EGDN), and pentaerythritol tetranitrate (PETN) was prepared containing 250 ppm of each analyte. ETN in acetonitrile was first evaporated and reconstituted in methanol using a nitrogen blowdown apparatus. Additionally, single component samples of NG, ETN, EGDN, PETN were prepared at 1000 ppm in methanol and diluted 100-fold.

Realistic samples were prepared by weighing out approximately 0.6 mg of each double-base smokeless powder (approximately 5 particles). The particles were extracted with 3 mL of dichloromethane (DCM) for an hour on a shaker table. Then, the DCM extract was filtered with a 0.45 µm PTFE filter and injected into the GC/VUV for analysis of smokeless powder components. The burned double-base smokeless powder samples were created by weighing out 50 mg of each double-base smokeless powder onto a watch glass. Then, the sample was ignited and allowed to self-extinguish. The residue was scraped from the watch glass and extracted with 1 mL of DCM for one hour. After filtering, the extract was analysed in the same manner as the intact smokeless powder.

### **2.3.3 Gas Chromatography**

Each experiment was run in triplicate with a methanol blank run between each set of triplicates. 1 µL of the mixture solution was injected into the gas chromatograph with hydrogen as the carrier gas at 1.8 mL/min (Agilent 7890B series GC equipped with a multimode inlet and Agilent 7390 autosampler). A ramped inlet temperature program was utilized (50 °C ramped to 280 °C at 900 °C/min) with a split injection (5:1).[22] Analytes were separated on a Phenomenex ZB-5MS column (10 m x 0.18 mm x 0.18 µm). For the mixture of EGDN, ETN, NG, and PETN,

the oven program began at 60 °C for 0.5 min, ramped at 20 °C/min to 170 °C. Realistic double-base smokeless powders were analysed with an oven program of 60 °C for 0.5 min, ramped at 20 °C/min to 220 °C.

#### **2.3.4 Vacuum Ultraviolet Spectroscopy**

After the GC effluent exited the transfer line, it was directed into a VUV Analytics VGA-101 VUV spectrometer with a spectral resolution of approximately 0.5 nm. All experiments were run with a spectral range of 125 nm to 430 nm with a 4.5 Hz scan rate, nitrogen as the make-up gas at a pressure of 0.35 psi, and a deuterium lamp as the light source. The transfer line and flow cell were adjusted, in tandem, for each triplicate run to 190 °C, 200 °C, 220 °C, 240 °C, 260 °C, and 280 °C. This was done to observe the thermal decomposition products of the nitrate esters in the VUV flow cell.

#### **2.3.5 Ultraviolet/Visible Spectroscopy**

Each sample was analyzed by a Thermo Scientific Evolution 201 UV-Visible Spectrophotometer with a scan range of 230 nm - 700 nm and a spectral bandwidth of 1.0 nm. Quartz cuvettes were utilized for spectral acquisition. The UV cut off for methanol (205 nm) is below the range of the UV-Vis instrument.

#### **2.3.6 Spectral Math**

Software for a Fourier Transform Infrared Spectrometer (FTIR), OMNIC Picta, was utilized to perform spectral subtraction on the VUV spectra at 280 °C to determine the relative contribution of each decomposition product to the nitrate ester spectra. This could be accomplished according to the Beer-Lambert law following the equation:  $\text{Spectrum 1} - (\text{Spectrum 2} * \text{Factor}) = \text{Result}$ . [23] The multiplication factor is determined by subtracting out spectrum 2 until the common peak(s) are, ideally, zeroed from spectrum 1. Using this approach, the thermal decomposition products were subtracted one at a time from the initial spectrum. The squared correlation coefficient ( $r^2$ ) and the sum-squared residuals (SSR) were calculated for the experimental VUV spectrum relative to the sum of the thermal decomposition components.

### **2.3.7 Calculations**

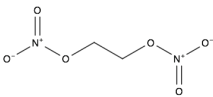
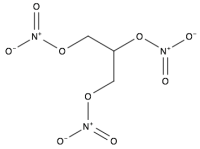
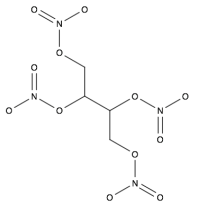
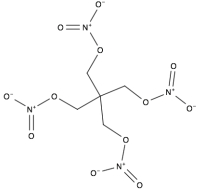
For calculations of signal-to-noise (S/N) ratio a single wavelength filter (128 - 129 nm) was considered. Signal was defined as the chromatographic peak height. Noise was defined as the standard deviation of ten baseline points that preceded the chromatographic peak. Seven calibration concentrations from 50 ppm to 1000 ppm run in triplicate were utilized for the calculations. A S/N ratio plot was constructed as  $\log(S/N)$  vs  $\log(S)$ . The limits of detection (LODs) were determined as the concentration with a S/N equal to 3 from the S/N plot.

## **2.4 Results and Discussion**

### **2.4.1 GC/VUV Analysis of EGDN, ETN, NG, and PETN**

Under the chromatographic conditions used here, the retention times for EGDN, NG, ETN, and PETN were 1.4 min, 3.4 min, 4.8 min, and 5.7 min, respectively. Standard VUV spectra were obtained for EGDN, NG, and ETN at flow cell temperatures of 170 °C and at 190 °C for PETN. As shown in Table 2.1, each VUV spectrum had two peak maxima around 135 nm and 187 - 188 nm, respectively.

Table 2.1. Experimentally determined wavelengths of maximum absorbance ( $\lambda_{\max} \pm 95\%$  confidence interval) of EGDN, ETN, EGDN, and PETN in the VUV at 190 °C (n = 3). In methanol, the  $\lambda_{\max}$  of these compounds are found at 278 - 280 nm (data not shown).

	Molecular Weight (g/mol)	Structure	VUV $\lambda_{\max}$ (nm)
EGDN	152.1		134.9 $\pm$ 0.2 187.3 $\pm$ 0.4
NG	227.09		135.1 $\pm$ 0.5 187.2 $\pm$ 1.1
ETN	302.11		134.9 $\pm$ 0.2 187.7 $\pm$ 0.3
PETN	316.1		136.1 $\pm$ 0.8 188.7 $\pm$ 0.4

The linear range,  $R^2$ , and slope for each analyte was determined from a calibration curve of peak area (at 128 - 129 nm) versus the concentration in ppm. Signal to noise was defined as the ratio of the height of a chromatographic peak divided by the standard deviation of the baseline noise preceding the peak. Plots of the log of the S/N ratio versus the log of the signal were constructed and confirmed that the S/N and S are linearly related and, hence, the instrument is blank noise limited. The calculated limit of detection for each compound (where S/N = 3) is shown in Table 2.2.

Table 2.2. Linearity, linear range, limit of detection and sensitivity of GC/VUV for EGDN, ETN, EGDN, and PETN.

Compound	Calculated LOD (ppm)	Linear Range (ppm)	R <sup>2</sup>	Slope (ppm <sup>-1</sup> ) X 100
EGDN	17.5	25 to 1000	0.9993	2.84
NG	33.4	50 to 1000	0.998	2.38
ETN	174.3	250 to 1000	0.9996	1.29
PETN	90.2	350 to 1000	0.995	0.45

With increasing molecular weight, the LOD listed in Table 2.2 exhibits a clear upward trend and sensitivity exhibits a clear downward trend with increasing molecular weight. This may be due to factors unrelated to the VUV detector, such as decreased efficiency of transfer of the analyte from the inlet to the stationary phase (i.e., discrimination effects related to volatility). A full optimization of inlet temperature and other parameters is planned to explore these effects. Another potential effect is that the thermal stability of these explosives decreases with increasing molecular weight, meaning degradation in the inlet would be more pronounced for ETN and PETN. A small peak that was specifically associated with PETN and deduced to be a degradation product formed in the inlet was observed.

#### 2.4.2 Temperature Effects and Thermal Degradation

When the VUV spectra of the nitrate esters are compared side-by-side with the EI mass spectra obtained from each compound, the overall lack of differentiation by either method is abundantly clear (see Figure 2.1).

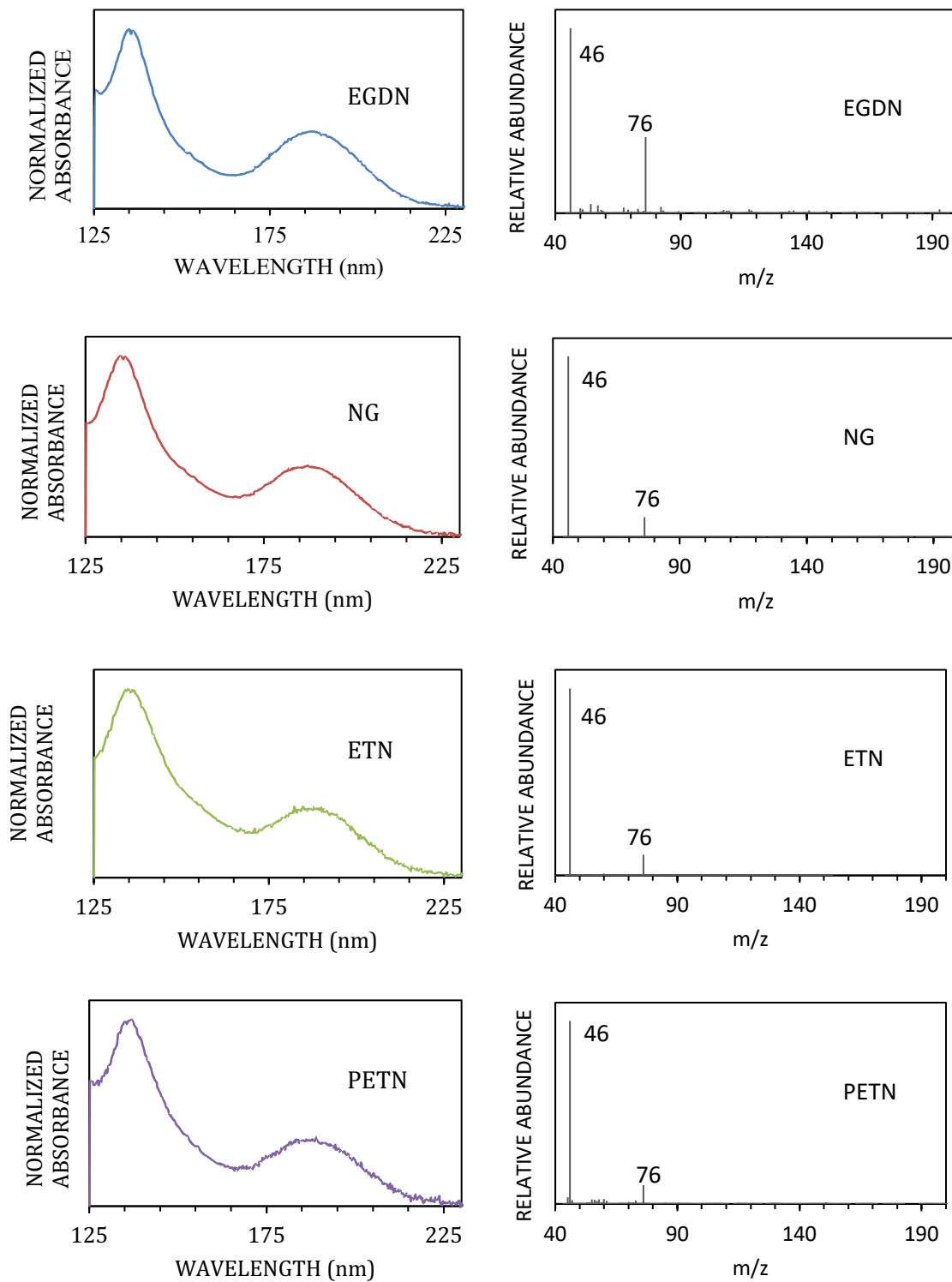


Figure 2.1. Comparison of “as is” VUV spectra at 190 °C and EI mass spectra for nitrate ester explosives.

However, increasing the flow cell temperature led to dramatic thermal decomposition of the four nitrate ester explosives. The decomposition process occurred in the flow cell, rather than in the GC inlet, as a single peak was observed for each explosive in the chromatogram. Partial decomposition was observed at 220 °C and nearly complete decomposition was observed at 280 °C (Figure 2.2). All spectra were truncated after 240 nm due to the lack of any spectral features at longer wavelengths.

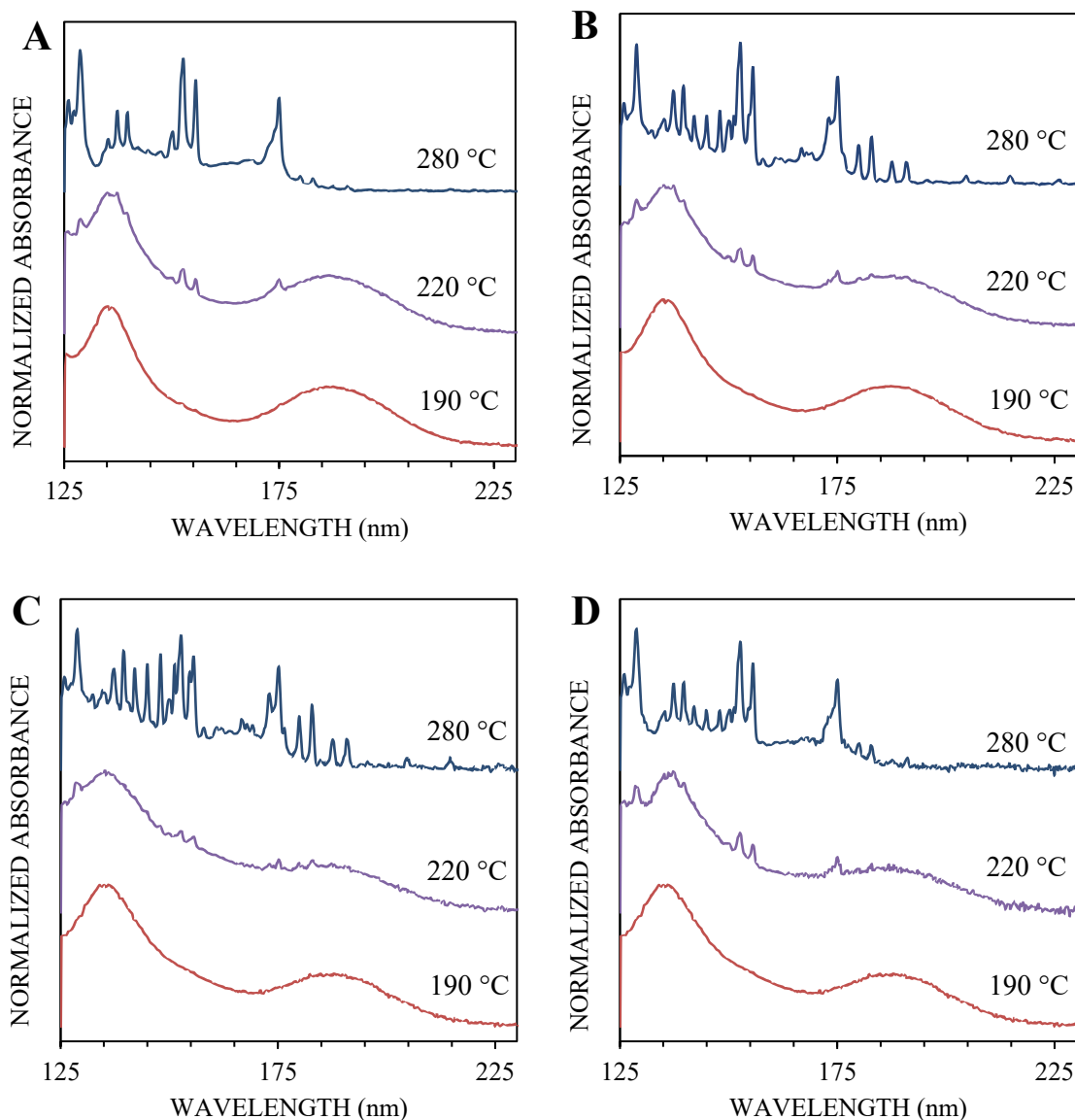


Figure 2.2. Stacked VUV spectra of (A) EGDN ( $T_{\text{dec}} = 198$ ), (B) NG ( $T_{\text{dec}} = 167$ ), (C) ETN ( $T_{\text{dec}} = 170$ ), and (D) PETN ( $T_{\text{dec}} = 157$ ) at 190 °C (bottom), 220 °C (middle), and 280 °C (top). Decomposition temperatures are derived from Differential Scanning Calorimetry (DSC).[24, 25]

Spectra at 190 °C have more broad spectral features than at higher temperatures (Figure 2.3). However, differences are apparent in the relative peak height ratios of the two peaks and in the valley between the peaks, which allows for differentiation between EGDN, ETN, NG, PETN at 190 °C.

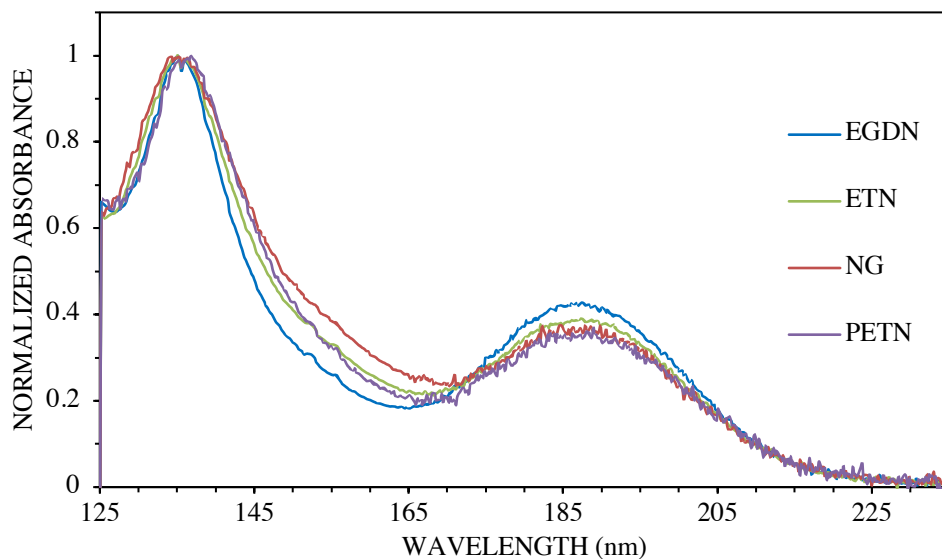


Figure 2.3. Overlay of VUV spectra of EGDN, NG, ETN, and PETN at 190 °C demonstrates the subtle and reproducible differences in the spectra.

### 2.4.3 Identification of Thermal Decomposition

Using a searchable VUV library, known decomposition products were compared to the decomposition spectra of EGDN, ETN, NG, and PETN. For example, we found that the spectral features in the decomposition spectrum of NG correspond to nitric oxide, carbon monoxide, and formaldehyde (Figure 2.4). In contrast, the EGDN VUV spectrum is dominated by formaldehyde with minimal contribution from nitric oxide and carbon monoxide (data not shown). In general, differences in the VUV spectra of the nitrate esters are observed in the differing contribution of nitric oxide (142 - 149 nm) and carbon monoxide (179 - 228 nm). In all cases, removal of the spectral contributions of these compounds from the nitrate ester VUV spectra resulted in broad featureless spectra consistent with the VUV spectra of water and oxygen (data not shown).

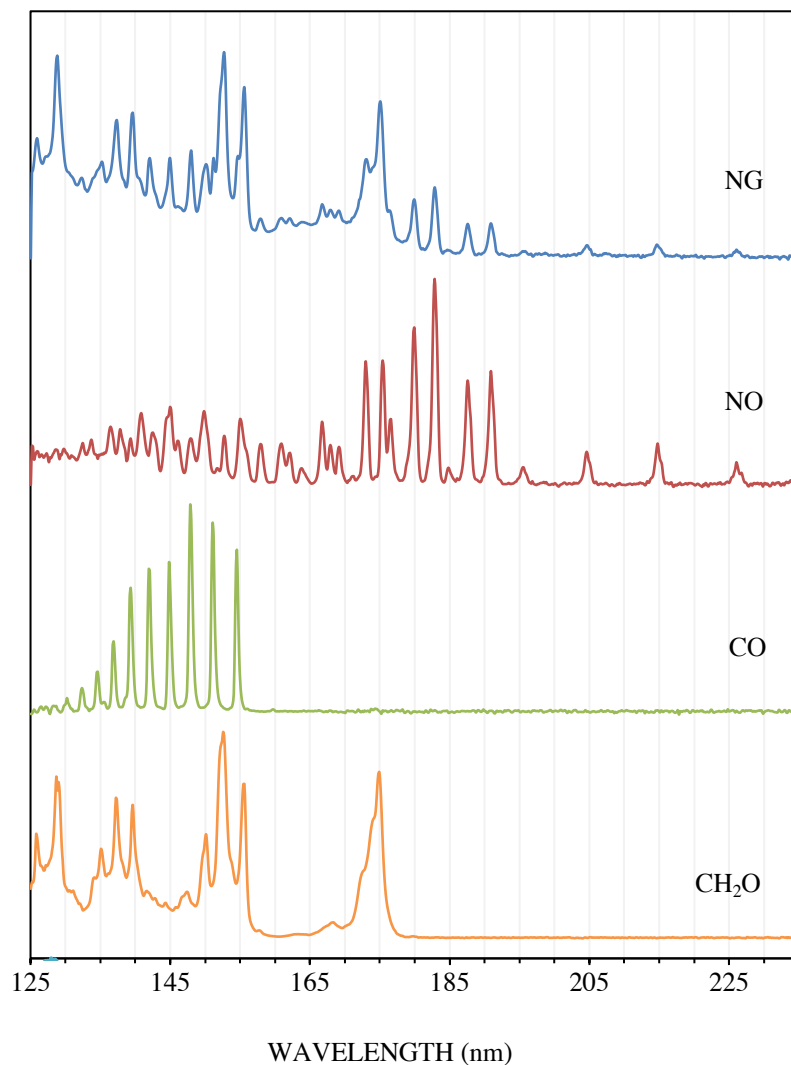


Figure 2.4. VUV spectra of NG and three of its thermal decomposition products: NO, CO, and CH<sub>2</sub>O.[26]

As the VUV spectrophotometer follows the Beer-Lambert Law[1, 3, 27], the absorptions of the decomposition products are additive to create the VUV spectra for each nitrate ester explosive. Therefore, the differentiation in the VUV spectra of EGDN, ETN, NG, and PETN at 280 °C could be attributed to the different spectral contribution ratios of the decomposition products. Spectral subtraction of nitric oxide, formaldehyde, carbon monoxide, water, and oxygen resulted in spectral multiplication factors that account for the differing contributions of each decomposition products.

As a check, the spectra of the decomposition products of NG were summed to attempt to recreate the NG spectra at 280 °C (Figure 2.5). This was accomplished by multiplying the

absorbance values of each decomposition product by the factor determined by the spectral subtraction. This was repeated for all explosives, where the absorbance values for the decomposition products were summed and the squared correlation coefficient ( $r^2$ ) and the sum of squares residual (SSR)[3-5, 11, 28] were calculated between each summed spectrum and experimental spectrum to quantify the spectral similarities (Table 2.3). SSR is related to the  $r^2$  through the following equation.[29]

$$r^2 = 1 - \frac{\text{sum of squares residual}}{\text{total sum of squares}}$$

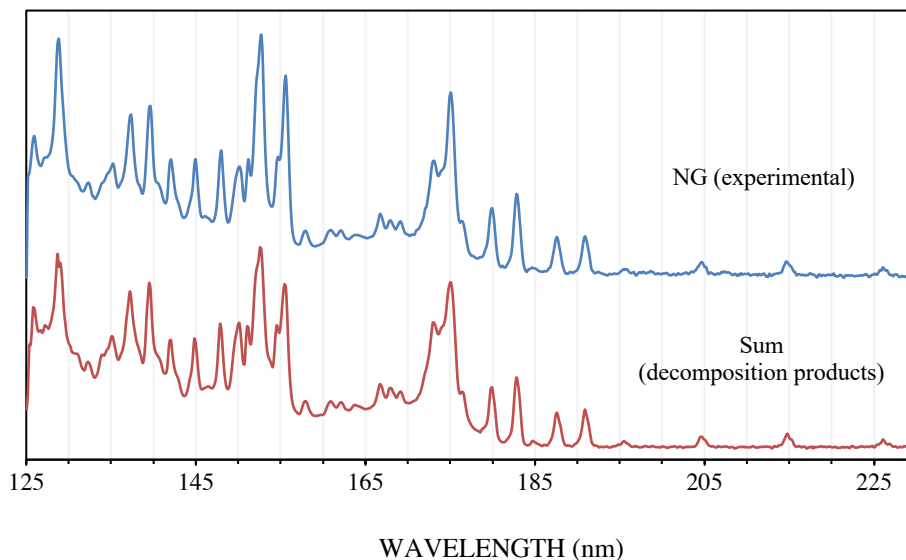


Figure 2.5. Experimental VUV spectra of NG (top) and the calculated sum of NG thermal decomposition products (bottom) per Table 2.3

Table 2.3. Relative percent composition of each decomposition product for EGDN, ETN, NG, and PETN at 280 °C and the squared correlation coefficients ( $r^2$ ) and the sum of squares residual (SSR) between the summed components and the experimental spectra.

	NO	CO	CH <sub>2</sub> O	H <sub>2</sub> O	O <sub>2</sub>	$r^2$	SSR
EGDN	0.05	0.00	0.65	0.23	0.10	0.955	3.99
NG	0.28	0.24	0.67	0.22	0.07	0.980	2.10
ETN	0.35	0.40	0.66	0.30	0.15	0.978	3.44
PETN	0.14	0.17	0.56	0.26	0.13	0.955	4.52

#### 2.4.4 Effect of Thermal Degradation on Sensitivity

Comparison of peak area over the range of VUV flow cell temperatures reveal a greater sensitivity at lower temperatures for ETN and NG with greater peak area at lower temperatures (Figure 2.6); indicating that pure ETN and NG have a higher molar absorptivity than the sum of the decomposition products, and thus, resulting in a higher absorption and a greater sensitivity. PETN has variable responses to the changes in flow cell temperatures, while EGDN does not have significant changes in peak area with changing temperatures.

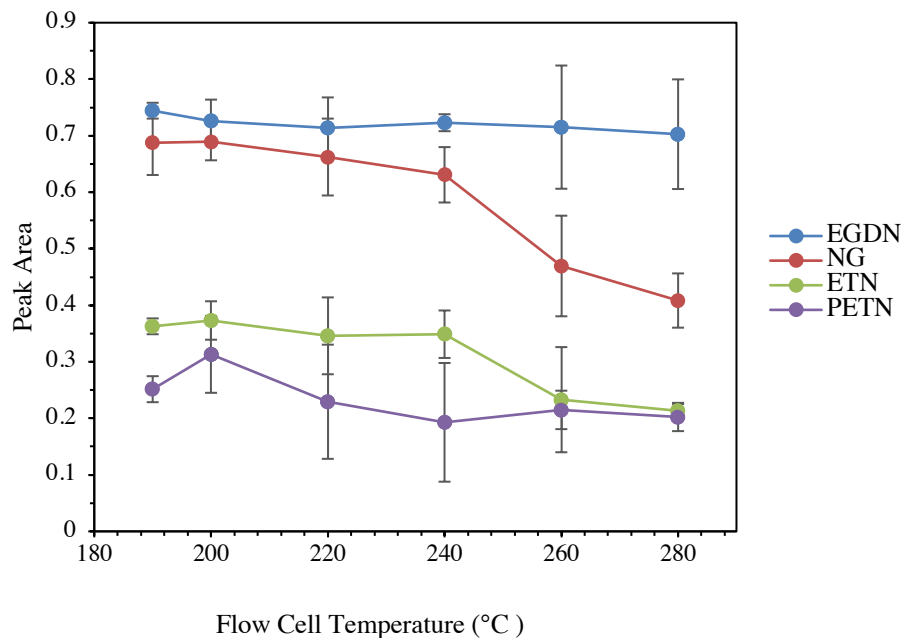


Figure 2.6. Effect of flow cell temperature on the peak area for nitrate ester explosives using a spectral filter from 125 nm - 240 nm.

#### 2.4.5 Analysis of Intact and Burned Double-Base Smokeless Powders

A low split ratio of 5:1 provided the best response of all analytes with a total flow (split vent flow and column flow) of 10.8 mL/min. Note that a minimum total flow of 10 mL/min is recommended for good chromatographic peak shape at low split ratios.[22] Spectral filters were created using the VUVision software to enhance the chromatographic signal by averaging the absorption in specified wavelength ranges; much in the same way as with extracted ion chromatograms in mass spectrometry.[9, 12]

All four of the nitrate ester decomposition VUV spectra absorbed light in the wavelength ranges 128 - 129 nm; therefore, a spectral filter was created that averages the absorbances in this wavelength range to improve the detection limits of nitroglycerine. A spectral filter from 175 - 205 nm improved the detection of aromatic double base-smokeless powder components such as diphenylamine, ethyl centralite, and di-n-butyl phthalate (Figure 2.7).

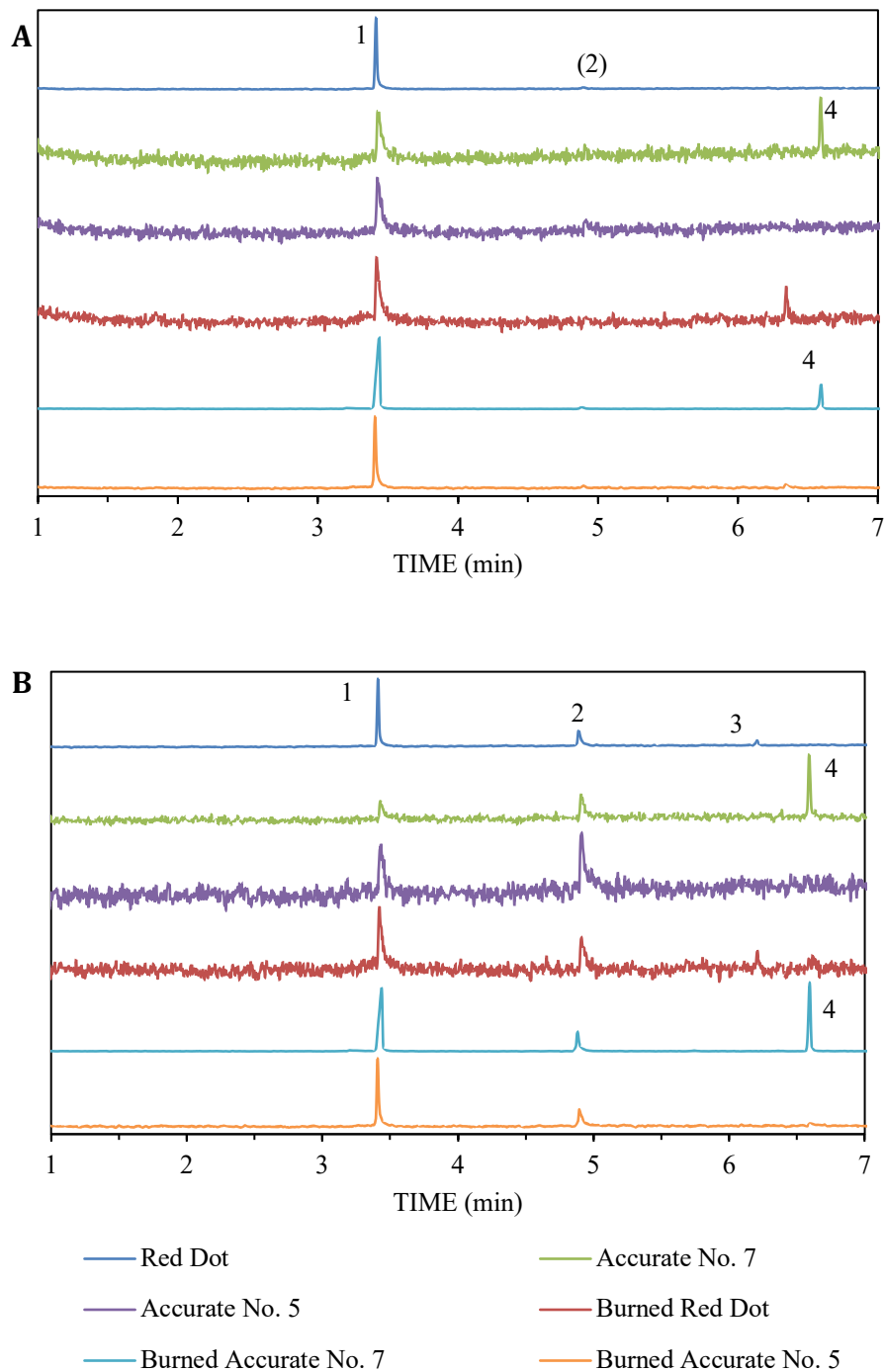


Figure 2.7. 5 mg of intact and 50 mg of burned Red Dot, Accurate No. 7, and Accurate No. 5 Double-Base Smokeless Powder with GC/VUV spectral filters (A) 175-205 nm, (B) 128-129 nm. (1) Nitroglycerine, (2) diphenylamine, (3) ethyl centralite, and (4) di-n-butyl phthalate. Each chromatogram normalized to unit absorbance. VUV spectra of smokeless powder components shown in Figure 2.8.

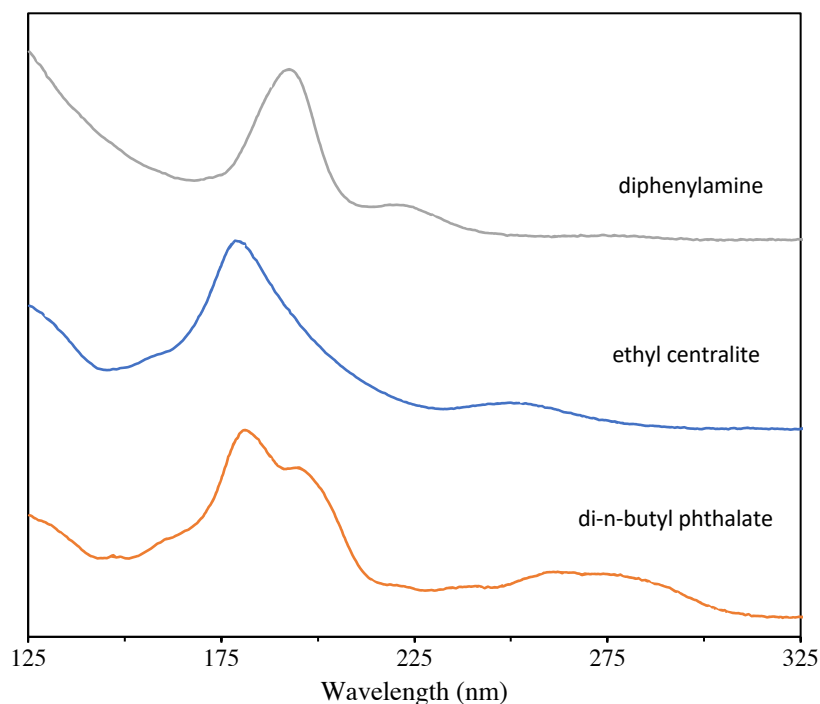


Figure 2.8. Stacked VUV spectra of double-base smokeless powder components.

## 2.5 Conclusions

GC/VUV has been used to investigate the thermal decomposition of nitrate ester explosives. In this work, increasing the transfer line and flow cell from 190 °C to 280 °C led to the decomposition of EGDN, ETN, NG, and PETN into nitric oxide, carbon monoxide, formaldehyde, water, and oxygen. It was determined that differing spectral contribution ratios of the decomposition products contribute to the variation in each nitrate ester explosive VUV spectrum. Additionally, GC/VUV was utilized to analyze realistic samples: double-base smokeless powders intact and burned (Red Dot, Accurate No. 5, and Accurate No. 7). Nitroglycerine, diphenylamine, ethyl centralite, and di-n-butyl phthalate were identified in the chromatograms of the realistic samples; thus, establishing the potential of GC/VUV to analyse post-blast debris for double-base smokeless powders. However, further method optimization is necessary to improve the LODs of these nitrate ester explosive compounds for application to post-blast analysis.

## 2.6 Acknowledgements

This work was partially supported via a National Institute of Justice Award 2017-R2-CX-0018. Opinions or points of view expressed here represent a consensus of the authors and do not necessarily represent the official position or policies of the U.S. Department of Justice.

## 2.7 References

1. Schug, K.A., et al., *Vacuum Ultraviolet Detector for Gas Chromatography*. Analytical Chemistry, 2014. **86**(16): p. 8329-8335.
2. Allegra, L., et al., *Detection of Cannabinoids and Cannabinoid Metabolites Using Gas Chromatography with Vacuum Ultraviolet Spectroscopy*. SEPARATION SCIENCE PLUS, 2018. **1**(1): p. 37-42.
3. Schenk, J., et al., *Analysis and Deconvolution of Dimethylnaphthalene Isomers Using Gas Chromatography Vacuum Ultraviolet Spectroscopy and Theoretical Computations*. Analytica Chimica Acta, 2016. **945**: p. 1-8.
4. Changling, Q., S. Jonathan, and S.K. A., *Analysis of Terpenes and Turpentine Using Gas Chromatography with Vacuum Ultraviolet Detection*. Journal of Separation Science, 2017. **40**(4): p. 869-877.
5. Weston, C., et al., *Investigation of Gas Phase Absorption Spectral Similarity for Stable-Isotopically Labeled Compounds in the 125–240nm Wavelength Range*. Talanta, 2018. **177**: p. 41-46.
6. Gröger, T., et al., *A Vacuum Ultraviolet Absorption Array Spectrometer as a Selective Detector for Comprehensive Two-Dimensional Gas Chromatography: Concept and First Results*. Analytical Chemistry, 2016. **88**(6): p. 3031-3039.
7. Bai, L., et al., *Comparison of Gc-Vuv, Gc-Fid, and Comprehensive Two-Dimensional Gc–Ms for the Characterization of Weathered and Unweathered Diesel Fuels*. Fuel, 2018. **214**: p. 521-527.
8. Bai, L., et al., *Pseudo-Absolute Quantitative Analysis Using Gas Chromatography – Vacuum Ultraviolet Spectroscopy – a Tutorial*. Analytica Chimica Acta, 2017. **953**: p. 10-22.
9. Santos, I.C., et al., *Analysis of Bacterial Fames Using Gas Chromatography – Vacuum Ultraviolet Spectroscopy for the Identification and Discrimination of Bacteria*. Talanta, 2018. **182**: p. 536-543.

10. Walsh, P., M. Garbalena, and K.A. Schug, *Rapid Analysis and Time Interval Deconvolution for Comprehensive Fuel Compound Group Classification and Speciation Using Gas Chromatography–Vacuum Ultraviolet Spectroscopy*. Analytical Chemistry, 2016. **88**(22): p. 11130-11138.
11. Skultety, L., et al., *Resolution of Isomeric New Designer Stimulants Using Gas Chromatography – Vacuum Ultraviolet Spectroscopy and Theoretical Computations*. Analytica Chimica Acta, 2017. **971**: p. 55-67.
12. Weber, B.M., P. Walsh, and J.J. Harynuk, *Determination of Hydrocarbon Group-Type of Diesel Fuels by Gas Chromatography with Vacuum Ultraviolet Detection*. Analytical Chemistry, 2016. **88**(11): p. 5809-5817.
13. Anthony, I.G.M., et al., *Vacuum Ultraviolet Spectroscopy and Mass Spectrometry: A Tandem Detection Approach for Improved Identification of Gas Chromatography-Eluting Compounds*. Analytical Chemistry, 2018. **90**(7): p. 4878-4885.
14. Beveridge, A., *Forensic Investigation of Explosions*. 2 ed. 2011: Taylor & Francis. 696.
15. Zhao, X. and J. Yinon, *Identification of Nitrate Ester Explosives by Liquid Chromatography–Electrospray Ionization and Atmospheric Pressure Chemical Ionization Mass Spectrometry*. Journal of Chromatography A, 2002. **977**(1): p. 59-68.
16. Beveridge, A., *Forensic Investigation of Explosions*. 2 ed. 2011: Taylor & Francis. 636, 696.
17. TWGFEX, *Recommended Guidelines for Forensic Identification of Post-Blast Explosive Residues*. 2007.
18. Takáts, Z., J.M. Wiseman, and R.G. Cooks, *Ambient Mass Spectrometry Using Desorption Electrospray Ionization (Desi): Instrumentation, Mechanisms and Applications in Forensics, Chemistry, and Biology*. Journal of Mass Spectrometry, 2005. **40**(10): p. 1261-1275.
19. Garcia-Reyes, J.F., et al., *Detection of Explosives and Related Compounds by Low-Temperature Plasma Ambient Ionization Mass Spectrometry*. Analytical Chemistry, 2011. **83**(3): p. 1084-1092.
20. Rowell, F., et al., *Detection of Nitro-Organic and Peroxide Explosives in Latent Fingermarks by Dart- and Saldi-Tof-Mass Spectrometry*. Forensic Science International, 2012. **221**(1): p. 84-91.
21. Jan, A., et al., *Analysis of Explosives by Gc-Uv*. Journal of Forensic Sciences, 2017. **62**(4): p. 1022-1027.
22. Rood, D., *Gas Chromatography Problem Solving and Troubleshooting*. Journal of Chromatographic Science, 1998. **36**(9): p. 476-477.

23. ThermoFisherScientific, *Omnic Picta User Guide*. 2009.
24. Lide, D.R., *Crc Handbook of Chemistry and Physics*. 2007, Boca Raton, FL: CRC Press, Taylor & Francis. 3-232.
25. Leppert, J., et al., *Hyper-Fast Flow-Field Thermal Gradient Gc/Ms of Explosives with Reduced Elution Temperatures*. Analytical Chemistry, 2018.
26. VUVAnalytics, *Vuv Spectral Database*. 2018: Austin, TX.
27. Fan, H., et al., *Gas Chromatography-Vacuum Ultraviolet Spectroscopy for Multiclass Pesticide Identification*. J Chromatogr A, 2015. **1389**: p. 120-7.
28. Schenk, J., et al., *Identification and Deconvolution of Carbohydrates with Gas Chromatography-Vacuum Ultraviolet Spectroscopy*. Journal of Chromatography A, 2017. **1513**: p. 210-221.
29. Draper, N.R., *Applied Regression Analysis*, H. Smith, Editor. 1998, Wiley: New York :. p. 15 - 45.

# CHAPTER 3. IDENTIFYING THERMAL DECOMPOSITION PRODUCTS OF NITRATE ESTER EXPLOSIVES USING GAS CHROMATOGRAPHY/VACUUM ULTRAVIOLET SPECTROSCOPY: AN EXPERIMENTAL AND COMPUTATIONAL STUDY

Courtney A. Cruse, Jingzhi Pu, John V. Goodpaster\*

Department of Chemistry and Chemical Biology, Indiana University - Purdue University Indianapolis (IUPUI), 402 North Blackford Street LD326, Indianapolis, Indiana 46202, United States

## 3.1 Abstract

Analysis of nitrate ester explosives (e.g., nitroglycerine) by gas chromatography/vacuum ultraviolet spectroscopy (GC/VUV) results in their thermal decomposition into nitric oxide, water, carbon monoxide, oxygen, and formaldehyde. These decomposition products exhibit highly structured spectra in the VUV that is not seen in larger molecules. Computational analysis using time dependent-density functional theory (TDDFT) was utilized to investigate the excited states and vibronic transitions of these decomposition products. The experimental and computational results are compared with those in previous literature using synchrotron spectroscopy, electron energy loss spectroscopy (EELS), photoabsorption spectroscopy and other computational excited state methods. It was determined that a benchtop GC/VUV detector gives comparable results to those previously reported and TDDFT could predict vibronic spacing and model molecular orbital diagrams.

## 3.2 Introduction

Benchtop vacuum ultraviolet (VUV) spectrometers are a recent addition to the family of detectors for gas chromatography (GC).[1] The energy range of these spectrometers is 2.88 eV to 9.92 eV (125 nm to 430 nm). GC/VUV has since been utilized to study fatty acids,[2-6] hydrocarbons,[7-13] pesticides,[14-18] flavors,[19-21] fragrances,[19] drugs,[22-25] and explosives.[23, 26] There has been little to no investigation into the performance of a benchtop GC/VUV in comparison to synchrotron facilities and no investigation in comparison to other

instrumentation that acquire data in this wavelength range.[1] This will be investigated here in an effort to further establish the benchtop GC/VUV as comparable to previously utilized techniques. Additionally, time dependent-density functional theory (TDDFT) has been used to compare calculated and experimental VUV spectra.[17, 27-29]

Previous analysis of nitrate ester explosives such as ethylene glycol dinitrate (EGDN), nitroglycerine (NG), and pentaerythritol tetranitrate (PETN) at temperatures exceeding 240 °C revealed various decomposition products such as nitric oxide, water, carbon monoxide, oxygen, and formaldehyde.[26, 30] These decomposition products were determined via the VUV spectral database.[31] The spectra of the decomposition products exhibited highly specific fine structure that has not been observed in the VUV spectra of the intact explosives; thus suggesting vibronic (transitions in the electronic and vibrational energy levels) or Rydberg transitions (high energy excitation beyond the valence shell). Some of these decomposition products have been extensively studied in the past as single species using electron energy loss spectroscopy and photoabsorption spectroscopy (synchrotron, dipole (e,e) spectrometer, vacuum ultraviolet spectrometer); thus, allowing for comparison of the same energy range of the benchtop VUV detector to previous research. The VUV spectra of oxygen, carbon monoxide, and water using the benchtop GC/VUV have been previously reported.[1, 32, 33] Formaldehyde and nitric oxide are available in the VUV reference library, however experimental acquisition of these compounds have not previously been published in an academic journal with wavelength acquisition down to 125 nm.[31] To the best of our knowledge, the VUV spectra of formaldehyde and nitric oxide have not been previously reported, nor has the use of TDDFT to predict spacing between vibronic transitions in the VUV[1, 32, 33].

Understanding and interpreting transitions occurring in the VUV region can be challenging as Rydberg transitions can be atomic-like or broad and featureless. Therefore, Rydberg transitions are similar to valence transitions (excitation of an electron within the valence shell), leading to difficulties distinguishing between the types of transitions.[34] Computational studies have been conducted to understand these transitions observed in this energy region. These studies, in addition to the experimental studies previously mentioned, are utilized in this work to understand and compare results obtained on the benchtop instrument. Additionally, in this work, computational analysis using TDDFT was utilized to understand and validate the observed experimental results and to predict vibronic spacing of the fine structure seen in these decomposition products. Finally,

the combination of past experimental and theoretical work, along with experimental acquisition via the benchtop GC/VUV and B3LYP computational analysis is utilized to investigate transitions observed and verify results with other established methods.

### **3.3 Materials and Methods**

#### **3.3.1 Chemicals**

Carbon monoxide Gasco Precision Gas Mixture (1% CO in N<sub>2</sub>) and nitric oxide Gasco Precision Gas Mixture (1000 ppm NO in N<sub>2</sub>) were purchased from Grainger. Formaldehyde was purchased from Santa Cruz Biotechnology. The formaldehyde was diluted to 1000 ppm in methanol for analysis. Oxygen (Bernzomatic) was purchased locally, and deionized water was purified through a Milli-Q system. Nitroglycerine (NG), ethylene glycol dinitrate (EGDN), pentaerythritol tetranitrate (PETN) (each as 1000 µg/mL in methanol), and erythritol tetranitrate (ETN) (1000 µg/mL in acetonitrile) were purchased from Restek as single-component standards. Methanol (optima LC/MS) was purchased from Fisher Scientific.

#### **3.3.2 Gas Chromatography**

An Agilent 7890B series GC equipped with an Agilent 7390 autosampler and Agilent Technologies, Inc HP-5MS UI column (30 m x 0.25 mm ID x 0.25 µm) was utilized. For the analysis of water and formaldehyde, the carrier gas was hydrogen with 100 °C inlet temperature, split ratio of 50:1, 1 ml/min flow rate, and 30 °C isothermal oven program. The column was utilized to introduce the sample into the VUV detector for the analysis of oxygen, carbon monoxide, and nitric oxide. For the analysis of oxygen, the carrier gas was hydrogen with 250 °C inlet temperature, split injection of 10:1, 2.2 ml/min flow rate, and 30 °C isothermal oven program. Carbon monoxide and nitric oxide were analyzed with nitrogen as the carrier gas with an inlet temperature of 250 °C inlet, split ratio of 10:1, 2.2 ml/min flow rate, and 30 °C isothermal oven program. Carbon monoxide and nitric oxide were standards in nitrogen gas. To obtain a VUV spectrum of these compounds, nitrogen gas was utilized as the carrier gas to ensure nitrogen was in the background constantly; thus, allowing for the ability to acquire the spectra. Without this, it is not possible to deconvolute the standard from the nitrogen in the sample.

Precision gas mixtures were introduced to the GC using a syringe connected to a regulator (by stainless steel tubing) on the gas canisters. As mixtures, the nitric oxide spectrum was obtained by deconvolution of oxygen and nitric oxide using the VUVision software. Additionally, the carbon monoxide spectrum was obtained by deconvolution of oxygen and carbon monoxide.[28, 35]

### 3.3.3 Vacuum Ultraviolet Spectroscopy

A VUV Analytics VGA-101 VUV spectrometer with a deuterium lamp was used as a detector. Experiments were run with the spectral range of 2.88 eV to 9.92 eV (125 nm to 430 nm) with a 4.5 Hz scan rate. Nitrogen was utilized as the make-up gas at 0.35 psi. The transfer line and flow cell were kept at 275 °C.

### 3.3.4 Theoretical Calculations

Gaussian 09 (Revision D.01) was used for optimization and TDDFT calculations.[36] Ground state optimization, excited state energy and frequency calculations, and population analysis were performed using the B3LYP[37-39] functional with the 6-31+G(d,p)[40] basis set, which has been shown to provide accurate results for Rydberg and valence transitions in this wavelength range.<sup>27</sup> Molecular orbitals were visualized with GaussView (Version 5.0.9).[41]

To understand and validate experimental results and to predict vibronic spacing of the fine structure of these compounds, the excited state calculations were performed to obtain the energy of each excited state (E in eV). Additionally, the frequencies of the excited states were calculated ( $\tilde{\nu}_{vib}$  in  $\text{cm}^{-1}$ ).

The following equation was utilized to calculate the theoretical energy difference between the spacings observed in the fine structure ( $\Delta E$  in eV).[42]

$$\left(\frac{1240}{E}\right) - \left(1240 * \left(\frac{1}{E * 10^{-9}} - \tilde{\nu}_{vib} * 10^3\right) * 10^{-9}\right) = \Delta E$$

Also, the observed energy of the excited state transition and the observed spacings between the fine structure of the vibronic transitions were utilized to calculate the vibrational frequency of the transition to compare to the computationally calculated frequency.

### 3.4 Results and Discussion

At a VUV flow cell temperature of 300 °C, the spectra of nitrate ester explosives exhibit fine structure (Figure 3.1a). In Figure 2.1b, illustrates that the degradation is temperature dependent. For example, the spectrum of NG at 200 °C lacks the fine structure observed at 300 °C, indicating a spectrum of intact NG. As the temperature increased to 240 °C, NG began to thermally decompose, and fine structure was observed. This was found to be true of the other nitrate ester explosives and to be reproducible. Furthermore, all nitrate ester explosives (i.e., NG, EGDN, ETN, and PETN) thermally decompose in the VUV into products such as nitric oxide, water, carbon monoxide, oxygen, and formaldehyde (Figure 3.2).[26]

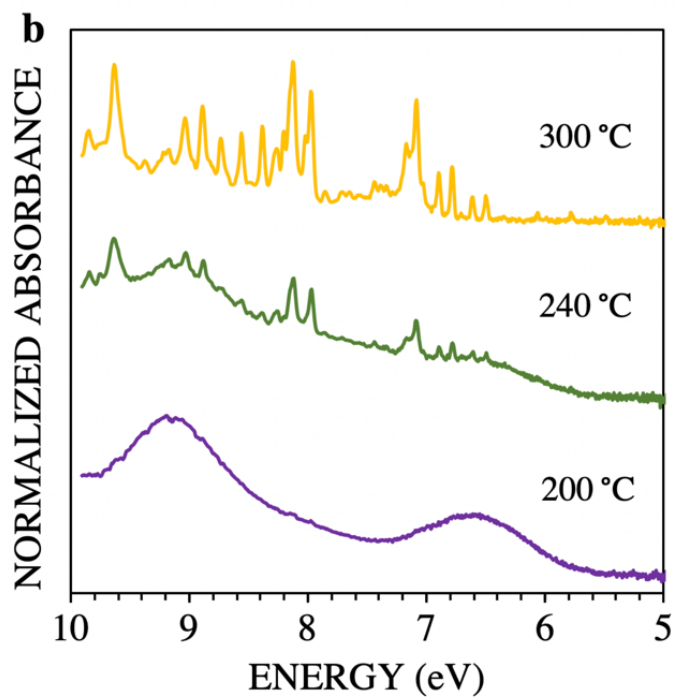
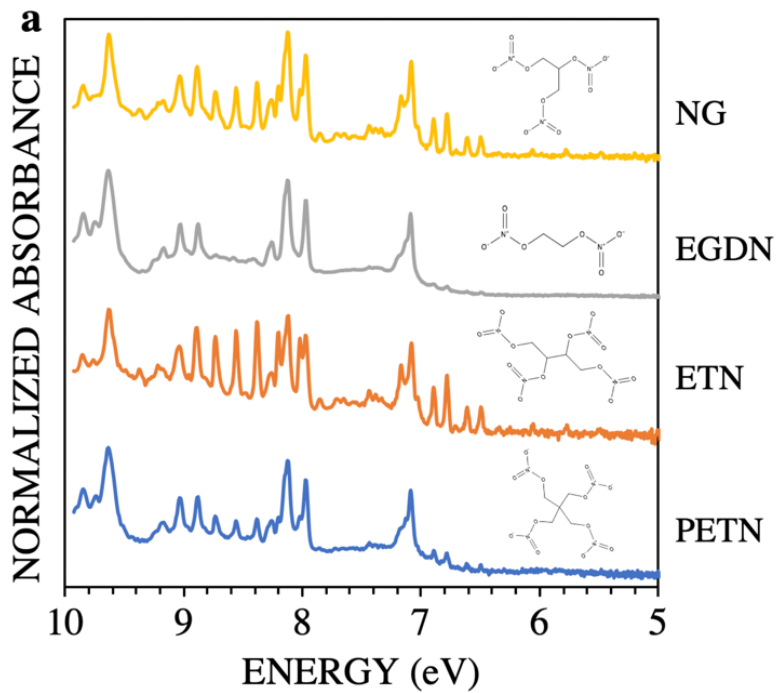


Figure 3.1. a) VUV spectra of nitrate ester explosives exhibiting fine structure at 300 °C. b) Thermal decomposition of nitroglycerine across the temperature range 200 °C (intact) to 300 °C (complete decomposition).

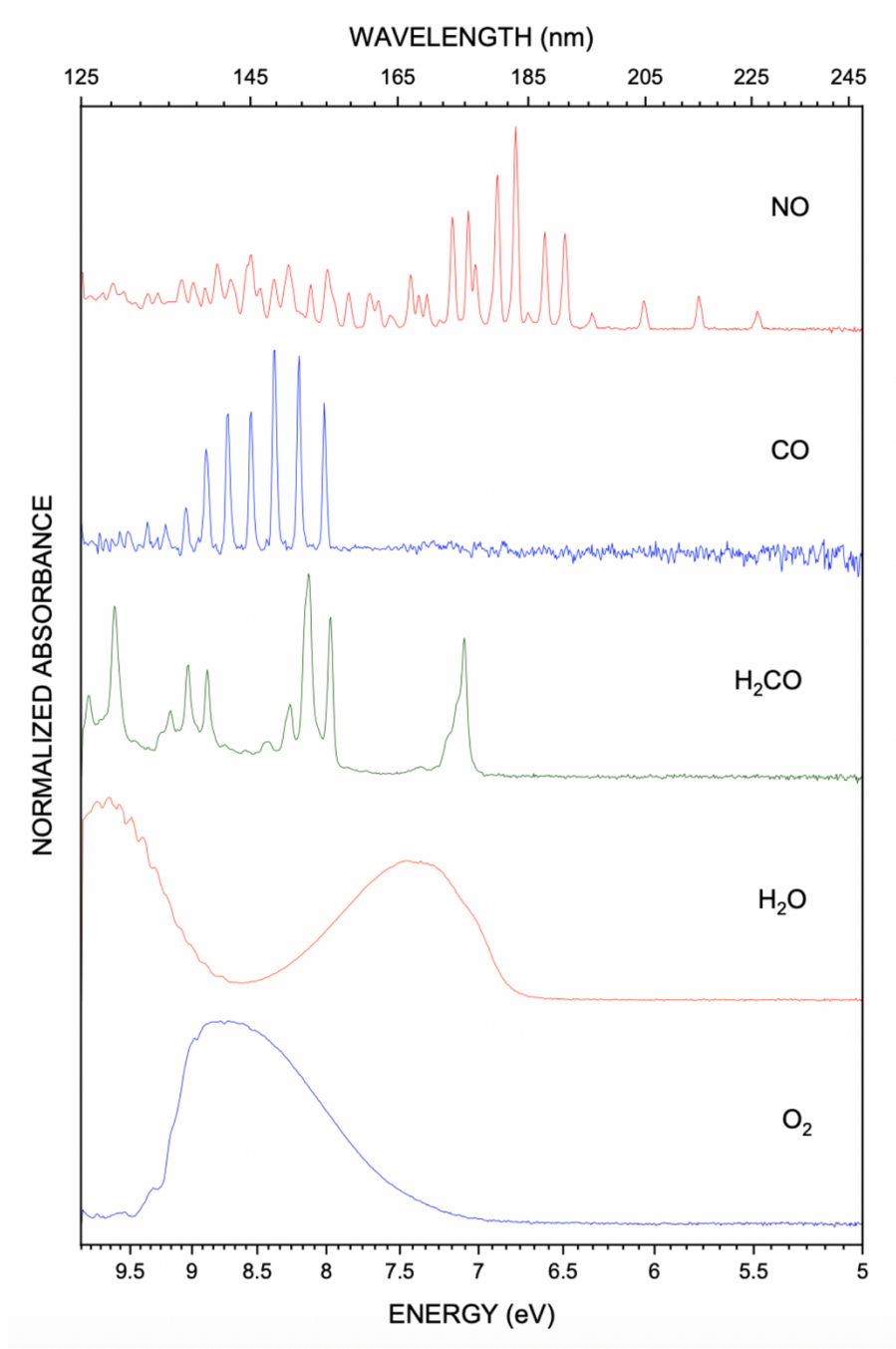


Figure 3.2. Thermal decomposition products of nitrate ester explosives.

The amount of NG that contributed to the spectrum was calculated by the Beer Lambert Law and a deconvolution algorithm that is a part of the VUV software. As reference spectra were known, the deconvolution was possible and is described previously in Ref. 26. The relationship between %NG and temperature from 200 °C to 300 °C can be characterized by a logistic function.

Below, the decomposition products of these nitrate ester explosives at higher temperatures were investigated experimentally, computationally, and in combination with previous literature.

### 3.4.1 Nitric Oxide

The VUV spectrum of nitric oxide (Figure 3.3) was obtained by deconvolution of the oxygen and nitric oxide spectra using the VUVision software.[28, 35] This was accomplished by subtracting the oxygen spectrum from the combined spectrum given the VUVision determined percent oxygen contribution. The nitric oxide spectrum is composed of the superposition of four electronic transitions with their associated vibrational levels. The first, third and fourth excited states ( $A \ ^2\Sigma^+ \leftarrow X \ ^2\Pi$ ,  $C \ ^2\Pi \leftarrow X \ ^2\Pi$ ,  $D \ ^2\Sigma^+ \leftarrow X \ ^2\Pi$ , respectively) are accessible via Rydberg transitions, while the second excited state ( $B \ ^2\Pi \leftarrow X \ ^2\Pi$ ) is reached via a valence transition (Figure 3.4).[34, 43-45] Previous literature values for these transitions are consistent with those seen in the VGA 101 VUV spectrometer. This is demonstrated in Table 3.1 for the first vibronic transition energies. Computationally, these excited states were visualized as molecular orbital diagrams in Figure 3.4.

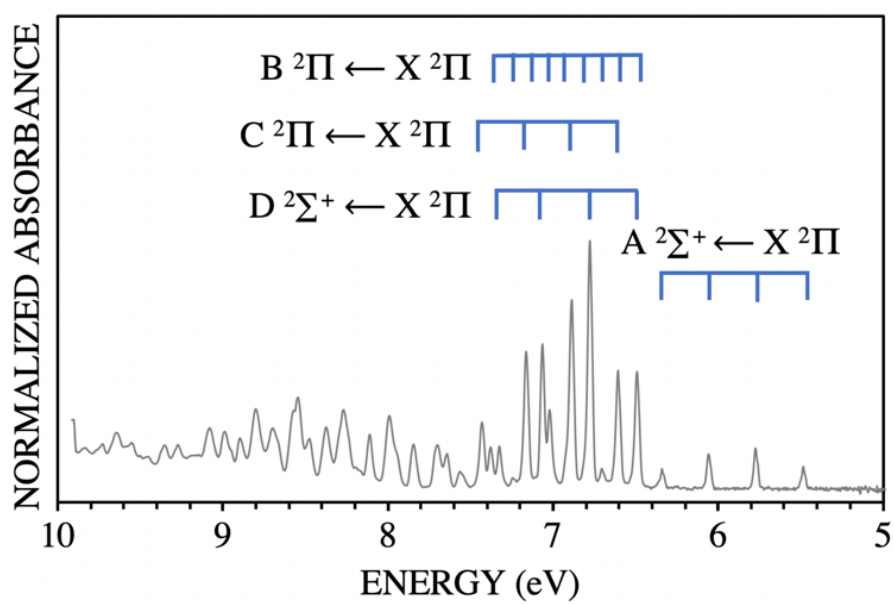


Figure 3.3. VUV spectra of nitric oxide (NO).

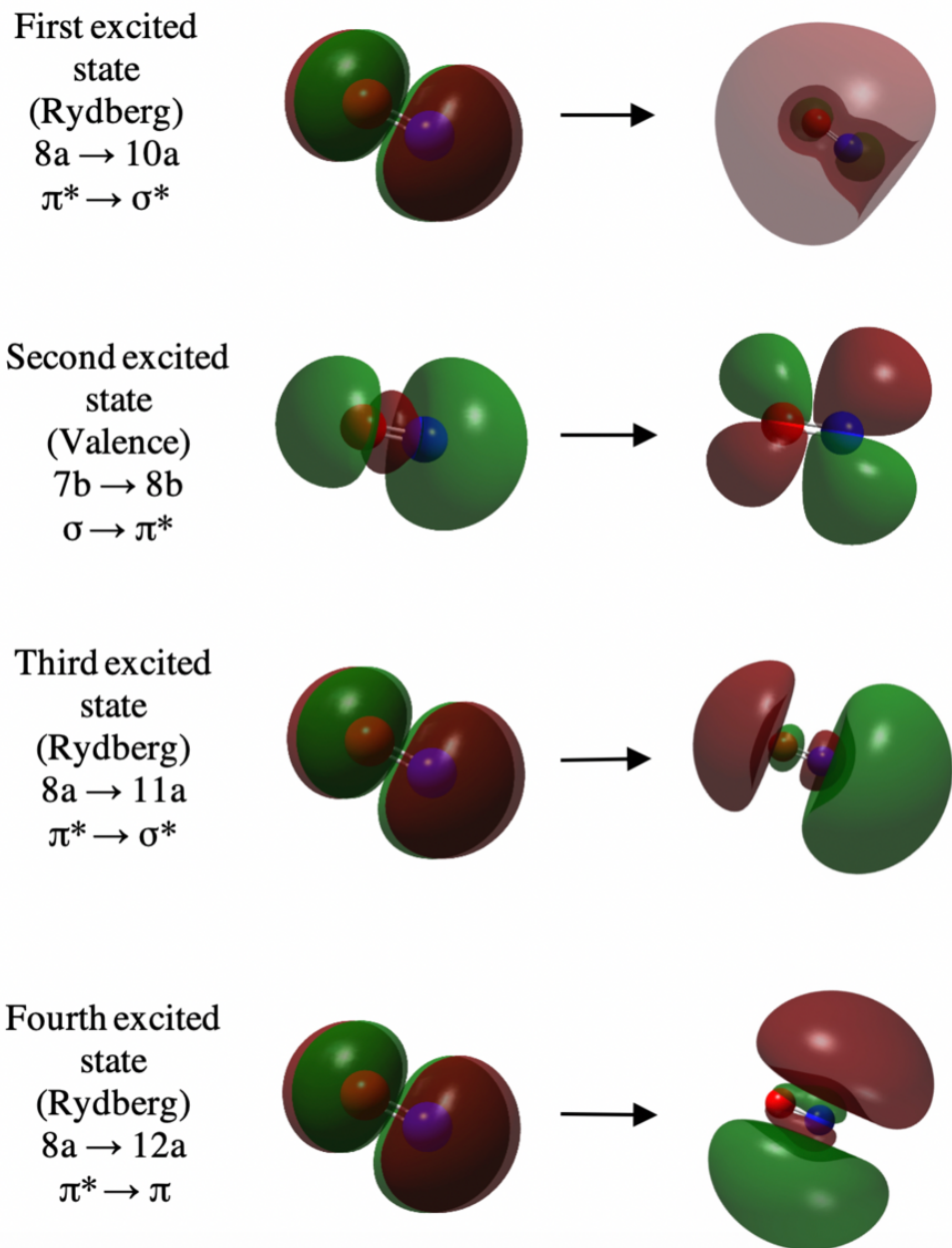


Figure 3.4. Molecular orbital diagram for visualization of the first four excited states of nitric oxide. The first, third, and fourth excited states result from Rydberg transitions and the second results from a valence transition, where 8 is the HOMO and 9 is the LUMO. The HOMO (8) and LUMO (9) transitions were not involved in the first four transitions.

Table 3.1. Comparison of VGA101 VUV vibronic transitions in nitric oxide to previously reported values. (Sync= Synchrotron, FTS= Fourier transform spectrometer, and PA= Photoabsorption).

	<b>EELS</b>	<b>SYNC-FTS</b>	<b>PA</b>	<b>CASSCF</b>	<b>THIS WORK</b>
	<b>[46]</b>	<b>[47]</b>	<b>[44]</b>	<b>[48]</b>	
<b>A <math>^2\Sigma^+ \leftarrow X^2\Pi</math></b>					
<b>(0,0)</b>	5.473		5.481	5.77	5.48
<b>(0,1)</b>	5.763		5.771		5.77
<b>(0,2)</b>	6.050		6.057		6.06
<b>(0,3)</b>	6.332	6.26	6.340		6.34
<b>(0,4)</b>	6.610		6.608		6.61
<b>(0,5)</b>	6.884		6.891		6.88
<b>(0,6)</b>	7.154		7.168		7.16
<b>B <math>^2\Pi \leftarrow X^2\Pi</math></b>					
<b>(0,0)</b>	5.642			7.57	
<b>(0,1)</b>	5.769				
<b>(0,2)</b>	5.894				
<b>(0,3)</b>	6.018				
<b>(0,4)</b>	6.139				
<b>(0,5)</b>	6.259		6.256		
<b>(0,6)</b>	6.376	6.26	6.374		
<b>(0,7)</b>	6.491	6.42	6.494		
<b>(0,8)</b>	6.605		6.608		6.61
<b>(0,9)</b>	6.715	6.67	6.718		6.70
<b>(0,10)</b>	6.824	6.78	6.782		6.78
<b>(0,11)</b>	6.930	6.89	6.939		
<b>(0,12)</b>	7.033	7.00	7.035		7.02
<b>(0,13)</b>	7.134	7.13	7.168		7.16

Table 3.1, continued

<b>(0,14)</b>	<b>7.231</b>	<b>7.17</b>	<b>7.259</b>		<b>7.25</b>
<b>(0,15)</b>	7.326		7.396		7.38
<b>(0,16)</b>	7.418				
<b>(0,17)</b>	7.506	7.51			
<b>(0,18)</b>	7.590	7.61			
<b>C <math>^2\Pi \leftarrow X ^2\Pi</math></b>					
<b>(0,0)</b>	6.499	6.42	6.494	6.74	6.49
<b>(0,1)</b>	6.790	6.70	6.782		6.78
<b>(0,2)</b>	7.078	7.00	7.063		7.06
<b>(0,3)</b>	7.361	7.38	7.342		7.32
<b>(0,4)</b>	7.641				
<b>(0,5)</b>	7.917				
<b>(0,6)</b>	8.189				
<b>D <math>^2\Sigma^+ \leftarrow X ^2\Pi</math></b>					
<b>(0,0)</b>	6.607	6.53	6.608	6.76	6.61
<b>(0,1)</b>	6.890	6.85	6.891		6.88
<b>(0,2)</b>	7.167	7.13	7.168		7.16
<b>(0,3)</b>	7.438	7.38	7.438		7.43
<b>(0,4)</b>	7.703				
<b>(0,5)</b>	7.963				

The vibronic spacings of these excited states of nitric oxide were calculated. The calculated and experimentally determined vibrational frequencies are compared in Table 3.2.

Table 3.2. Computationally predicted vibrational frequencies ( $\tilde{\nu}_{vib_{calc}}$ ) and calculated energy differences between the vibronic transitions ( $\Delta E$ ) for the first four excited state of nitric oxide compared to experimental data. \*Approximated B  $^2\Pi \leftarrow X \ ^2\Pi$  (0,0) energy using the known distances between the second excited state vibrational transitions.

EXCITED STATE	OBSERVED			CALCULATED		
	$E_{obs}$ (eV)	$\tilde{\nu}_{vib_{exp}}$ ( $cm^{-1}$ )	$\Delta E_{obs}$ (eV)	$E_{calc}$ (eV)	$\tilde{\nu}_{vib_{calc}}$ ( $cm^{-1}$ )	$\Delta E_{calc}$ (eV)
<b>1</b>	5.48	2120.2	0.29	6.07	2519.8	0.31
<b>2</b>	7.29*	573.3	0.09	6.35	1244.4	0.15
<b>3</b>	6.49	2154.3	0.29	7.29	2711.9	0.34
<b>4</b>	6.61	2023.5	0.27	7.51	3029.1	0.38

### 3.4.2 Water

The VUV spectrum of water (Figure 3.5a) consists primarily of electronic transitions from the ground state to Rydberg states. The nature of these transitions have been determined for the two broad absorption bands observed in water.[49, 50] The maximum at 7.43 eV is due to excitation to the  $\tilde{A} \ ^1B_1$  Rydberg state and the maximum at 9.72 eV is due to excitation to the  $\tilde{B} \ ^1A_1$  Rydberg state with associated vibronic transitions.[51-53] These maxima are consistent with previously reported values (Table 3.3). However, in a small number of previous studies, the relative intensity of the maxima are reversed in Skerbele et al (1968),[54] Skerbele and Lassette (1964),[55] and Skerbele and Lassette (1966).[56] This could be a result in the experimental design of the EELS instrumentation, such as the kinetic energy of incidence or the scattering angle. The experimental vibrational progression spacings of the second excited state were also compared to previous studies and were consistent with what has previously been observed (Table 3.4). Previous literature attributes a shoulder at 7.1 eV to the  $\tilde{a} \ ^3B_1$  transition.[52, 53, 57] Computationally, the second excited state in the TDDFT calculation was observed at 10.02 eV and the molecular orbital diagram for this valence transition is seen in Figure 3.5b.

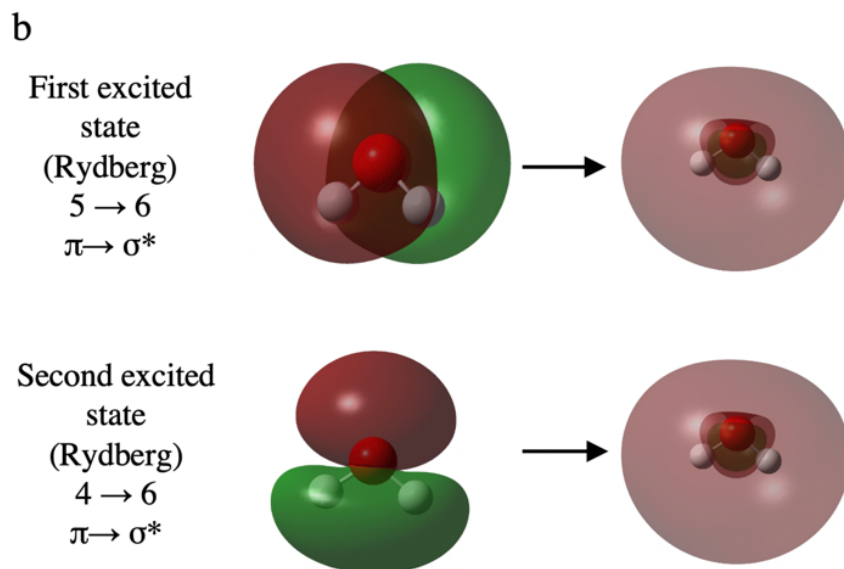
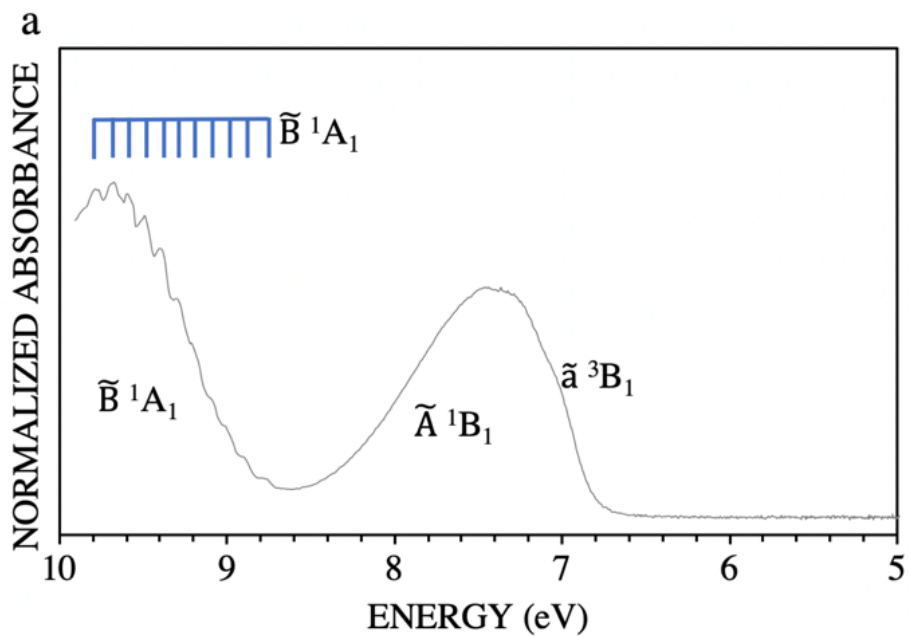


Figure 3.5. a) VUV spectra of water ( $H_2O$ ) normalized to 1 and b) molecular orbital diagram for visualization of the first and second excited states of water (Rydberg transitions), where 5 is the HOMO and 6 is the LUMO.

Table 3.3. Comparison of the VGA101 VUV absorption maxima of the first and second excited state electronic transitions of water to previously reported experimental values. (PA= Photoabsorption).

	EELS	EELS	EELS	EELS	EELS	PA	PA	TDDFT	THIS
	[49]	[58]	[55]	[56]	[59]	[52]	[51]		WORK
$\tilde{A}^1B_1 \leftarrow \tilde{X}^1A_1$	7.4	7.4	7.44	7.42	7.42	7.42	7.45	7.89	7.43
$\tilde{B}^1A_1 \leftarrow \tilde{X}^1A_1$	9.7	9.7	9.7	9.67	9.67	9.69	9.67	10.02	9.72

Table 3.4. Comparison of VGA101 VUV vibrational transitions in the second excited state of water to previously reported experimental values. \*Shoulder approximation. (PA= Photoabsorption).

$\tilde{\nu}$	PA	PA	PA	THIS
	[50]	[52]	[51]	WORK
			8.60	
		8.66	8.66	8.66
	8.79	8.79	8.78	8.79
	8.90	8.90	8.88	8.91*
	9.0	9.01	8.98	9.01*
	9.09	9.10	9.08	9.09*
	9.20	9.20	9.20	9.22*
	9.29	9.30	9.29	9.31
	9.39	9.39		9.40
	9.48	9.49		9.49
	9.57	9.58		9.60
	9.68	9.68		9.67
	9.77	9.77		9.79
	9.87	9.86		

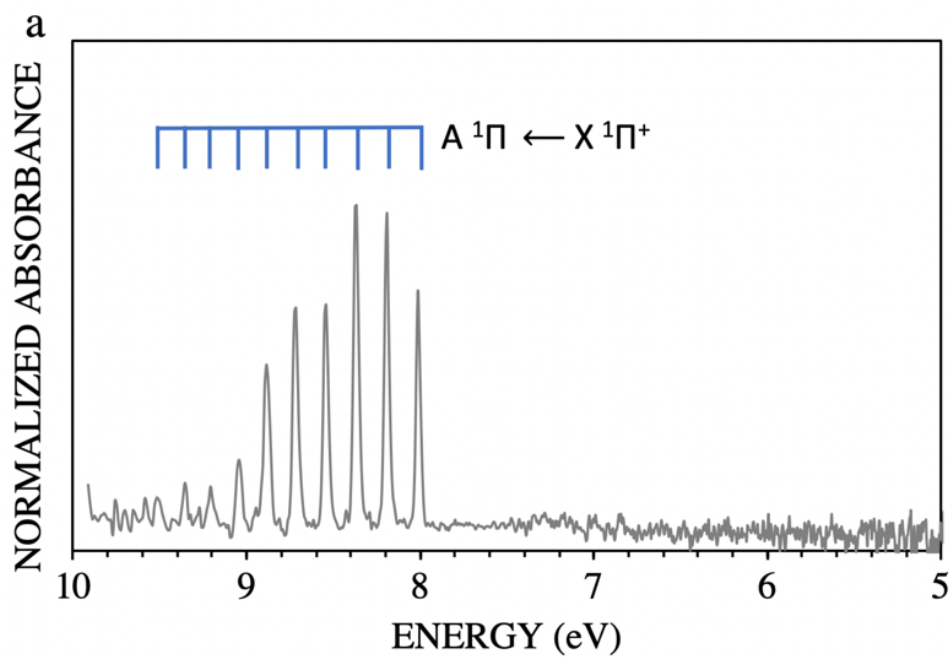
The vibronic spacings of the second excited state were calculated and compared to the experimentally calculated vibrational frequencies are compared in Table 3.5. As a computational method, the TDDFT prediction of the energy of the second excited state transition and frequency of this transition agrees with the experimentally observed; thus, further confirming the presence of vibronic transitions in the VGA 101 VUV spectrum of water.

Table 3.5. Computationally predicted vibrational frequency ( $\tilde{\nu}_{vib_{calc}}$ ) and calculated energy difference between the vibronic transitions ( $\Delta E$ ) for the second excited state of water compared to experimental data.

EXCITED STATE	OBSERVED			CALCULATED		
	$E_{obs}$ (eV)	$\tilde{\nu}_{vib_{exp}}$ ( $cm^{-1}$ )	$\Delta E_{obs}$ (eV)	$E_{calc}$ (eV)	$\tilde{\nu}_{vib_{calc}}$ ( $cm^{-1}$ )	$\Delta E_{calc}$ (eV)
2	8.79	967.74	0.12	10.02	765.62	0.09

### 3.4.3 Carbon Monoxide

The carbon monoxide spectrum (Figure 3.6a) was obtained by deconvolution of oxygen and carbon monoxide.[28, 35] It is composed of the vibronic transition of the first excited state  $A \ ^1\Pi \leftarrow X \ ^1\Pi^+$ .<sup>[55, 60-66]</sup> The experimental energies of the vibronic spacing were compared to previous literature (Table 3.6). The experimental values observed here are consistent with previously reported values.



b

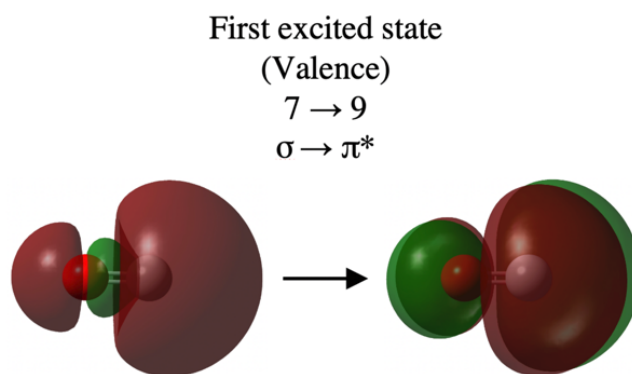


Figure 3.6. a) VUV spectra of carbon monoxide (CO) normalized to 1 and b) molecular orbital diagram for visualization of the first excited state resulting in a valence transition of carbon monoxide, where 7 is the HOMO and 8 is the LUMO.

Table 3.6. Comparison of VGA101 VUV vibronic transitions of the first excited state in carbon monoxide to previously reported values. (PA= Photoabsorption).

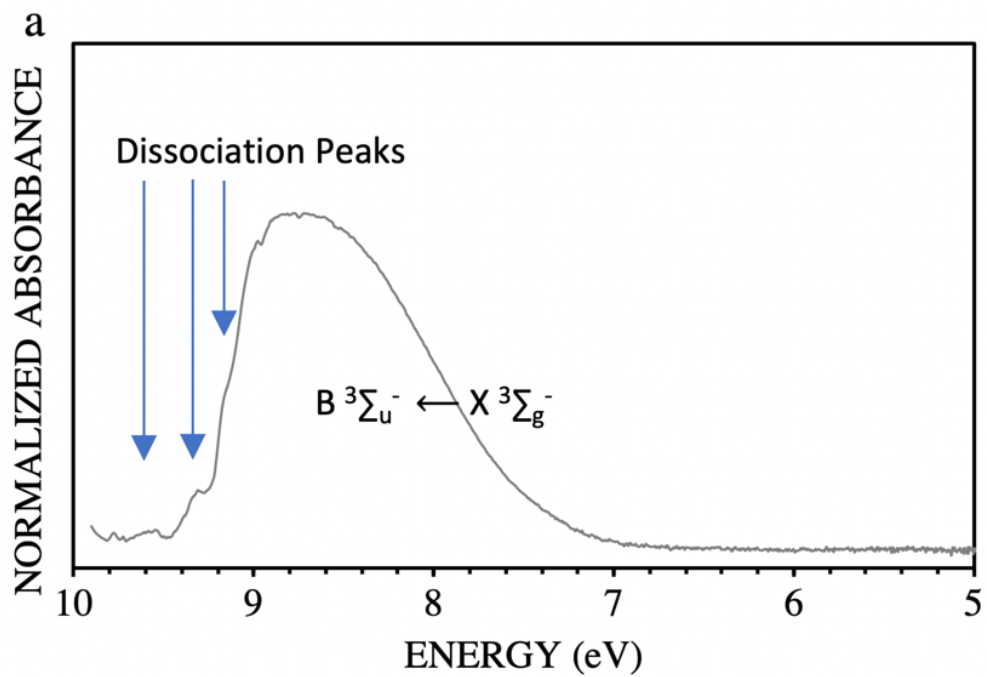
$A^1\Pi \leftarrow X^1\Pi^+$	EELS[43]	EELS[67]	PA [62]	PA [66]	CIS[63]	THIS WORK
(0,0)	8.028	8.03	8.029	8.027	8.076	8.02
(0,1)	8.212	8.21	8.212	8.209	8.246	8.19
(0,2)	8.390	8.39	8.391	8.387	8.413	8.37
(0,3)	8.566	8.57	8.566	8.560	8.576	8.55
(0,4)	8.737	8.74	8.737	8.730	8.736	8.72
(0,5)	8.903	8.90	8.903	8.896	8.893	8.89
(0,6)	9.064	9.06	9.065	9.058	9.047	9.05
(0,7)	9.223	9.22	9.224	9.214	9.20	9.21
(0,8)	9.375	9.38	9.378	9.367		9.36
(0,9)	9.525		9.527	9.516		9.52
(0,10)	9.671		9.671	9.660		
(0,11)	9.812		9.812	9.801		

Computationally, the first excited state was calculated at 8.36 eV (Figure 3.6b) . However, using this computational method, the first and second energy levels are degenerate. Therefore, an excited state vibrational frequency analysis was not possible as the optimization of the first excited state was not achieved.

### 3.4.4 Oxygen

Oxygen has been reported to contain the  $B^3\Sigma_u^- \leftarrow X^3\Sigma_g^-$  electronic transition in the Schumann-Runge Continuum (135-175 nm).[43, 68-76] The absorption maxima observed in the VGA-101 instrument at 8.75 eV (Figure 3.7a). In addition to this electronic transition, the absorption spectrum of oxygen in the VUV region contains dissociative state. Mainly the continuum is composed of the  $B^3\Sigma_u^-$  valence state crossed with absorption maxima at 9.19 eV, 9.35 eV, and 9.58 eV.[43, 68, 70, 77-79] This has been attributed to the photodissociation of  $O_2$

into a combination of  $O(^1D)$ ,  $O(^3P)$ , and  $O(^1S)$ . [43, 70, 71, 79-82] Tanaka (1952) assigned the maximum at 9.61 eV to the dissociation of  $O_2$  into  $O(^3P) + O(^1S)$  and the other two maxima to either  $O(^1D) + O(^1D)$  or  $O(^3P) + O(^1S)$ . [80] Lee et al (1977) suggest the features at 9.22 eV and 6.53 eV are due to dissociation into  $O(^3P) + O(^3P)$  and that 9.22 eV occurs from the  $^3\Pi_u$  valence state. [83] Comparison of experimental data to the absorption of oxygen in the VGA-101 instrument are given in Table 3.7.



b

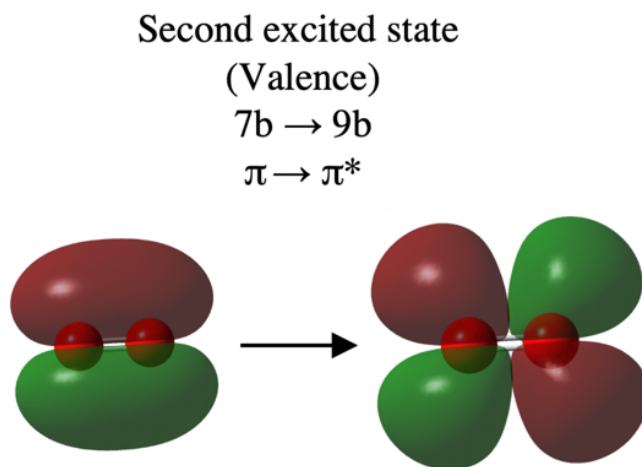


Figure 3.7. a) VUV spectra of Oxygen ( $O_2$ ) normalized to 1 and b) Molecular orbital diagram for visualization of the second excited state (valence transition) of oxygen, where 9 is the HOMO and 10 is the LUMO.

Table 3.7. Comparison of the continuum maxima and dissociation peaks of the VGA101 VUV transitions in oxygen to previously reported experimental values. \*Shoulder approximation (Sync= Synchrotron and PA= Photoabsorption).

	SYNC [68]	PA [70]	PA [80]	PA [79]	PA [84]	PA [85]	EELS [74]	EELS [76]	THIS WORK
<b>CONTINUUM MAXIMUM</b>				8.73	8.57	8.57		8.57	8.72
<b>O(<sup>3</sup>P)+O(<sup>1</sup>S)[80]</b>									
<b>or</b>	9.20	9.16	9.19	9.17			9.15		9.15*
<b>O(<sup>3</sup>P)+O(<sup>3</sup>P)[83]</b>									
<b>O(<sup>1</sup>D)+O(<sup>1</sup>D)[80]</b>									
<b>or</b>	9.29	9.29	9.29	9.31			9.27		9.32
<b>O(<sup>3</sup>P)+O(<sup>1</sup>S)[80]</b>									
<b>O(<sup>1</sup>D)+O(<sup>1</sup>D)[80]</b>									
<b>or</b>	9.60	9.58	9.61	9.59			9.58		9.59
<b>O(<sup>3</sup>P)+O(<sup>1</sup>S)[80]</b>									

Computationally, the second excited state in the TDDFT calculation was observed at 5.96 eV and the molecular orbital diagram for this valence transition is seen in Figure 3.7b.

### 3.4.5 Formaldehyde

The formaldehyde VUV spectrum (Figure 3.8) is composed of vibronic Rydberg transitions where the Rydberg transitions are intense and the vibrational progression are weak.[86, 87] The Rydberg transitions resulting from the ground state (<sup>1</sup>A<sub>1</sub>) have been previously observed using a VGA 101 VUV spectrometer.[86, 88-90] However, the vibrational transitions were not distinguishable. The identification of the transitions was based on previous literature and the comparison between these values are in Table 3.8. The energies of the transitions in the GC/VUV spectra are consistent with the literature values. The computationally determined excitation energies and symmetry of the molecular orbitals are consistent with other computational studies on formaldehyde (Figure 3.9), but these energy values differ from those observed experimentally (Table 3.9).

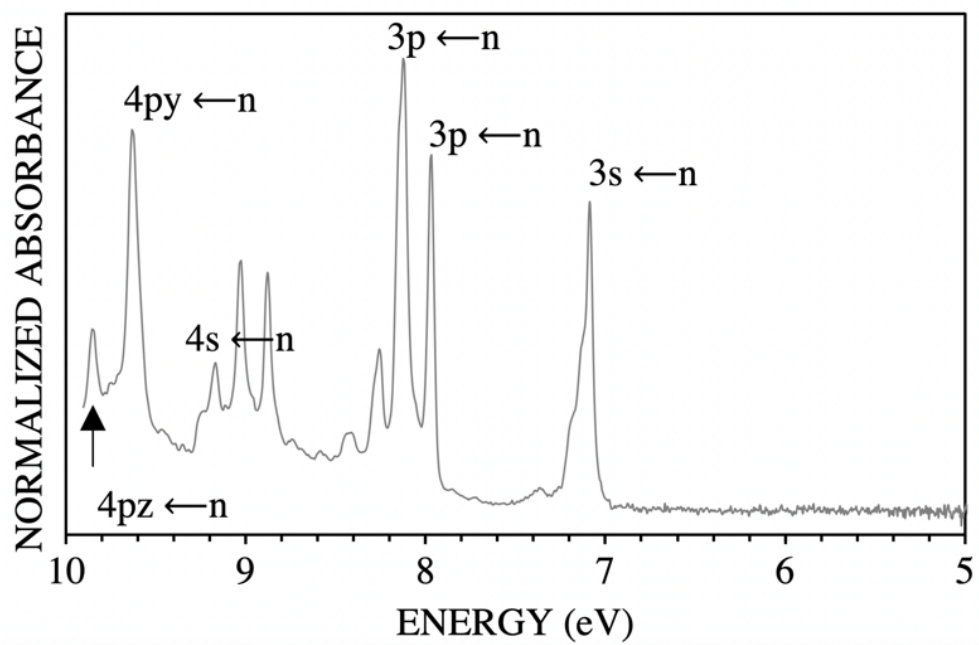


Figure 3.8. VUV spectra of formaldehyde (H<sub>2</sub>CO) normalized to 1.

Table 3.8. Comparison of VGA101 VUV transitions in formaldehyde to previously reported experimental values. \*Shoulder approximation (Sync= Synchrotron and PA= Photoabsorption).

<b>n →</b>	<b>SYNC[87]</b>	<b>PA[91]</b>	<b>PA[92]</b>	<b>PA[93]</b>	<b>EELS[89]</b>	<b>THIS WORK</b>
<b>3s (3s<sub>a1</sub>)</b>	7.086	7.09	7.09	7.09	7.10	7.08
	7.124	7.13				
	7.178	7.18				
<b>4s</b>	9.176	9.25	9.26	9.26		9.17
<b>3py (3p<sub>b2</sub>)</b>	8.122	7.97	7.98	7.97	7.98	
<b>3pz (3p<sub>b1</sub>)</b>	7.969		8.13	8.13	8.14	
<b>4py</b>	9.629	9.58	9.59	9.58		9.64
<b>4pz (4p)</b>	9.592	9.63	9.63	9.63	9.65	9.70*
<b>3d</b>	8.884	8.88	8.88	8.88	8.88	8.88
<b>4d</b>	9.846	9.84	9.85	9.84		9.88

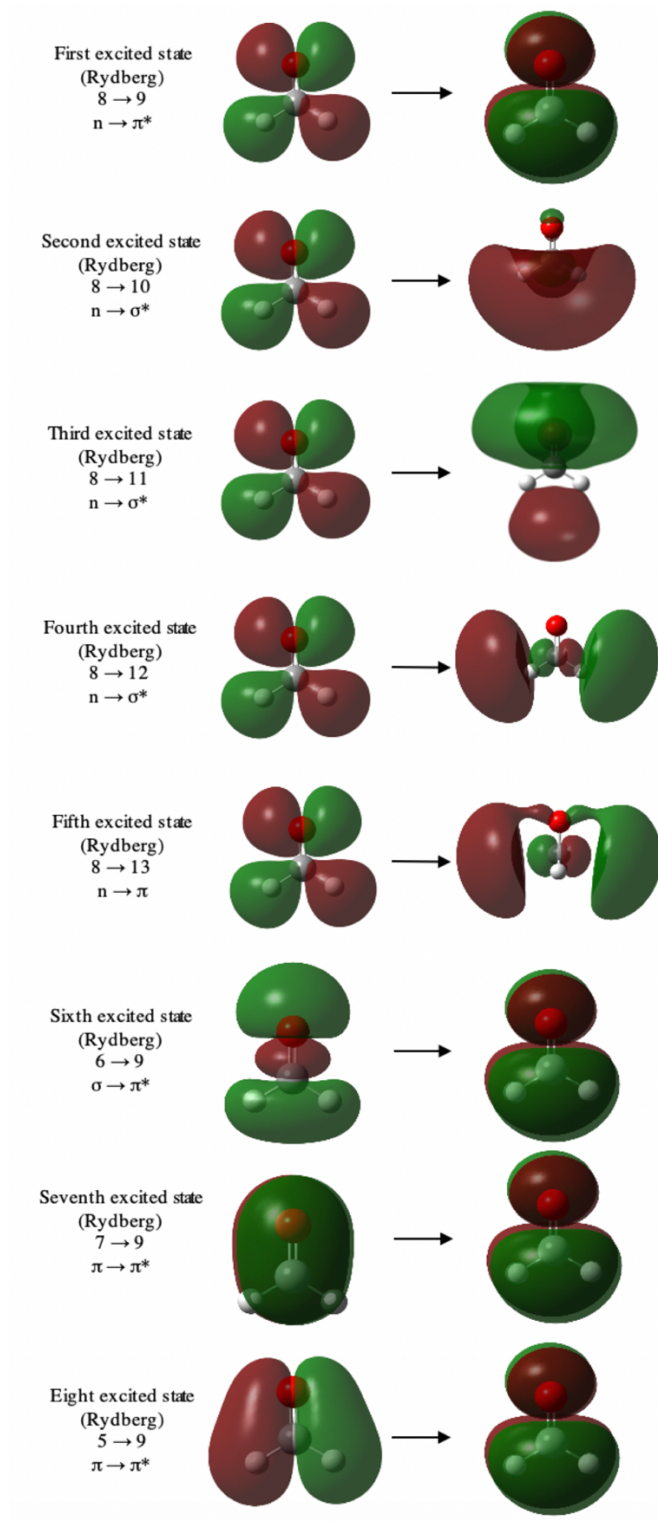


Figure 3.9. Molecular orbital diagram for visualization of the excited states in formaldehyde, where 8 is the HOMO and 9 is the LUMO.

Table 3.9. Comparison of B3LYP computational transitions in formaldehyde to previously reported computational values.

TRANSITION	CIS [94]	CIS [95]	CIS [96]	CIS [87]	SCF+ CIS [88]	SCF [91]	MRCC [97]	EOM [98]	B3LYP [94]	B3LYP [87]	THIS WORK B3LYP
${}^1A_2 n \rightarrow \pi^*$	3.94	3.80		4.36					4.58	3.40	3.95
${}^1B_2 n \rightarrow 3s$	6.47	7.48	7.52	8.84	7.38			7.28	8.59	6.59	6.88
${}^1B_2 n \rightarrow 3p_z$	7.27		8.69	9.69	8.14			8.12	9.38	7.63	7.63
${}^1A_1 n \rightarrow 3p_y$	7.27		8.90	9.93	7.97			8.15	9.51	7.49	7.87
${}^1A_2 n \rightarrow 3p_x$	7.57			10.5				8.35	9.76	8.40	8.37
${}^1B_1 5a_1(\sigma) \rightarrow \pi^*$	8.98	9.35		9.18		8.43	8.40	9.19	9.80	7.92	9.01
${}^1A_1 \pi \rightarrow \pi^*$	9.34		9.65	9.15		9.8	9.91	9.40	9.76	8.27	9.49
${}^1B_1 \pi \rightarrow 3s$	9.96		9.66	10.8						9.31	10.1

### 3.5 Conclusions

GC/VUV has been utilized to study the thermal decomposition products of nitrate ester explosives: NO, CO, H<sub>2</sub>O, O<sub>2</sub>, H<sub>2</sub>CO. TDDFT using B3LYP was successfully used to understand and validate experimental results by investigating their excited state energies and molecular orbital diagrams. Computational analysis was also utilized to predict vibronic spacing of the fine structure of NO and H<sub>2</sub>O. By comparison to existing instrumentation that investigates the energy range observed in the VGA 101, it was determined that transitions in the VUV region using the VGA 101 benchtop spectrometer were consistent with the transitions seen in non-benchtop instruments (EELS, photoabsorption, and synchrotron).

### 3.6 Acknowledgements

This work was supported via a h 2017-R2-CX- 0018 and 2018-R2-CX-0015. Opinions or points of view expressed here represent a consensus of the authors and do not necessarily represent the official position or policies of the U.S. Department of Justice.

The computational analysis via Big Red II was supported in part by the Lilly Endowment, Inc., through its support for the Indiana University Pervasive Technology Institute, and in part by

the Indiana METACyt Initiative. The Indiana METACyt Initiative at IU was also supported in part by Lilly Endowment, Inc.

### 3.7 References

1. Schug, K.A., et al., *Vacuum Ultraviolet Detector for Gas Chromatography*. Anal Chem, 2014. **86**(16): p. 8329-35.
2. Santos, I.C., et al., *Large-Volume Injection Gas Chromatography-Vacuum Ultraviolet Spectroscopy for the Qualitative and Quantitative Analysis of Fatty Acids in Blood Plasma*. Anal Chim Acta, 2019. **1053**: p. 169-177.
3. Zoccali, M., et al., *Flow-Modulated Comprehensive Two-Dimensional Gas Chromatography Combined with a Vacuum Ultraviolet Detector for the Analysis of Complex Mixtures*. J Chromatogr A, 2017. **1497**: p. 135-143.
4. Fan, H., et al., *Gas Chromatography-Vacuum Ultraviolet Spectroscopy for Analysis of Fatty Acid Methyl Esters*. Food Chem, 2016. **194**: p. 265-71.
5. Weatherly, C.A., et al., *Analysis of Long-Chain Unsaturated Fatty Acids by Ionic Liquid Gas Chromatography*. J Agric Food Chem, 2016. **64**(6): p. 1422-32.
6. Santos, I.C., et al., *Analysis of Bacterial Fames Using Gas Chromatography - Vacuum Ultraviolet Spectroscopy for the Identification and Discrimination of Bacteria*. Talanta, 2018. **182**: p. 536-543.
7. Liu, H., et al., *Hyphenation of Short Monolithic Silica Capillary Column with Vacuum Ultraviolet Spectroscopy Detector for Light Hydrocarbons Separation*. J Chromatogr A, 2019. **1595**: p. 174-179.
8. Garcia-Cicourel, A.R. and H.G. Janssen, *Direct Analysis of Aromatic Hydrocarbons in Purified Mineral Oils for Foods and Cosmetics Applications Using Gas Chromatography with Vacuum Ultraviolet Detection*. J Chromatogr A, 2019. **1590**: p. 113-120.
9. Dunkle, M.N., et al., *Quantification of the Composition of Liquid Hydrocarbon Streams: Comparing the Gc-Vuv to Dha and Gcxcg*. J Chromatogr A, 2019. **1587**: p. 239-246.
10. Bai, L., et al., *Comparison of Gc-Vuv, Gc-Fid, and Comprehensive Two-Dimensional Gc-Ms for the Characterization of Weathered and Unweathered Diesel Fuels*. Fuel, 2018. **214**: p. 521-527.
11. Isaacman, G., et al., *Improved Resolution of Hydrocarbon Structures and Constitutional Isomers in Complex Mixtures Using Gas Chromatography-Vacuum Ultraviolet-Mass Spectrometry*. Anal Chem, 2012. **84**(5): p. 2335-42.

12. Walsh, P., M. Garbalena, and K.A. Schug, *Rapid Analysis and Time Interval Deconvolution for Comprehensive Fuel Compound Group Classification and Speciation Using Gas Chromatography-Vacuum Ultraviolet Spectroscopy*. Anal Chem, 2016. **88**(22): p. 11130-11138.
13. Weber, B.M., P. Walsh, and J.J. Harynyuk, *Determination of Hydrocarbon Group-Type of Diesel Fuels by Gas Chromatography with Vacuum Ultraviolet Detection*. Anal Chem, 2016. **88**(11): p. 5809-17.
14. Fan, H., et al., *Gas Chromatography-Vacuum Ultraviolet Spectroscopy for Multiclass Pesticide Identification*. J Chromatogr A, 2015. **1389**: p. 120-7.
15. Leghissa, A., Z.L. Hildenbrand, and K.A. Schug, *A Review of Methods for the Chemical Characterization of Cannabis Natural Products*. J Sep Sci, 2018. **41**(1): p. 398-415.
16. Zheng, J., C. Huang, and S. Wang, *Challenging Pharmaceutical Analyses by Gas Chromatography with Vacuum Ultraviolet Detection*. J Chromatogr A, 2018. **1567**: p. 185-190.
17. Skultety, L., et al., *Resolution of Isomeric New Designer Stimulants Using Gas Chromatography - Vacuum Ultraviolet Spectroscopy and Theoretical Computations*. Anal Chim Acta, 2017. **971**: p. 55-67.
18. Leghissa, A., et al., *Detection of Cannabinoids and Cannabinoid Metabolites Using Gas Chromatography with Vacuum Ultraviolet Spectroscopy*. Separation Science Plus, 2018. **1**(1): p. 37-42.
19. Hodgson, A. and J. Cochran, *Vacuum Ultraviolet Spectroscopy as a New Tool for Gc Analysis of Terpenes in Flavors and Fragrances*. J AOAC Int, 2019. **102**(2): p. 655-658.
20. Santos, I.C., J. Smuts, and K.A. Schug, *Rapid Profiling and Authentication of Vanilla Extracts Using Gas Chromatography-Vacuum Ultraviolet Spectroscopy*. Food Analytical Methods, 2017. **10**(12): p. 4068-4078.
21. Qiu, C., J. Smuts, and K.A. Schug, *Analysis of Terpenes and Turpentine Using Gas Chromatography with Vacuum Ultraviolet Detection*. J Sep Sci, 2017. **40**(4): p. 869-877.
22. Roberson, Z.R. and J.V. Goodpaster, *Differentiation of Structurally Similar Phenethylamines Via Gas Chromatography-Vacuum Ultraviolet Spectroscopy (Gc-Vuv)*. Forensic Chemistry, 2019. **15**: p. 100172.
23. Reiss, R., et al., *Evaluation and Application of Gas Chromatography - Vacuum Ultraviolet Spectroscopy for Drug- and Explosive Precursors and Examination of Non-Negative Matrix Factorization for Deconvolution*. Spectrochim Acta A Mol Biomol Spectrosc, 2019. **219**: p. 129-134.

24. Kranenburg, R.F., et al., *Distinguishing Drug Isomers in the Forensic Laboratory: Gc-Vuv in Addition to Gc-Ms for Orthogonal Selectivity and the Use of Library Match Scores as a New Source of Information*. Forensic Sci Int, 2019. **302**: p. 109900.
25. Buchalter, S., et al., *Gas Chromatography with Tandem Cold Electron Ionization Mass Spectrometric Detection and Vacuum Ultraviolet Detection for the Comprehensive Analysis of Fentanyl Analogues*. J Chromatogr A, 2019. **1596**: p. 183-193.
26. Cruse, C.A. and J.V. Goodpaster, *Generating Highly Specific Spectra and Identifying Thermal Decomposition Products Via Gas Chromatography / Vacuum Ultraviolet Spectroscopy (Gc/Vuv): Application to Nitrate Ester Explosives*. Talanta, 2019. **195**: p. 580-586.
27. Mao, J.X., P. Kroll, and K.A. Schug, *Vacuum Ultraviolet Absorbance of Alkanes: An Experimental and Theoretical Investigation*. Structural Chemistry, 2019. **30**(6): p. 2217-2224.
28. Schenk, J., et al., *Analysis and Deconvolution of Dimethylnaphthalene Isomers Using Gas Chromatography Vacuum Ultraviolet Spectroscopy and Theoretical Computations*. Anal Chim Acta, 2016. **945**: p. 1-8.
29. Mao, J.X., et al., *Simulation of Vacuum Ultraviolet Absorption Spectra: Paraffin, Isoparaffin, Olefin, Naphthene, and Aromatic Hydrocarbon Class Compounds*. Appl Spectrosc, 2020. **74**(1): p. 72-80.
30. Andrasko, J., et al., *Analysis of Explosives by Gc-Uv*. J Forensic Sci, 2017. **62**(4): p. 1022-1027.
31. VUVAnalytics, *Vuv Spectral Database*. 2018: Austin, TX.
32. Bai, L., et al., *Permanent Gas Analysis Using Gas Chromatography with Vacuum Ultraviolet Detection*. J Chromatogr A, 2015. **1388**: p. 244-50.
33. Schenk, J., et al., *Lab-Simulated Downhole Leaching of Formaldehyde from Proppants by High Performance Liquid Chromatography (Hplc), Headspace Gas Chromatography-Vacuum Ultraviolet (Hs-Gc-Vuv) Spectroscopy, and Headspace Gas Chromatography-Mass Spectrometry (Hs-Gc-Ms)*. Environ Sci Process Impacts, 2019. **21**(2): p. 214-223.
34. Robin, M.B., *Higher Excited States of Polyatomic Molecules*. Vol. 1. 1974, New York and London: Academic Press.
35. Schenk, J., et al., *Identification and Deconvolution of Carbohydrates with Gas Chromatography-Vacuum Ultraviolet Spectroscopy*. J Chromatogr A, 2017. **1513**: p. 210-221.

36. M. J. Frisch, G.W.T., H. B. Schlegel, G. E. Scuseria, M. A. Robb, J. R. Cheeseman, G. Scalmani, V. Barone, G. A. Petersson, H. Nakatsuji, X. Li, M. Caricato, A. Marenich, J. Bloino, B. G. Janesko, R. Gomperts, B. Mennucci, H. P. Hratchian, J. V. Ortiz, A. F. Izmaylov, J. L. Sonnenberg, D. Williams-Young, F. Ding, F. Lipparini, F. Egidi, J. Goings, B. Peng, A. Petrone, T. Henderson, D. Ranasinghe, V. G. Zakrzewski, J. Gao, N. Rega, G. Zheng, W. Liang, M. Hada, M. Ehara, K. Toyota, R. Fukuda, J. Hasegawa, M. Ishida, T. Nakajima, Y. Honda, O. Kitao, H. Nakai, T. Vreven, K. Throssell, J. A. Montgomery, Jr., J. E. Peralta, F. Ogliaro, M. Bearpark, J. J. Heyd, E. Brothers, K. N. Kudin, V. N. Staroverov, T. Keith, R. Kobayashi, J. Normand, K. Raghavachari, A. Rendell, J. C. Burant, S. S. Iyengar, J. Tomasi, M. Cossi, J. M. Millam, M. Klene, C. Adamo, R. Cammi, J. W. Ochterski, R. L. Martin, K. Morokuma, O. Farkas, J. B. Foresman, and D. J. Fox,, *Gaussian 09*. 2013, Gaussian, Inc.: Wallingford CT.
37. Becke, A.D., *Density-Functional Thermochemistry. Iii. The Role of Exact Exchange*. The Journal of Chemical Physics, 1993. **98**(7): p. 5648-5652.
38. Lee, C., W. Yang, and R.G. Parr, *Development of the Colle-Salvetti Correlation-Energy Formula into a Functional of the Electron Density*. Phys Rev B Condens Matter, 1988. **37**(2): p. 785-789.
39. Stephens, P.J., et al., *Ab-Initio Calculation of Vibrational Absorption and Circular-Dichroism Spectra Using Density-Functional Force-Fields*. Journal of Physical Chemistry, 1994. **98**(45): p. 11623-11627.
40. Francel, M.M., et al., *Self-Consistent Molecular Orbital Methods. Xxiii. A Polarization-Type Basis Set for Second-Row Elements*. The Journal of Chemical Physics, 1982. **77**(7): p. 3654-3665.
41. Dennington, R., T.A. Keith, and J.M. Millam, *Gaussview*. 2013, Semichem, Inc.: Shawnee Mission, KS.
42. McQuarrie, D.A. and J.D. Simon, *Physical Chemistry: A Molecular Approach*. 1997, Sausalito, CA: University Science Books.
43. Lassetre, E.N., et al., *High-Resolution Study of Electron-Impact Spectra at Kinetic Energies between 33 and 100 Ev and Scattering Angles to 16°*. The Journal of Chemical Physics, 1968. **48**(11): p. 5066-5096.
44. Chan, W.F., G. Cooper, and C.E. Brion, *Absolute Optical Oscillator-Strengths for the Photoabsorption of Nitric-Oxide (5-30 Ev) at High-Resolution*. Chemical Physics, 1993. **170**(1): p. 111-121.
45. Brunger, M.J., et al., *Electron-Impact Excitation of Rydberg and Valence Electronic States of Nitric Oxide: I. Differential Cross Sections*. Journal of Physics B-Atomic Molecular and Optical Physics, 2000. **33**(4): p. 783-808.

46. Campbell, L., et al., *Deconvolution of Overlapping Features in Electron Energy-Loss Spectra: Determination of Absolute Differential Cross Sections for Electron-Impact Excitation of Electronic States of Molecules*. Australian Journal of Physics, 1997. **50**(3): p. 525-537.
47. Yoshino, K., et al., *The Application of a Vacuum-Ultraviolet Fourier Transform Spectrometer and Synchrotron-Radiation Source to Measurements of Bands of No. Vii. The Final Report*. J Chem Phys, 2006. **124**(5): p. 054323.
48. Shi, H. and A.L. East, *Improved Results for the Excited States of Nitric Oxide, Including the B/C Avoided Crossing*. J Chem Phys, 2006. **125**(10): p. 104311.
49. Chan, W.F., G. Cooper, and C.E. Brion, *The Electronic-Spectrum of Water in the Discrete and Continuum Regions - Absolute Optical Oscillator-Strengths for Photoabsorption (6-200 Ev)*. Chemical Physics, 1993. **178**(1-3): p. 387-400.
50. Watanabe, K. and M. Zelikoff, *Absorption Coefficients of Water Vapor in the Vacuum Ultraviolet*. Journal of the Optical Society of America, 1953. **43**(9): p. 753-755.
51. Mota, R., et al., *Water Vuv Electronic State Spectroscopy by Synchrotron Radiation*. Chemical Physics Letters, 2005. **416**(1-3): p. 152-159.
52. Wang, H.t., W.S. Felps, and S.P. McGlynn, *Molecular Rydberg States. Vii. Water*. The Journal of Chemical Physics, 1977. **67**(6): p. 2614-2628.
53. Thorn, P.A., et al., *Cross Sections and Oscillator Strengths for Electron-Impact Excitation of the a 1b1 Electronic State of Water*. J Chem Phys, 2007. **126**(6): p. 064306.
54. Skerbele, A., M.A. Dillon, and E.N. Lassette, *Excitation by Electron Impact of Vibrational Transitions in Water and Carbon Dioxide at Kinetic Energies between 30 and 60 Ev*. The Journal of Chemical Physics, 1968. **49**(11): p. 5042-5046.
55. Skerbele, A. and E.N. Lassette, *Electron-Impact Spectra*. The Journal of Chemical Physics, 1965. **42**(1): p. 395-401.
56. Skerbele, A. and E.N. Lassette, *Intensity Variation with Scattering Angle of Electronic Transitions in H2o Excited by Electron Impact*. The Journal of Chemical Physics, 1966. **44**(11): p. 4066-4069.
57. Matsui, M., et al., *Measuring Electron-Impact Cross Sections of Water: Elastic Scattering and Electronic Excitation of the  $\tilde{A}3b1$  and  $\tilde{A}1b1$  States*. The European Physical Journal D, 2016. **70**(4).
58. Trajmar, S., W. Williams, and A. Kuppermann, *Electron Impact Excitation of H2o*. The Journal of Chemical Physics, 1973. **58**(6): p. 2521-2531.

59. Skerbele, A., V.D. Meyer, and E.N. Lassette, *Relative Intensities of Two Rydberg Transitions in the Electron-Impact Spectrum of Water*. The Journal of Chemical Physics, 1965. **43**(3): p. 817-820.
60. Chan, W.F., G. Cooper, and C.E. Brion, *Absolute Optical Oscillator Strengths for Discrete and Continuum Photoabsorption of Carbon Monoxide (7–200 Ev) and Transition Moments for the  $X\ 1\sigma^+ \rightarrow a\ 1\pi$  System*. Chemical Physics, 1993. **170**(1): p. 123-138.
61. Lassette, E.N. and A. Skerbele, *Absolute Generalized Oscillator Strengths for Four Electronic Transitions in Carbon Monoxide*. The Journal of Chemical Physics, 1971. **54**(4): p. 1597-1607.
62. Tanaka, Y., A.S. Jursa, and F. LeBlanc, *Absorption Spectrum of Co in the Vacuum Ultraviolet Region*. The Journal of Chemical Physics, 1957. **26**(4): p. 862-866.
63. Chantranupong, L., et al., *A Configuration-Interaction Study of the Oscillator-Strengths for Various Low-Lying Transitions of the Co Molecule*. Chemical Physics, 1992. **161**(3): p. 351-362.
64. Kato, H., et al., *Cross Sections for Electron Impact Excitation of the Vibrationally Resolved a  $1\pi$  Electronic State of Carbon Monoxide*. J Chem Phys, 2007. **126**(6): p. 064307.
65. Lassette, E.N. and S.M. Silverman, *Inelastic Collision Cross Sections of Carbon Monoxide*. The Journal of Chemical Physics, 1964. **40**(5): p. 1256-1261.
66. Majumder, M., et al., *Photoabsorption of Carbon Monoxide: A Time-Dependent Quantum Mechanical Study*. Journal of Physics B-Atomic Molecular and Optical Physics, 2012. **45**(18): p. 185101.
67. Meyer, V.D., A. Skerbele, and E.N. Lassette, *Intensity Distribution in the Electron-Impact Spectrum of Carbon Monoxide at High-Resolution and Small Scattering Angles*. The Journal of Chemical Physics, 1965. **43**(3): p. 805-816.
68. Nee, J.B. and P.C. Lee, *Detection of O(1d) Produced in the Photodissociation of O<sub>2</sub> in the Schumann–Runge Continuum*. The Journal of Physical Chemistry A, 1997. **101**(36): p. 6653-6657.
69. Chan, W.F., G. Cooper, and C.E. Brion, *Absolute Optical Oscillator-Strengths for the Photoabsorption of Molecular-Oxygen (5-30 Ev) at High-Resolution*. Chemical Physics, 1993. **170**(1): p. 99-109.
70. Blake, A.J., J.H. Carver, and G.N. Haddad, *Photo-Absorption Cross Sections of Molecular Oxygen between 1250 Å and 2350 Å*. Journal of Quantitative Spectroscopy and Radiative Transfer, 1966. **6**(4): p. 451-459.
71. Goldstein, R. and F.N. Mastrup, *Absorption Coefficients of the O<sub>2</sub> Schumann–Runge Continuum from 1270 Å ↔ 1745 Å Using a New Continuum Source*. Journal of the Optical Society of America, 1966. **56**(6): p. 765-769.

72. Gibson, S.T., et al., *Temperature Dependence in the Schumann-Runge Photoabsorption Continuum of Oxygen*. Journal of Quantitative Spectroscopy and Radiative Transfer, 1983. **30**(5): p. 385-393.
73. Krupenie, P.H., *The Spectrum of Molecular Oxygen*. Journal of Physical and Chemical Reference Data, 1972. **1**(2): p. 423-534.
74. Huebner, R.H., et al., *Apparent Oscillator Strengths for Molecular Oxygen Derived from Electron Energy-Loss Measurements*. The Journal of Chemical Physics, 1975. **63**(1): p. 241-248.
75. Suzuki, D., et al., *Electron Excitation of the Schumann-Runge Continuum, Longest Band, and Second Band Electronic States in O<sub>2</sub>*. J Chem Phys, 2011. **134**(6): p. 064311.
76. Geiger, J. and B. Schröder, *High-Resolution Energy-Loss Spectrum of Molecular Oxygen*. The Journal of Chemical Physics, 1968. **49**(2): p. 740-744.
77. Buenker, R.J. and S.D. Peyerimhoff, *Ab Initio Study of the Mixing of Valence and Rydberg States in O<sub>2</sub>: Ci Potential Curves for The  $3\sigma_u$ -,  $3\delta_u$  And  $3\pi_u$  States*. Chemical Physics Letters, 1975. **34**(2): p. 225-231.
78. Allison, A.C., S.L. Guberman, and A. Dalgarno, *A Model of the Schumann-Runge Continuum of O<sub>2</sub>*. Journal of Geophysical Research, 1986. **91**(A9): p. 10193-10198.
79. Watanabe, K., E.C.Y. Inn, and M. Zelikoff, *Absorption Coefficients of Oxygen in the Vacuum Ultraviolet*. The Journal of Chemical Physics, 1953. **21**(6): p. 1026-1030.
80. Tanaka, Y., *On the New Absorption Bands of the Oxygen Molecule in the Far Ultraviolet Region*. The Journal of Chemical Physics, 1952. **20**(11): p. 1728-1733.
81. Saxon, R.P. and B. Liu, *Ab Initio Configuration Interaction Study of the Rydberg States of O<sub>2</sub>. I. A General Computational Procedure for Diabatic Molecular Rydberg States and Test Calculations on the  $3\pi_g$  States of O<sub>2</sub>*. The Journal of Chemical Physics, 1980. **73**(2): p. 870-875.
82. Newell, W.R., M.A. Khakoo, and A.C.H. Smith, *Electron Impact Spectroscopy of O<sub>2</sub> for Energy Losses in the Range 6.5 to 10.5 Ev*. Journal of Physics B: Atomic and Molecular Physics, 1980. **13**(24): p. 4877.
83. Lee, L.C., et al., *Quantum Yields for the Production of O(1d) from Photodissociation of O<sub>2</sub> at 1160–1770 Å*. The Journal of Chemical Physics, 1977. **67**(12): p. 5602-5606.
84. Ladenburg, R. and C.C. Van Voorhis, *The Continuous Absorption of Oxygen between 1750 and 1300 Å and Its Bearing Upon the Dispersion*. Physical Review, 1933. **43**(5): p. 315-321.

85. Ditchburn Robert, W., D.W.O. Heddle, and W. Massey Harrie Stewart, *Absorption Cross-Sections in the Vacuum Ultra-Violet. - I. Continuous Absorption of Oxygen (1800 to 1300 Å)*. Proceedings of the Royal Society of London. Series A. Mathematical and Physical Sciences, 1953. **220**(1140): p. 61-70.
86. Cooper, G., J.E. Anderson, and C.E. Brion, *Absolute Photoabsorption and Photoionization of Formaldehyde in the Vuv and Soft X-Ray Regions (3-200 Ev)*. Chemical Physics, 1996. **209**(1): p. 61-77.
87. Sunanda, K., et al., *Photo-Absorption Studies on Formaldehyde Using Synchrotron Radiation at Indus I*. Vol. 45. 2012. 65-73.
88. Peyerimhoff, S., et al., *Calculation of the Electronic Spectrum of Formaldehyde*. Vol. 8. 1971. 129-135.
89. Weiss, M.J., C.E. Kuyatt, and S. Mielczarek, *Inelastic Electron Scattering from Formaldehyde*. The Journal of Chemical Physics, 1971. **54**(10): p. 4147-4150.
90. Tanaka, H.K., et al., *Photoabsorption and Photoionization Cross Sections for Formaldehyde in the Vacuum-Ultraviolet Energy Range*. Journal of Chemical Physics, 2017. **146**(9): p. 094310.
91. Mentall, J.E., et al., *Photoionization and Absorption Spectrum of Formaldehyde in the Vacuum Ultraviolet*. The Journal of Chemical Physics, 1971. **55**(12): p. 5471-5479.
92. Brint, P., et al., *The Vacuum Ultraviolet Absorption Spectrum of Formaldehyde*. Vol. 81. 1985.
93. Drury-Lessard, C.R. and D.C. Moule, *The Higher Rydberg States of Formaldehyde*. Chemical Physics Letters, 1977. **47**(2): p. 300-303.
94. Matsuzawa, N., et al., *Time-Dependent Density Functional Theory Calculations of Photoabsorption Spectra in the Vacuum Ultraviolet Region*. Vol. 105. 2001.
95. Whitten, J.L. and M. Hackmeyer, *Configuration Interaction Studies of Ground and Excited States of Polyatomic Molecules. I. The Ci Formulation and Studies of Formaldehyde*. The Journal of Chemical Physics, 1969. **51**(12): p. 5584-5596.
96. Langhoff, P., S. Langhoff, and C. T. Corcoran, *Photoabsorption in Formaldehyde*. Vol. 67. 1977.
97. Pal, S., et al., *Multireference Coupled-Cluster Methods Using an Incomplete Model Space: Application to Ionization Potentials and Excitation Energies of Formaldehyde*. Vol. 137. 1987. 273-278.

98. Yeager, D.L. and V. McKoy, *Equations of Motion Method: Excitation Energies and Intensities in Formaldehyde*. The Journal of Chemical Physics, 1974. **60**(7): p. 2714-2716.

## **CHAPTER 4. THERMAL AND SPECTROSCOPIC ANALYSIS OF NITRATED COMPOUNDS AND THEIR BREAK-DOWN PRODUCTS USING GAS CHROMATOGRAPHY/VACUUM UV SPECTROSCOPY (GC/VUV)**

Courtney A. Cruse, John V. Goodpaster\*

Department of Chemistry and Chemical Biology, Indiana University - Purdue University Indianapolis (IUPUI), 402 North Blackford Street LD326, Indianapolis, Indiana 46202, United States

### **4.1 Abstract**

Gas chromatography/vacuum UV spectroscopy (GC/VUV) was utilized to study various explosives and pharmaceuticals in the nitrate ester and nitramine structural classes. In addition to generating specific VUV spectra for each compound, VUV was used to indicate the onset of thermal decomposition based upon the appearance of break-down products such as nitric oxide, carbon monoxide, formaldehyde, water, and molecular oxygen. The effect of temperature on decomposition could be fit to a logistical function where the fraction of intact compound remaining decreased as the transfer line/flow cell temperature was increased from 200 °C to 300 °C. Utilizing this relationship, the decomposition temperatures for the nitrate ester and nitramine compounds were determined to range between 244 °C and 277 °C. It was also discovered that the decomposition temperature was dependent on the GC carrier gas flow rate and, therefore, the residence time of the compounds in the transfer line/flow cell. For example, the measured decomposition temperature of nitroglycerine ranged from 222 °C to 253 °C across four flow rates. Tracking the appearance/disappearance of decomposition products across this temperature range indicated that NO, CO, and H<sub>2</sub>CO are final decomposition products while O<sub>2</sub> and H<sub>2</sub>O increase to a maximum before decreasing again. The decomposition temperatures for all explosives were highly correlated to similar decomposition measurements taken by differential scanning calorimetry (DSC) ( $r = 0.91$ ) and thermal gravimetric analysis (TGA) ( $r = 0.90 - 0.98$ ). In addition, the decomposition temperatures for all explosives were negatively correlated to the heat of explosion at constant volume ( $r = -0.68$ ) and strongly positively correlated to the oxygen balance ( $r = 0.92$ ).

## 4.2 Introduction

Assessing the decomposition temperature of a sample is critical in several areas of research, such as fuels and energy,[1-4] polymer science,[5-7] pharmaceuticals,[8-11] food science,[12, 13] nanomaterials,[14, 15] and energetic/explosive compounds.[16-18] Thermal degradation is typically studied using differential scanning calorimetry (DSC) and/or thermal gravimetric analysis (TGA).[19] Both of these techniques can measure a number of thermal properties of a sample, such as glass transition temperature, enthalpic relaxation, melting point, onset of thermal degradation, and enthalpy of melting/crystallization. DSC measures the change in heat capacity as a function of temperature while TGA measures the change in mass as a function of temperature.[4, 11, 20] However, in DSC/TGA the results are dependent on the temperature ramp utilized.[21] For example, nitrate ester explosives (*e.g.*, ethylene glycol dinitrate (EGDN), nitroglycerine (NG), and pentaerythritol tetranitrate (PETN)) have been analyzed by DSC and TGA at numerous temperature ramps ranging from 5 - 20 °C/min.[22-27] Lastly, the identification of the breakdown products typically requires interfacing a TGA with a mass spectrometer or infrared spectrometer.[28-30]

The technique of gas chromatography/vacuum UV spectroscopy (GC/VUV) has applications in areas such as drugs,[31-37] hydrocarbons,[38-47] flavors and fragrance,[48-52] fatty acids,[53-56] environmental samples.[57, 58] and explosives.[59, 60] It has also been shown that nitrate ester explosives thermally decompose during analysis by GC/VUV - this decomposition occurs in the transfer line/flow cell of the VUV at higher temperatures, producing a complex mixture of compounds such as nitric oxide, carbon monoxide, formaldehyde, water, and molecular oxygen.[59] This adds significant specificity to the technique. For example, compounds such as nitroglycerine, PETN and EGDN have very similar or indistinguishable (electron ionization) mass spectra, but the VUV spectra of their degradation products were visibly differentiable.[59]

In this work, we establish GC/VUV as a new way to measure the temperature at which thermal decomposition occurs as well as identify the decomposition products that result. Various nitrated compounds were analyzed which fell into two different structural classes (*i.e.*, nitrate esters and nitramines). Nitrate esters have the basic structure of  $R-CH_2-NO_2$  and nitramines have the basic structure  $R_2N-NO_2$ . These compounds find application in forensic science, environmental

science, and medicine. Of the six compounds analyzed here, only three have been analyzed by GC/VUV previously (*i.e.*, nitroglycerine, ethylene glycol dinitrate, pentaerythritol tetranitrate).[59]

Degradation was monitored by spectral deconvolution of the VUV spectra and break-down products were identified via their structured spectra. Compounds were analyzed at various temperatures from 200 °C to 300 °C and the data fit to a logistic function for determination of the exact decomposition temperature. These decomposition temperatures determined via GC/VUV were correlated with various thermodynamic properties, including DSC and TGA decomposition temperatures, melting points, heat of explosion and heat of detonation; thus, establishing the utilization of GC/VUV for the study and determination of thermolysis.

### **4.3 Materials and Methods**

#### **4.3.1 Chemicals**

Nitroglycerine (1000 µg/mL in methanol), ethylene glycol dinitrate (1000 µg/mL in methanol), pentaerythritol tetranitrate (1000 µg/mL in methanol), EPA method 8330 calibration mix #1 (1000 µg/mL each in acetonitrile) were purchased from Restek. Isosorbide mononitrate was purchased from MEDCHEMEXPRESS LLC and isosorbide dinitrate was purchased from Cayman Chemical. Methanol (optima LC/MS) and chloroform (stabilized HPLC grade) were purchased from Fisher Scientific.

#### **4.3.2 Sample Preparation**

Nitroglycerine, ethylene glycol dinitrate, pentaerythritol tetranitrate, and EPA 8330 calibration mix #1 were analyzed as received. Standard concentrations of 1000 ppm of isosorbide mononitrate and isosorbide dinitrate were each made by dissolving in chloroform.

Temperature studies were performed using a 250-ppm mixture of NG, EGDN, and PETN; a 500-ppm mixture of isosorbide mononitrate and isosorbide dinitrate; a 500-ppm standard of RDX; and a 1000-ppm mixture of EPA method 8330 Calibration mix #1 (for analysis of HMX and a duplicate analysis of RDX). The flow rate study was performed with a 250-ppm standard of NG in methanol.

### 4.3.3 Gas Chromatography

An Agilent 7890B series GC equipped with a multimode inlet and Agilent 7390 autosampler was utilized with hydrogen carrier gas at a 3.2 mL/min flow rate, a ramped inlet temperature program (50 °C ramped to 280 °C at 900 °C/min), and splitless injection. A Restek Rtx®-5MS column (15 m x 0.32 mm x 0.25 µm) was utilized for analysis of the EPA 8330 and remaining compounds. The EPA 8330 calibration mix 1 was analyzed with an oven program of 50 °C held for 2 min, ramped 10 °C/min to 170 °C then 20 °C/min to 280 °C. For the thermal decomposition analysis of HMX, the temperature program for the GC oven was ramped to 240 °C rather than 280 °C to be able to analyze HMX at a transfer line/flow cell temperature of 240 °C. The remainder of the compounds were analyzed with a splitless injection and an oven program of 50 °C held for 0.5 min, ramped at 20 °C/min to 200 °C.

The impact of flow rate on the thermal decomposition temperature of NG was assessed using an oven program of 50 °C held for 0.5 min, ramped 20 °C/min to 180 °C with a ramped inlet temperature program of 50 °C ramped to 280 °C at 900 °C/min splitless. The flow rates analyzed were 0.7 mL/min, 1 mL/min, 3.2 mL/min, and 6 mL/min.

### 4.3.4 Vacuum Ultraviolet Spectroscopy

GC effluent was directed into a VUV Analytics VGA-101 VUV spectrometer. All experiments were run with a spectral range of 120 nm to 430 nm with a 4.5 Hz scan rate, nitrogen make-up gas at a pressure of 0.35 psi, and a deuterium lamp as the light source. Standards of compound spectra were run with a transfer line and flow cell temperature of 300 °C. Compounds displaying thermal decomposition were analyzed over a flow cell temperature range of 200 °C to 300 °C at 20 °C intervals. For the flow rate study, temperatures from 180 °C to 300 °C at 20 °C intervals were investigated.

### 4.3.5 JMP Analysis

Analysis of the thermal decomposition was modeled utilizing a logistic 2-parameter curve fit in JMP Pro 14 via the following equation:

$$\text{Logistic } 2P = \frac{1}{1 + \text{Exp}(-a * (\text{Temperature} - b))}$$

where a is the growth rate and b is the inflection point. A 2-parameter fit was not applicable for the flow rate study of NG at 0.7 mL/min and 1 mL/min or for modeling the logistic curves of the decomposition products (NO, CO, and H<sub>2</sub>CO) as the 2-parameter equation assumes limits of zero/one and these logistic curves did not reach the upper boundary. Therefore, the following 3-parameter curve fit was utilized for the flow rate study:

$$\text{Logistic } 3P = \frac{c}{1 + \text{Exp}(-a * (\text{Temperature} - b))}$$

where c is the asymptote.

## 4.4 Results and Discussion

### 4.4.1 VUV Spectra of Nitrate Esters and Nitramines

All nitrate esters and nitramines thermally decomposed upon reaching the VUV flow cell at its highest temperature. Based on prior research, the degradation products have been identified (e.g., water, formaldehyde, nitrogen oxide, carbon monoxide and oxygen)[59, 61]. The thermal decomposition into these small compounds contribute to spectra that display fine structure, while the intact compound spectra have broader absorption bands (Fig. 4.1).

The nitramine compounds, RDX and HMX, partially decomposed into NO and H<sub>2</sub>CO with remaining intact compound at higher flow cell temperatures. An intact RDX spectrum was observed at 200 °C and partial decomposition was observed at 300 °C (Fig. 4.1). Due to the high elution temperature of HMX at 240 °C, the lowest flow cell temperature analyzed was 240 °C at which HMX was already partially decomposed into NO and H<sub>2</sub>CO (Fig. 4.1). It is established that chromatographic analysis of HMX via GC is problematic which led to additional difficulties in further analysis of HMX[62, 63]. Therefore, direct analysis via VUV (without hyphenation with GC) would be advantageous for compounds that are difficult to analyze chromatographically (e.g., HMX); however, hyphenation allows for the analysis of several compounds at once and for realistic samples that are not pure (e.g., pharmaceutical and explosive analyses).

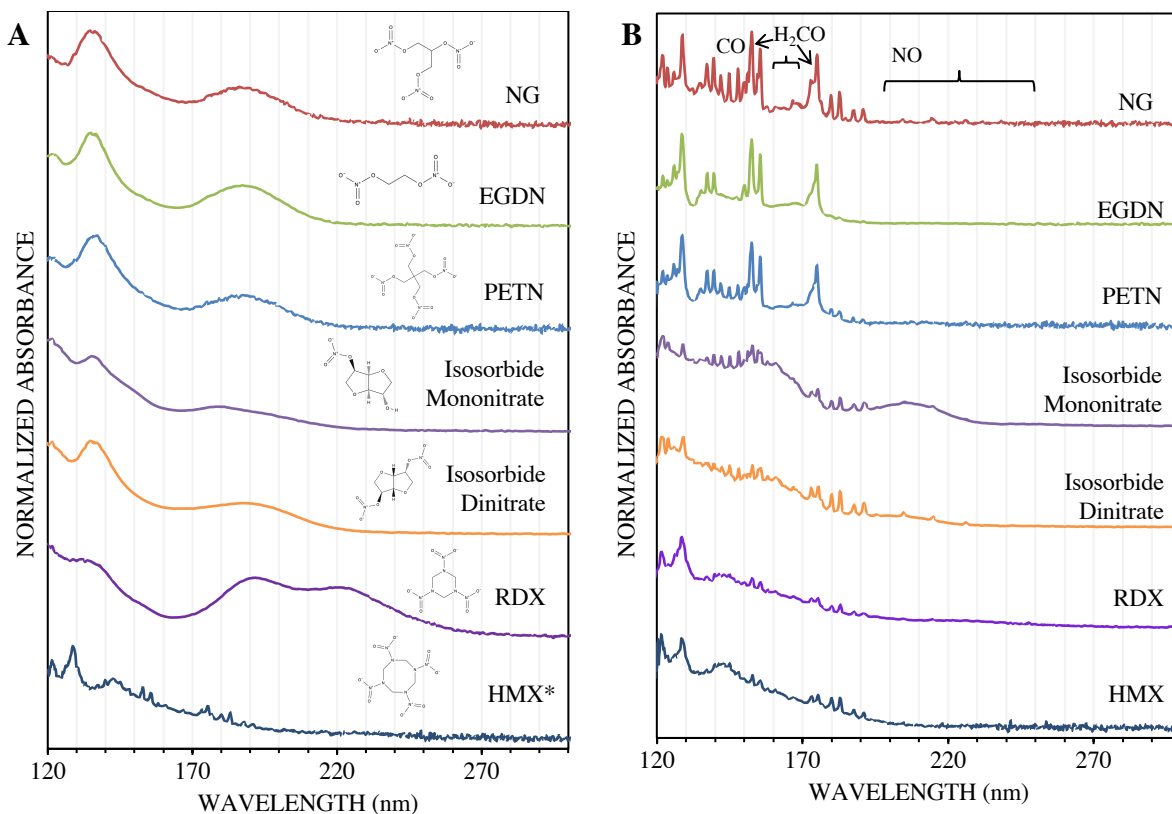


Figure 4.1. Nitrate ester and nitramine VUV spectra A) intact at 200 °C; and B) decomposed at 300 °C measured at 3.2 mL/min. Fine structure in the spectra are labelled with corresponding decomposition product. \* The minimum flow cell temperature for HMX was 240 °C due to its high elution temperature.

Isosorbide mono- and dinitrate compounds (ISMN and ISDN, respectively) thermally decomposed into NO, CO, H<sub>2</sub>CO, and additional unknown compounds. At 300 °C, a broad absorption was observed for ISMN and ISDN that overlapped the fine structure of NO (185 nm - 225 nm). This absorption characteristic is inconsistent with the intact compounds, indicating an unidentified decomposition compound that is not in the VUV library or previous literature (Fig. 4.1B). Additional work using mass spectrometry and/or infrared spectroscopy is likely needed to identify these compounds

#### 4.4.2 Effect of GC Flow Rate on Decomposition Temperature

It is known that DSC and TGA yield lower decomposition temperatures at slower temperature ramps. Based on this, the 50% decomposition temperature for NG was analyzed using

four different GC carrier gas flow rates. Changes in the decomposition temperature due to changing the velocity at which the compounds traveled through the transfer line are shown in (Fig. 4.2). Like trends observed in DSC and TGA, as the flow rate increased, the 50% decomposition temperature also increased due to a shorter time spent in the transfer line and flow cell. The shortest and longest dwell times investigated were 0.7 sec (6 mL/min) and 5.0 sec (0.70 mL/min), respectively. However, there exists a positive bias in values determined by GC/VUV compared to reported values by DSC and TGA, which was hypothesized to be due to the residence time in GC/VUV being equivalent to a much larger temperature ramp program than those utilized in DSC and TGA leading to higher decomposition temperatures that are more consistent with HyperDSC.[62, 63]

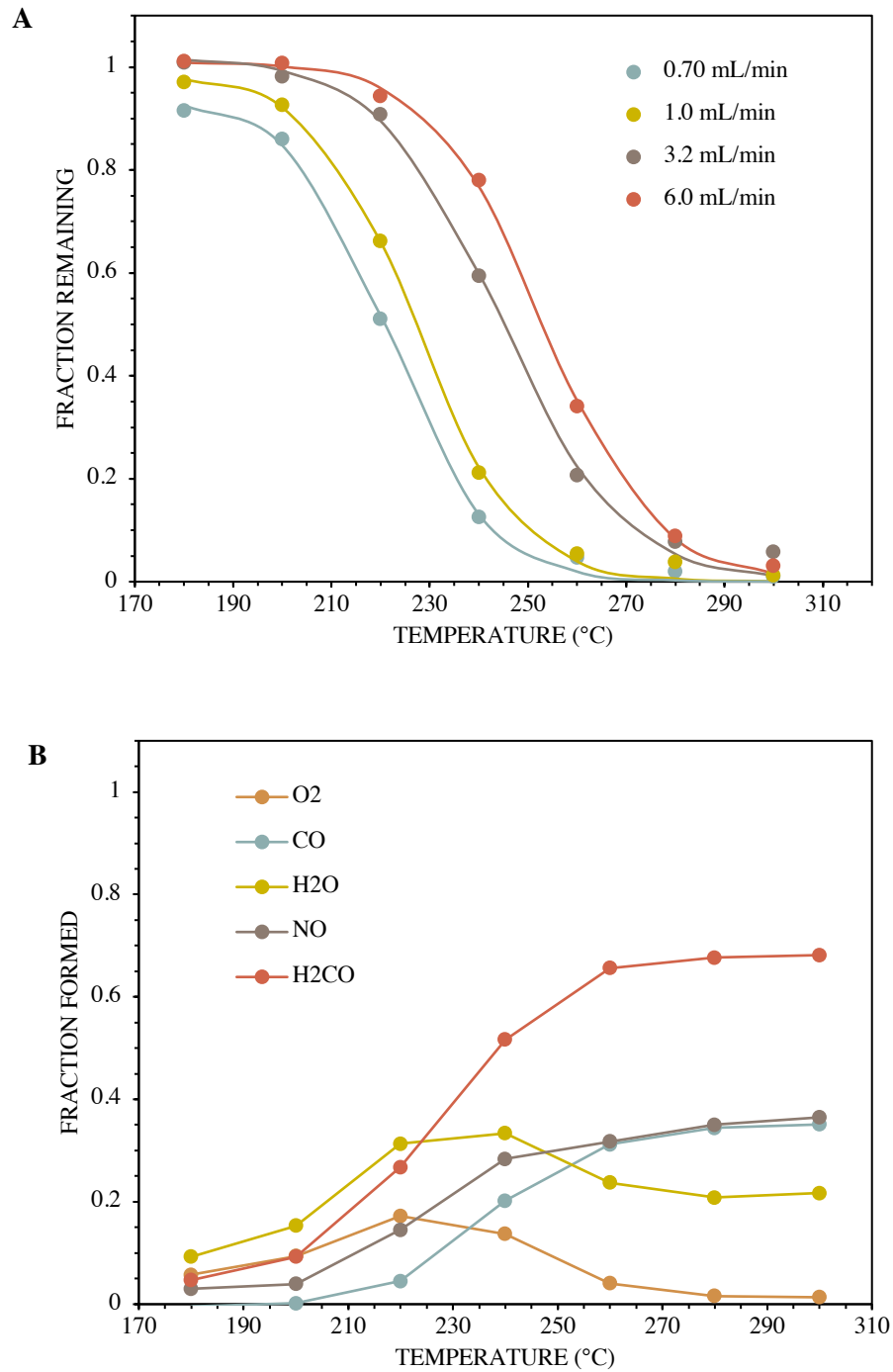


Figure 4.2. A. Trends in decomposition of NG at various flow rates. B. Trends in the formation of decomposition products at a 0.70 mL/min flow rate.

Table 4.1. Inflection points determined by a 3-parameter logistic function for 50% decomposition of NG and 50% formation of the decomposition products H<sub>2</sub>CO, NO, and CO across four flow rates and the corresponding residence time in the transfer line/flow cell.

<b>Flow Rate (mL/min)</b>	<b>NG (°C)</b>	<b>H<sub>2</sub>CO (°C)</b>	<b>NO (°C)</b>	<b>CO (°C)</b>	<b>Residence Time (sec)</b>
<b>0.70</b>	222.0±1.0	225.5±1.2	224.6±2.1	237.3±0.75	5.0
<b>1.0</b>	227.26±1.0	231.8±0.8	230.4±2.0	245.4±2.0	3.5
<b>3.2</b>	244.3±1.4	247.7±2.0	248.6±1.5	255.7±2.3	1.2
<b>6.0</b>	253.0±0.6	256.8±2.7	254.4±1.7	265.2±0.8	0.70

Of the decomposition products, NO and H<sub>2</sub>CO had inflection points like that of NG (Table 4.1). The CO inflection point was shifted by about 15 °C higher than the inflection point observed for NG. The contributions of O<sub>2</sub> and H<sub>2</sub>O to the decomposed NG spectra gradually increased until a maximum was reached at approximately 220 °C and 240 °C, respectively. O<sub>2</sub> levels continued to decrease toward zero, while H<sub>2</sub>O decreased until leveling out at approximately 21% of the total VUV spectrum. Thus, suggesting that NO, H<sub>2</sub>CO, CO and H<sub>2</sub>O are final reaction products of the decomposition.

Additionally, the relationship between the decomposition temperature and the flow rate behaved in a logarithmic function (Fig. 4.3A). This is consistent with a logarithmic relationship between the reported TGA temperature program and the temperature of onset of decomposition for NG (Fig. 4.3B). Since the same process is undergone by NG (decomposition) and the same logarithmic relationship exists between the decomposition temperature and the rate and ramp, it can be assumed that an equivalent GC/VUV flow rate and TGA temperature ramp can be calculated for a given decomposition temperature. Therefore, the TGA temperature program equivalent to the GC/VUV flow rate that results in the same decomposition temperature can be calculated by:

$$22.63 \ln(x_{TGA}) = 14.23 \ln(x_{VUV}) + 117.37^{\circ}C.$$

The calculated TGA temperature ramps were considerably higher than standard TGA temperature ramps. The calculated ramps ranged from 142 °C/min to 544 °C/min, which are more consistent with temperature ramps observed in HyperDSC analysis (Table 4.2).[62, 63] A calculated flow rate that would be equivalent to a 20 °C/min ramp was 0.03 mL/min (88 sec

residence time). Due to limited literature values for DSC decomposition temperatures of NG at multiple ramps, comparison of GC/VUV flow rate to DSC temperature ramps was not completed.

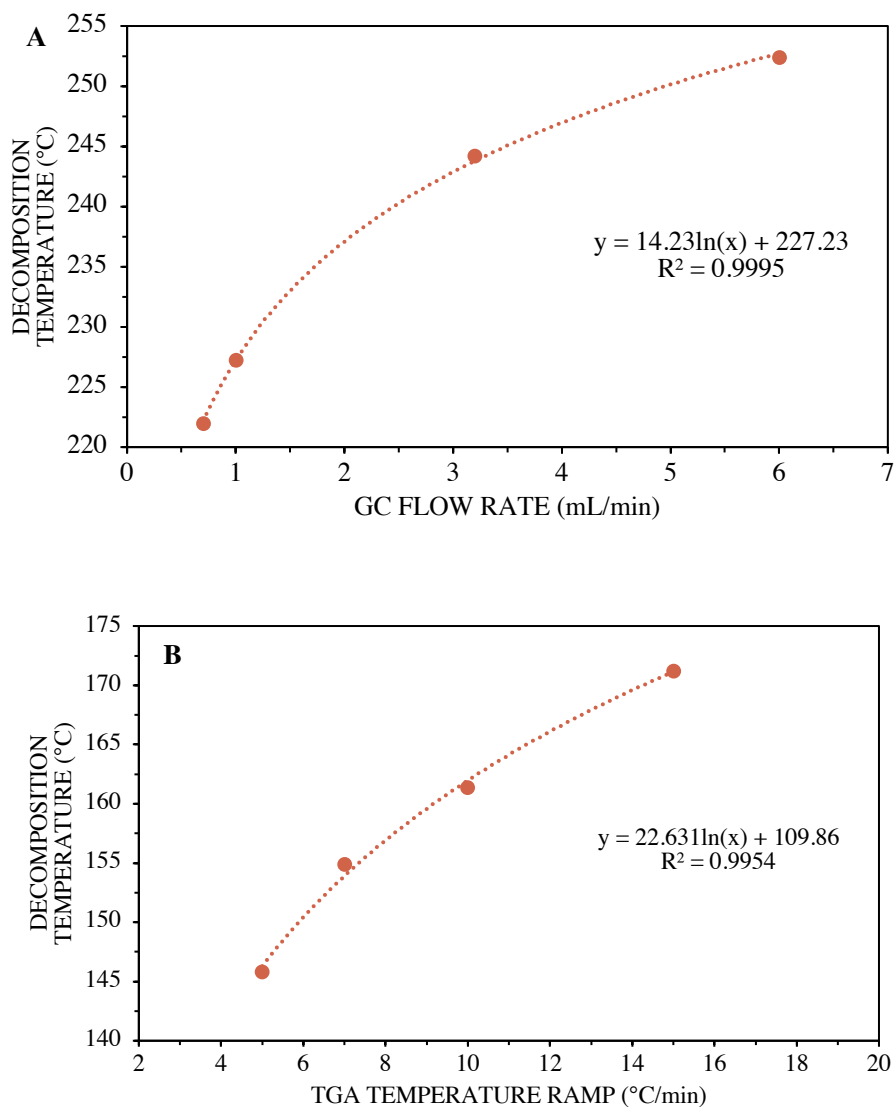


Figure 4.3. A) logarithmic relationship between the calculated 50% decomposition temperature for NG across the four flow rates B) logarithmic relationship between the TGA onset temperature of decomposition for NG (literature data) across four temperature ramps.[64]

#### 4.4.3 Determination of Decomposition Temperatures of Nitrated Compounds

All compounds that could be analyzed intact as well as thermally degraded (*i.e.*, NG, EGDN, PETN, RDX, ISMN, and ISDN) were analyzed between 200 °C and 300 °C to find their decomposition temperature (Fig. 4.4).

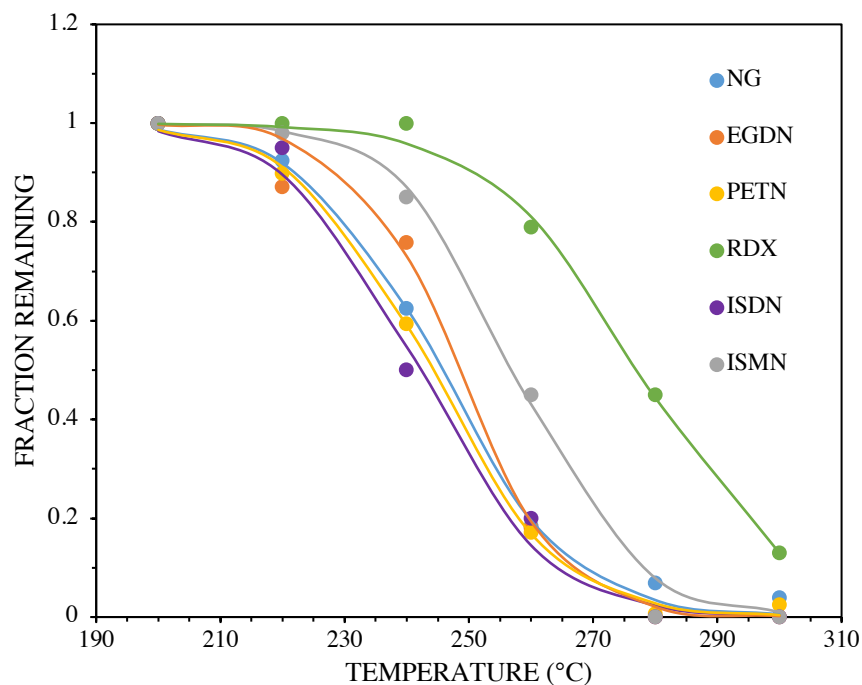


Figure 4.4. Decomposition curves of nitrate ester and nitramine compounds at a flow rate of 3.2 mL/min via a 2-parameter logistic function.

The growth rates and inflection points (at which 50% of the compound has decomposed) are reported in Table 4.2. The 50% decomposition temperatures ranged from 241.9 °C to 277.3 °C with a general trend of increasing 50% decomposition temperature with increasing molecular weight (exception is the 50% decomposition temperature of ISDN). Additionally, values for DSC and TGA at various temperature programs (ranging from 1 °C/min to 20 °C/min) are reported for the nitrate ester compounds. A correlation analysis between the inflection point, literature data, and thermodynamic properties is reported in Table 4.3. The thermodynamic properties include oxygen balance, melting point, heat of detonation at constant volume ( $\Delta H_d$ ), and heat of explosion at constant volume ( $Q_v$ ) are reported and a correlation between these values and the 50% decomposition temperatures are investigated.

The oxygen balance ( $\Omega$ ) was calculated for any explosive compound with empirical formula  $C_aH_bN_cO_d$  by the following equation:

$$\Omega = \frac{(d - (2a) - (\frac{b}{2})) \times 1600}{\text{molecular mass}}$$

Where a negative oxygen balance indicates the molecule requires oxygen from the environment for a completely efficient detonation to occur; while a positive oxygen balance indicates the molecule's high oxygen content does not require additional oxygen.[65]

$\Delta H_d$  and  $Q_v$  are related via the following equation:

$$Q_v = \frac{\Delta H_d \times 1000}{\text{molecular mass}};$$

where  $Q$  is the amount of heat released in an explosion through the formation of products (i.e. carbon monoxide, carbon and hydrogen gases) under adiabatic conditions and  $\Delta H_d$  is the amount of heat released during detonation of an explosive.[65]

Table 4.2. JMP curve fitting results (plus or minus standard error). Literature values for reported decomposition temperatures via DSC and TGA reported at various temperature programs (DSC and TGA decomposition temperatures reported as peak temperature of decomposition).

	This Work (n = 3)			Literature		Ref.
	Growth Rate $\pm$ Std Error (°C)	Inflection Pt. $\pm$ Std Error (°C)	R <sup>2</sup>	DSC T <sub>dec</sub> (°C) (°C/min)	TGA T <sub>dec</sub> (°C) (°C/min)	
<b>PETN</b>	-0.098±0.005	243.7±0.6	0.999	202 (5)		[26]
				197.6 (5)		[23]
				205.4 (10)		
				210.2 (15)		
				212.8 (20)		
				202.9 (10)	186.9 (5) 190.1 (7) 194.5 (10) 199.4 (15)	[24]
				201 (5)		[25]
				208 (10)		
				212 (15)		
				216 (20)		
				185 (5)		[26]
<b>NG</b>	-0.096±0.007	245.3±0.92	0.997	199.9 (10)	165.8 (5) 177.4 (7) 183.8 (10) 191.9 (15)	[24]
<b>EGDN</b>	-0.121±0.020	248.2±1.70	0.980	201.9 (5)		[22]
<b>ISDN</b>	-0.098±0.014	241.9±1.7	0.991			
<b>ISMN</b>	-0.109±0.008	257.5±0.7	0.998			
<b>RDX</b>	-0.084±0.008	277.3±1.3	0.995	218 (1)		[25]
				225 (2)		
				240 (5)		
				247 (10)		
				231 (5)		[66]
				241 (10)		
				245 (15)		
				251 (20)		
					214.74 (2) 216.77 (4) 227.25 (8) 230.80 (16)	[67]
					218.43 (5) 230.62 (10) 232.90 (15) 239.01 (20)	[64]

Table 4.3. Correlation analysis between the 50% decomposition temperature of nitrated compounds and reported thermodynamic properties (decomposition temperature, oxygen balance, melting point, heat of explosion and heat of detonation). The standard deviation is included for averaged values.

	<i>Inflection Pt.</i>	<i>Avg. DSC 5 °C/min</i>	<i>TGA 5 °C/min</i>	<i>TGA 10 °C/min</i>	<i>TGA 15 °C/min</i>	<i>Oxygen Balance</i>	<i>M.P. (°C)</i>	<i>ΔH<sub>d</sub> (kJ/mol)</i>	<i>Q<sub>v</sub> (kJ/kg)</i>	<i>Ref.</i>
<i>PETN</i>	243.7	202±2.4	186.9	194.5	199.4	-10.13	143	-1831	5794	[26, 65]
<i>NG</i>	245.3	185	165.8	183.8	191.9	3.5	13	-1406	6194	[26, 65]
<i>EGDN</i>	248.2	201.9	-	-	-	0	-23	-1012	6658	[22, 65]
<i>ISDN</i>	241.9	-	-	-	-	-	-	-	-	-
<i>ISMN</i>	257.5	-	-	-	-	-	-	-	-	-
<i>RDX</i>	277.3	231±6.4	218.43	230.62	232.90	21.6	206	-1118	5036	[25, 26, 64, 65]
<i>r</i>	-	0.910	0.900	0.966	0.977	0.923	0.676	0.509	-0.792	-

There exists a strong positive correlation between the 50% decomposition temperature via GC/VUV and the average reported DSC and TGA decomposition temperatures with a higher correlation with the higher temperature ramp programs (10 °C/min and 15 °C/min) in TGA. Additionally, there is a strong positive correlation between with the oxygen balance and melting point and a negative correlation between the inflection point and the heat of explosion. Therefore, it is concluded that the energy required to achieve 50% decomposition correlates to thermodynamic properties and suggests the use of GC/VUV to study thermodynamic processes or properties of explosives.

## 4.5 Conclusions

Within the temperature range of the GC/VUV, nitrate ester and nitramine compounds thermally decomposed. The nitrate ester and nitramine compounds were analyzed from 200 °C to 300 °C and revealed a logistic function relationship between the spectral contribution from NG and the flow cell/transfer line temperature. Therefore, a 50% decomposition temperature could be determined from the inflection point in the logistic fit. The values for PETN, NG, and EGDN are negatively correlated to the heat of explosion and positively correlated to oxygen balance and decomposition temperatures determined by DSC and TGA. This suggests the use of GC/VUV to study thermodynamic properties of compounds that thermally decompose. Additionally, analysis of NG across four GC flow rates revealed a dependence of the decomposition temperature on the

flow rate and, therefore, the time spent in the transfer line. This is consistent with trends observed in DSC and TGA with higher temperature ramps corresponding to higher decomposition temperatures; thus, suggesting the GC/VUV residence time being equivalent to a DSC and TGA temperature ramp that is larger than those observed in literature. Investigation of trends observed for the fraction formed for the decomposition products revealed that NO, CO, and H<sub>2</sub>CO are final decomposition products; thus, suggesting the utilization of GC/VUV to study oxidative decomposition processes. This highlights the advantage of GC/VUV for studying thermal decomposition when compared to DSC and TGA as GC/VUV permits identification of decomposition products in addition to decomposition temperature. As with reporting decomposition temperatures with DSC and TGA, it is necessary to report the experimental parameters utilized to understand the contextualized decomposition temperature. Variation in reported decomposition temperatures exist within and between established techniques (DSC and TGA). Future work includes further investigation on the correlations observed between the thermal decomposition temperatures and thermodynamic properties, including comparison of GC/VUV flow rate and DSC temperature ramp for NG; as well as the trends observed in the formation of decomposition products between 200 °C and 300 °C.

#### 4.6 Acknowledgements

This work was supported via a National Institute of Justice Award 2017-R2-CX- 0018 and 2018-R2-CX-0015. Opinions or points of view expressed here represent a consensus of the authors and do not necessarily represent the official position or policies of the U.S. Department of Justice.

#### 4.7 References

1. Yuen, F.T.C., et al., *Novel Experimental Approach to Studying the Thermal Stability and Coking Propensity of Jet Fuel*. Energy & Fuels, 2017. **31**(4): p. 3585-3591.
2. Wang, L., T. Maxisch, and G. Ceder, *A First-Principles Approach to Studying the Thermal Stability of Oxide Cathode Materials*. Chemistry of Materials, 2007. **19**(3): p. 543-552.
3. Maleki, H., et al., *Thermal Stability Studies of Binder Materials in Anodes for Lithium-Ion Batteries*. Journal of the Electrochemical Society, 2000. **147**(12): p. 4470-4475.

4. Ahmadi Khoshooei, M., et al., *A Review on the Application of Differential Scanning Calorimetry (Dsc) to Petroleum Products*. Journal of Thermal Analysis and Calorimetry, 2019. **138**(5): p. 3485-3510.
5. Chattopadhyay, D.K. and D.C. Webster, *Thermal Stability and Flame Retardancy of Polyurethanes*. Progress in Polymer Science, 2009. **34**(10): p. 1068-1133.
6. El-Sayed, S., et al., *Dsc, Tga and Dielectric Properties of Carboxymethyl Cellulose/Polyvinyl Alcohol Blends*. Physica B-Condensed Matter, 2011. **406**(21): p. 4068-4076.
7. Lewandowska, K., *Miscibility and Thermal Stability of Poly(Vinyl Alcohol)/Chitosan Mixtures*. Thermochimica Acta, 2009. **493**(1-2): p. 42-48.
8. Khan, W. and N. Kumar, *Characterization, Thermal Stability Studies, and Analytical Method Development of Paromomycin for Formulation Development*. Drug Test Anal, 2011. **3**(6): p. 363-72.
9. Chakravarty, S. and R. Varadarajan, *Elucidation of Factors Responsible for Enhanced Thermal Stability of Proteins: A Structural Genomics Based Study*. Biochemistry, 2002. **41**(25): p. 8152-61.
10. Herbrink, M., et al., *Thermal Stability Study of Crystalline and Novel Spray-Dried Amorphous Nilotinib Hydrochloride*. J Pharm Biomed Anal, 2018. **148**: p. 182-188.
11. Chiu, M.H. and E.J. Prenner, *Differential Scanning Calorimetry: An Invaluable Tool for a Detailed Thermodynamic Characterization of Macromolecules and Their Interactions*. J Pharm Bioallied Sci, 2011. **3**(1): p. 39-59.
12. Santos, J.C.O., et al., *Thermal Stability and Kinetic Study on Thermal Decomposition of Commercial Edible Oils by Thermogravimetry*. Journal of Food Science, 2002. **67**(4): p. 1393-1398.
13. Bernal, V. and P. Jelen, *Thermal Stability of Whey Proteins – a Calorimetric Study*. Journal of Dairy Science, 1985. **68**(11): p. 2847-2852.
14. Wang, Y.M., et al., *Study on Mechanical Properties, Thermal Stability and Crystallization Behavior of Pet/Mmt Nanocomposites*. Composites Part B-Engineering, 2006. **37**(6): p. 399-407.
15. Kundu, S., et al., *Thermal Stability and Reducibility of Oxygen-Containing Functional Groups on Multiwalled Carbon Nanotube Surfaces: A Quantitative High-Resolution Xps and Tpd/Tpr Study*. Journal of Physical Chemistry C, 2008. **112**(43): p. 16869-16878.

16. Abrishami, F., et al., *Study on Thermal Stability and Decomposition Kinetics of Bis (2,2-Dinitropropyl) Fumarate (Bdnpf) as a Melt Cast Explosive by Model-Free Methods*. Propellants Explosives Pyrotechnics, 2019. **44**(11): p. 1446-1453.
17. Green, S.P., et al., *Thermal Stability and Explosive Hazard Assessment of Diazo Compounds and Diazo Transfer Reagents*. Org Process Res Dev, 2020. **24**(1): p. 67-84.
18. Anniyappan, M., et al., *1-Methyl-2,4,5-Trinitroimidazole (Mtni), a Melt-Cast Explosive: Synthesis and Studies on Thermal Behavior in Presence of Explosive Ingredients*. Journal of Energetic Materials, 2020. **38**(1): p. 111-125.
19. Nazarian, A. and C. Presser, *Forensic Analysis Methodology for Thermal and Chemical Characterization of Homemade Explosives*. Thermochemica Acta, 2014. **576**: p. 60-70.
20. Coats, A.W. and J.P. Redfern, *Thermogravimetric Analysis. A Review*. The Analyst, 1963. **88**(1053): p. 906-924.
21. Brill, T.B. and K.J. James, *Kinetics and Mechanisms of Thermal-Decomposition of Nitroaromatic Explosives*. Chemical Reviews, 1993. **93**(8): p. 2667-2692.
22. Jones, D.E.G., R.A. Augsten, and K.K. Feng, *Detection Agents for Explosives*. Journal of Thermal Analysis and Calorimetry, 1995. **44**(3): p. 533-546.
23. Song, X., Y. Wang, and C. An, *Thermochemical Properties of Nanometer Cl-20 and Petn Fabricated Using a Mechanical Milling Method*. AIP Advances, 2018. **8**(6): p. 065009.
24. Dong, J., et al., *The Correlations among Detonation Velocity, Heat of Combustion, Thermal Stability and Decomposition Kinetics of Nitric Esters*. Journal of Thermal Analysis and Calorimetry, 2018. **131**(2): p. 1391-1403.
25. Lee, J.-S., C.-K. Hsu, and C.-L. Chang, *A Study on the Thermal Decomposition Behaviors of Petn, Rdx, Hns and Hmx*. Thermochemica Acta, 2002. **392-393**: p. 173-176.
26. Fischer, D., T.M. Klapotke, and J. Stierstorfer, *Tetranitratoethane*. Chem Commun (Camb), 2016. **52**(5): p. 916-8.
27. Altenburg, T., T.M. Klapötke, and A. Penger, *Primary Nitramines Related to Nitroglycerine: 1-Nitramino-2, 3-Dinitroxypropane and 1, 2, 3-Trinitraminopropane*. Central European Journal of Energetic Materials, 2009. **6**(3-4): p. 255-275.
28. Rothgery, E.F., et al., *The Study of the Thermal-Decomposition of 3-Nitro-1,2,4-Triazol-5-One (Nto) by Dsc, Tga-Ms, and Arc*. Thermochemica Acta, 1991. **185**(2): p. 235-243.
29. Singh, S., C.F. Wu, and P.T. Williams, *Pyrolysis of Waste Materials Using Tga-Ms and Tga-Ftir as Complementary Characterisation Techniques*. Journal of Analytical and Applied Pyrolysis, 2012. **94**: p. 99-107.

30. Ozsin, G. and A.E. Putun, *Kinetics and Evolved Gas Analysis for Pyrolysis of Food Processing Wastes Using Tga/Ms/Ft-Ir*. Waste Manag, 2017. **64**: p. 315-326.
31. Zheng, J., C. Huang, and S. Wang, *Challenging Pharmaceutical Analyses by Gas Chromatography with Vacuum Ultraviolet Detection*. J Chromatogr A, 2018. **1567**: p. 185-190.
32. Roberson, Z.R. and J.V. Goodpaster, *Differentiation of Structurally Similar Phenethylamines Via Gas Chromatography-Vacuum Ultraviolet Spectroscopy (Gc-Vuv)*. Forensic Chemistry, 2019. **15**: p. 100172.
33. Kranenburg, R.F., et al., *Distinguishing Drug Isomers in the Forensic Laboratory: Gc-Vuv in Addition to Gc-Ms for Orthogonal Selectivity and the Use of Library Match Scores as a New Source of Information*. Forensic Sci Int, 2019. **302**: p. 109900.
34. Buchalter, S., et al., *Gas Chromatography with Tandem Cold Electron Ionization Mass Spectrometric Detection and Vacuum Ultraviolet Detection for the Comprehensive Analysis of Fentanyl Analogues*. J Chromatogr A, 2019. **1596**: p. 183-193.
35. Roberson, Z.R., H.C. Gordon, and J.V. Goodpaster, *Instrumental and Chemometric Analysis of Opiates Via Gas Chromatography-Vacuum Ultraviolet Spectrophotometry (Gc-Vuv)*. Anal Bioanal Chem, 2020. **412**(5): p. 1123-1128.
36. Leghissa, A., Z.L. Hildenbrand, and K.A. Schug, *A Review of Methods for the Chemical Characterization of Cannabis Natural Products*. J Sep Sci, 2018. **41**(1): p. 398-415.
37. Weston, C., et al., *Investigation of Gas Phase Absorption Spectral Similarity for Stable-Isotopically Labeled Compounds in the 125-240nm Wavelength Range*. Talanta, 2018. **177**: p. 41-46.
38. Dunkle, M.N., et al., *Quantification of the Composition of Liquid Hydrocarbon Streams: Comparing the Gc-Vuv to Dha and Gcxcg*. J Chromatogr A, 2019. **1587**: p. 239-246.
39. Mao, J.X., et al., *Simulation of Vacuum Ultraviolet Absorption Spectra: Paraffin, Isoparaffin, Olefin, Naphthene, and Aromatic Hydrocarbon Class Compounds*. Appl Spectrosc, 2020. **74**(1): p. 72-80.
40. Mao, J.X., P. Kroll, and K.A. Schug, *Vacuum Ultraviolet Absorbance of Alkanes: An Experimental and Theoretical Investigation*. Structural Chemistry, 2019. **30**(6): p. 2217-2224.
41. Schenk, J., et al., *Analysis and Deconvolution of Dimethylnaphthalene Isomers Using Gas Chromatography Vacuum Ultraviolet Spectroscopy and Theoretical Computations*. Anal Chim Acta, 2016. **945**: p. 1-8.

42. Liu, H., et al., *Hyphenation of Short Monolithic Silica Capillary Column with Vacuum Ultraviolet Spectroscopy Detector for Light Hydrocarbons Separation*. J Chromatogr A, 2019. **1595**: p. 174-179.
43. Bai, L., et al., *Comparison of Gc-Vuv, Gc-Fid, and Comprehensive Two-Dimensional Gc-Ms for the Characterization of Weathered and Unweathered Diesel Fuels*. Fuel, 2018. **214**: p. 521-527.
44. Isaacman, G., et al., *Improved Resolution of Hydrocarbon Structures and Constitutional Isomers in Complex Mixtures Using Gas Chromatography-Vacuum Ultraviolet-Mass Spectrometry*. Anal Chem, 2012. **84**(5): p. 2335-42.
45. Walsh, P., M. Garbalena, and K.A. Schug, *Rapid Analysis and Time Interval Deconvolution for Comprehensive Fuel Compound Group Classification and Speciation Using Gas Chromatography-Vacuum Ultraviolet Spectroscopy*. Anal Chem, 2016. **88**(22): p. 11130-11138.
46. Weber, B.M., P. Walsh, and J.J. Harynuk, *Determination of Hydrocarbon Group-Type of Diesel Fuels by Gas Chromatography with Vacuum Ultraviolet Detection*. Anal Chem, 2016. **88**(11): p. 5809-17.
47. Schug, K.A., et al., *Vacuum Ultraviolet Detector for Gas Chromatography*. Anal Chem, 2014. **86**(16): p. 8329-35.
48. Hodgson, A. and J. Cochran, *Vacuum Ultraviolet Spectroscopy as a New Tool for Gc Analysis of Terpenes in Flavors and Fragrances*. J AOAC Int, 2019. **102**(2): p. 655-658.
49. Santos, I.C., J. Smuts, and K.A. Schug, *Rapid Profiling and Authentication of Vanilla Extracts Using Gas Chromatography-Vacuum Ultraviolet Spectroscopy*. Food Analytical Methods, 2017. **10**(12): p. 4068-4078.
50. Garcia-Cicourel, A.R., et al., *Comprehensive Off-Line Silver Phase Liquid Chromatography X Gas Chromatography with Flame Ionization and Vacuum Ultraviolet Detection for the Detailed Characterization of Mineral Oil Aromatic Hydrocarbons*. J Chromatogr A, 2019. **1607**: p. 460391.
51. Garcia-Cicourel, A.R. and H.G. Janssen, *Direct Analysis of Aromatic Hydrocarbons in Purified Mineral Oils for Foods and Cosmetics Applications Using Gas Chromatography with Vacuum Ultraviolet Detection*. J Chromatogr A, 2019. **1590**: p. 113-120.
52. Qiu, C., J. Smuts, and K.A. Schug, *Analysis of Terpenes and Turpentine Using Gas Chromatography with Vacuum Ultraviolet Detection*. J Sep Sci, 2017. **40**(4): p. 869-877.
53. Fan, H., et al., *Gas Chromatography-Vacuum Ultraviolet Spectroscopy for Analysis of Fatty Acid Methyl Esters*. Food Chem, 2016. **194**: p. 265-71.

54. Santos, I.C., et al., *Large-Volume Injection Gas Chromatography-Vacuum Ultraviolet Spectroscopy for the Qualitative and Quantitative Analysis of Fatty Acids in Blood Plasma*. *Anal Chim Acta*, 2019. **1053**: p. 169-177.
55. Weatherly, C.A., et al., *Analysis of Long-Chain Unsaturated Fatty Acids by Ionic Liquid Gas Chromatography*. *J Agric Food Chem*, 2016. **64**(6): p. 1422-32.
56. Santos, I.C., et al., *Analysis of Bacterial Fames Using Gas Chromatography - Vacuum Ultraviolet Spectroscopy for the Identification and Discrimination of Bacteria*. *Talanta*, 2018. **182**: p. 536-543.
57. Schenk, J., et al., *Lab-Simulated Downhole Leaching of Formaldehyde from Proppants by High Performance Liquid Chromatography (Hplc), Headspace Gas Chromatography-Vacuum Ultraviolet (Hs-Gc-Vuv) Spectroscopy, and Headspace Gas Chromatography-Mass Spectrometry (Hs-Gc-Ms)*. *Environ Sci Process Impacts*, 2019. **21**(2): p. 214-223.
58. Qiu, C., et al., *Gas Chromatography-Vacuum Ultraviolet Detection for Classification and Speciation of Polychlorinated Biphenyls in Industrial Mixtures*. *J Chromatogr A*, 2017. **1490**: p. 191-200.
59. Cruse, C.A. and J.V. Goodpaster, *Generating Highly Specific Spectra and Identifying Thermal Decomposition Products Via Gas Chromatography / Vacuum Ultraviolet Spectroscopy (Gc/Vuv): Application to Nitrate Ester Explosives*. *Talanta*, 2019. **195**: p. 580-586.
60. Reiss, R., et al., *Evaluation and Application of Gas Chromatography - Vacuum Ultraviolet Spectroscopy for Drug- and Explosive Precursors and Examination of Non-Negative Matrix Factorization for Deconvolution*. *Spectrochim Acta A Mol Biomol Spectrosc*, 2019. **219**: p. 129-134.
61. Cruse, C.A., J. Pu, and J.V. Goodpaster, *Identifying Thermal Decomposition Products of Nitrate Ester Explosives Using Gas Chromatography-Vacuum Ultraviolet Spectroscopy: An Experimental and Computational Study*. *Appl Spectrosc*, 2020. **74**(12): p. 1486-1495.
62. Gramaglia, D., et al., *High Speed Dsc (Hyper-Dsc) as a Tool to Measure the Solubility of a Drug within a Solid or Semi-Solid Matrix*. *Int J Pharm*, 2005. **301**(1-2): p. 1-5.
63. McGregor, C. and E. Bines, *The Use of High-Speed Differential Scanning Calorimetry (Hyper-Dsc) in the Study of Pharmaceutical Polymorphs*. *Int J Pharm*, 2008. **350**(1-2): p. 48-52.
64. Tong, Y., R. Liu, and T. Zhang, *The Effect of a Detonation Nanodiamond Coating on the Thermal Decomposition Properties of Rdx Explosives*. *Phys Chem Chem Phys*, 2014. **16**(33): p. 17648-57.
65. Akhavan, J., *The Chemistry of Explosives*. 2 ed. 2004: The Royal Society of Chemistry.

66. Li, J.-S., et al., *Study on Thermal Characteristics of Tnt Based Melt-Cast Explosives*. Propellants, Explosives, Pyrotechnics, 2019. **44**(10): p. 1270-1281.
67. Abd-Elghany, M., A. Elbeih, and S. Hassanein, *Thermal Behavior and Decomposition Kinetics of Rdx and Rdx/Htpb Composition Using Various Techniques and Methods*. Central European Journal of Energetic Materials, 2016. **13**(3): p. 714-735.

## CHAPTER 5. A SYSTEMATIC STUDY OF THE ABSORBANCE OF THE NITRO FUNCTIONAL GROUP IN THE VACUUM UV REGION

Courtney A. Cruse, John V. Goodpaster\*

Department of Chemistry and Chemical Biology, Indiana University - Purdue University Indianapolis (IUPUI), 402 North Blackford Street LD326, Indianapolis, Indiana 46202, United States

### 5.1 Abstract

The nitro functional group ( $\text{NO}_2$ ) features strongly in compounds such as explosives, pharmaceuticals, and fragrances. However, its gas phase absorbance characteristics in the vacuum UV region (120 – 200 nm) have not been systematically studied. Gas chromatography/vacuum UV spectroscopy (GC/VUV) was utilized to study the gas phase VUV spectra of various nitrated compounds (*e.g.*, nitrate esters ( $-\text{R-O-NO}_2$ ), nitramines ( $\text{R-N-NO}_2$ ), nitroaromatics ( $\text{Ar-NO}_2$ ), and nitroalkanes ( $\text{R-NO}_2$ )). The nitro absorption maximum appeared over a wide range (170 – 270 nm) and its wavelength and intensity were highly dependent upon the structure of the rest of the molecule. For example, the nitroalkanes exhibited a trend in that the ratio of the relative absorption intensity between these two absorption features between the alkyl group ( $< 150$  nm) and the nitro group (200 nm) increases as the molecular weight increases. It was observed that the addition of multiple nitro functional groups on benzene or toluene resulted in an increase in intensity and blue shift from approximately 240 nm to 210 nm. Nitrate esters exhibited an absorption between 170 nm to 210 nm and absorbance increased with increasing nitrogen content. The relative diversity of the spectra obtained was analyzed by Principal Component Analysis (PCA) and Linear Discriminant Analysis (LDA). These calculations revealed that the spectra of all the compounds analyzed could be reliably differentiated without any misclassifications.

### 5.2 Introduction

Since the development of the benchtop vacuum ultraviolet spectrometer as a detector for gas chromatography, GC/VUV has been utilized to study a variety of compounds in several applications.[1] One key advantage of GC/VUV is its spectral range (120 - 430 nm), which

produces spectra that can differentiate compounds that are difficult or impossible to distinguish by mass spectrometry. Hence, there has been a focus in the literature on the discriminating power of GC/VUV in the analysis of structurally similar compounds and isomers.[2-17] Additionally, the differentiation of spectra based on structural classes has been studied. Most notably is attributing specific wavelength ranges to specific compound classes to create spectral filters (*i.e.*, aromatics, saturates, and di-olefins). This approach has been extended to the analysis and characterization of Paraffins, Isoparaffins, Olefins, Naphthenes and Aromatics (PIONA) in petroleum products.[18-20]

However, less has been written about differentiation of the same functional group or trends in spectra for different chemical structures.[21-23] To date, analysis of aromatic hydrocarbons in mineral oils,[24] organosilanes,[22] and alkanes[25] have revealed changes in VUV spectral features due to corresponding chemical structure changes. Other trends include a red shift with each of the following: increasing number of double bonds present,[26] increase in the number of aromatic rings,[5] and increase in the dihedral angle of polychlorinated biphenyls.[10] Additionally, the impact of silylation of cannabinoid spectra was also investigated in detail, attributing structural features (aromaticity, oxygenation, saturation/unsaturation) to specific wavelength ranges.[27] Similarly, GC/UV has been utilized to extensively characterize the UV spectra of various compounds; however, the minimum wavelength was limited to 168 nm.[28, 29] Furthermore, using GC/VUV to identify unknown compounds has been less explored. A recent publication was the first to establish simultaneous use of VUV, MS, and retention indices for untargeted analysis and classification of beer volatiles.[30]

In this work, the spectral characteristics of various nitrated compounds from differing structural classes (*i.e.*, nitrate esters, nitramines, nitroaromatics, and nitroalkanes) were investigated. Nitrated compounds are of interest in several areas of application including forensic science, environmental science, medicine, and flavors/fragrances.

Of the 24 compounds analyzed, only 11 have been analyzed by GC/VUV previously (Table 5.1). In addition, this is the first time that the mono-nitrotoluene structural isomers (2-nitrotoluene, 3-nitrotoluene, and 4-nitrotoluene) have been compared and differentiated by GC/VUV. The absorption band attributed to the nitro group was investigated for each structural class to assess its utility as a reliable marker. A figure characterizing the nitro group of nitroalkanes, nitrobenzenes, nitrotoluenes, and nitrate esters was also developed. Lastly, Principal Component Analysis (PCA)

and Linear Discriminant Analysis (LDA) were completed to further investigate spectral differences of nitroaromatic, nitrate ester and nitramine compounds. All 12 compounds analyzed were successfully discriminated via LDA with an 80:20 validation: training set with zero misclassifications.

Table 5.1 Summary of previously analyzed compounds via GC/VUV.

\*approximation of absorbance maximum.

<b>Compound</b>	<b>MW (g/mol)</b>	<b>Abs. Max (nm)</b>	<b>Ref</b>
Nitromethane	61.0	130.6	[31, 32]
Nitrobenzene	123.1	178.75	[33]
2-Nitrotoluene	137.1	182.8	[31, 32]
Ethylene Glycol Dinitrate	152.1	134.9±0.2	[7]
2,4-Dinitrobenzene	182.1	166.8	[31, 32]
2,6-Dinitrobenzene	182.1	174.6	[31, 32]
Isosorbide Mononitrate	191.1	<125*	[34]
RDX	222.1	120	[34]
Nitroglycerine	227.1	134.9±0.2	[7]
Isosorbide Dinitrate	236.1	130-140*	[34]
Pentaerythritol Tetranitrate	316.1	136.1±0.4	[7]

## 5.3 Materials and Methods

### 5.3.1 Chemicals

Nitroglycerine (1000 µg/mL in methanol), ethylene glycol dinitrate (1000 µg/mL in methanol), pentaerythritol tetranitrate (1000 µg/mL in methanol), EPA method 8330 calibration mix #1 (1000 µg/mL each in acetonitrile) and #2 (1000 µg/mL each in acetonitrile) were purchased from Restek. 2,3-dimethyl-2,3-dinitrobutane, musk xylene (1000 µg/ml in acetonitrile), nitromethane, nitroethane, and 1-nitropropane were purchased from Sigma-Aldrich. Isosorbide mononitrate was purchased from MEDCHEMEXPRESS LLC, isosorbide dinitrate was purchased from Cayman Chemical, and nitroquinoline was purchased from Santa Cruz Biotechnology.

Methanol (optima LC/MS), chloroform (stabilized HPLC grade), and acetonitrile (HPLC Grade) were purchased from Fischer Scientific.

### 5.3.2 Sample Preparation

A 1000 ppm standard of 2,3-dimethyl-2,3-dinitrobutane was prepared in methanol. 1000 ppm standards of isosorbide mononitrate and isosorbide dinitrate were each made by dissolving in chloroform. A 1000 ppm standard of nitroquinoline was created by dissolving in acetonitrile. Nitroglycerine, ethylene glycol dinitrate, pentaerythritol tetranitrate, EPA 8330 calibration mix #1 and #2, and musk xylene standards were analyzed as received. 1000 ppm standards of nitromethane, nitroethane, and 1-nitropropane were prepared in methanol.

### 5.3.3 Gas Chromatography

An Agilent 7890B series GC equipped with a multimode inlet and Agilent 7390 autosampler was utilized with hydrogen carrier gas at 3.2 mL/min and a splitless ramped inlet temperature program (50 °C ramped to 280 °C at 900 °C/min). A Restek Rtx®-5MS column (15 m x 0.32 mm x 0.25 µm) was utilized for analysis of the EPA 8330 and remaining compounds, other than the nitroalkanes. The EPA 8330 calibration mix 1 and 2 were analyzed with an oven program of 50 °C held for 2 min, ramped 10 °C/min to 170 °C then 20 °C/min to 240 °C. The remainder of the compounds (other than the nitroalkanes) were analyzed with a splitless injection and an oven program of 50 °C held for 0.5 min, ramped at 20 °C/min to 200 °C.

A flow rate of 2.5 mL/min was utilized for the nitroalkanes with a 5:1 split injection at 200°C and an HP-5MS UI column (30 m x 0.25 mm ID x 0.25 µm). An isothermal oven program of 45°C for 3 min was utilized to resolve nitromethane from the solvent front.

### 5.3.4 Vacuum Ultraviolet Spectroscopy

GC effluent was directed into a VUV Analytics VGA-101 VUV spectrometer. All experiments were run with a spectral range of 120 nm to 430 nm with a 4.5 Hz scan rate, nitrogen make-up gas at a pressure of 0.35 psi, and a deuterium lamp as the light source. Nitroalkane and nitroaromatic compounds were analyzed at a transfer line and flow cell temperature of 300 °C, while nitrate ester and nitramine compounds were analyzed at 200 °C due to their thermal

decomposition at higher temperatures.[7, 35] Spectra obtained for PCA and LDA analysis were obtained at a flow cell temperature of 300 °C.

### 5.3.5 Principal Component Analysis and Discriminant Analysis

JMP Pro 15 by SAS Institute was utilized to complete Principal Component Analysis (PCA) and Linear Discriminant Analysis (LDA). For PCA analysis, spectra were normalized via the square root of the sum of squares normalization. The spectra were then truncated to 120 nm - 300 nm. Five replicates of each compound were acquired. The first four principal components were utilized for LDA.

## 5.4 Results and Discussion

### 5.4.1 Nitroalkanes

The VUV spectra of four nitroalkanes are similar with absorption features around 200 nm and below 150 nm (Fig. 5.1). The ratio of the relative absorption intensity between these two absorption features ( $< 150 \text{ nm} / 200 \text{ nm}$ ) increases as the molecular weight increases ( $r = 0.81$ ). When compared to the VUV spectra of their corresponding alkanes (not shown), these spectra confirm that the contribution of the alkyl nitro group in gas phase VUV spectra is a single broad absorption that appears between 185 and 215 nm. This was confirmed previously via experimental and computational analysis of nitromethane as the  $\pi^* \leftarrow \pi$  transition associated with the nitro group.[36-38].

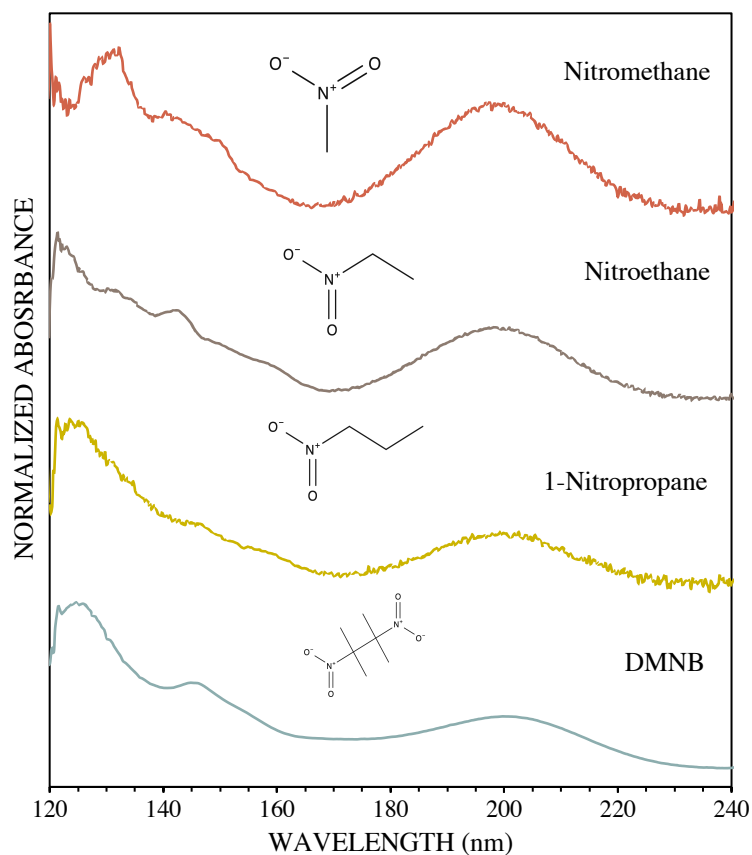


Figure 5.1. Nitroalkane VUV spectra at 300 °C.

## 5.4.2 Nitroaromatics

VUV spectra of the nitroaromatics are organized by similar structures (*i.e.*, nitrobenzenes (Fig. 5.2A), mononitrotoluenes (Fig. 5.2B), and di- and tri- nitrotoluenes (Figure 5.2C)). More complex structures that did not correspond to these categories are grouped into Fig. 5.2D.

In nitrobenzenes (Figure 5.2A), the nitro functional group generates a broad absorption around 240 nm. As additional nitro groups are added, this absorption increases in intensity and exhibits a blue shift, appearing at the shoulder of the absorption band at 210 nm in trinitrobenzene. This absorption band has been established for nitrobenzene as the  $\pi^* \leftarrow \pi$  charge transfer transition from the benzene ring to the nitro group.[39-42]

Mononitrotoluenes (Figure 5.2B) have a similar broad absorption between 240 and 250 nm. A decrease in the absorption intensity of the nitro group charge transfer for 2-nitrotoluene is observed. This is attributed to the ortho position of the nitro group to the methyl group that

sterically forces the nitro group out of plane and decreasing the energy of charge transfer state.[43-46] Similar to nitrobenzenes, as additional nitro groups are added to the toluene sub-structure (Figure 5.2C) the absorption increases in intensity and shifts to shorter wavelengths, appearing at 240 nm on the shoulder of the absorption band at 210 nm in 2,4,6-trinitrotoluene. The spectra of 2-amino-4,6-dinitrotoluene and 4-amino-2,6-dinitrotoluene became more complex with the addition of two nitro groups when compared to the VUV spectra of o-toluidine and p-toluidine (not shown), respectively. The nitrated VUV spectra of the toluidine compounds resulted in a more complex and broader absorption band around 215 nm due to increased overlapping of multiple absorption bands (Figure 5.2D).[47] Additionally, the presence of the nitro groups on musk xylene (2,4,6-trinitro-1,3-dimethyl-5-tert-butylbenzene) shifts the maximum absorbance to a slightly longer wavelength (198 nm for musk xylene) when compared to 5-tert-butyl-m-xylene (195 nm) (Figure 5.2C).[47]

Note that several compounds in this class exhibit EI mass spectra that are extremely similar (e.g., 2,4- and 2,6- dinitrotoluene[31] and 3- and 4- nitrotoluene). These compounds can be readily differentiated based upon their VUV spectra. This underscores the discriminating power of VUV spectroscopy as a detector for GC.

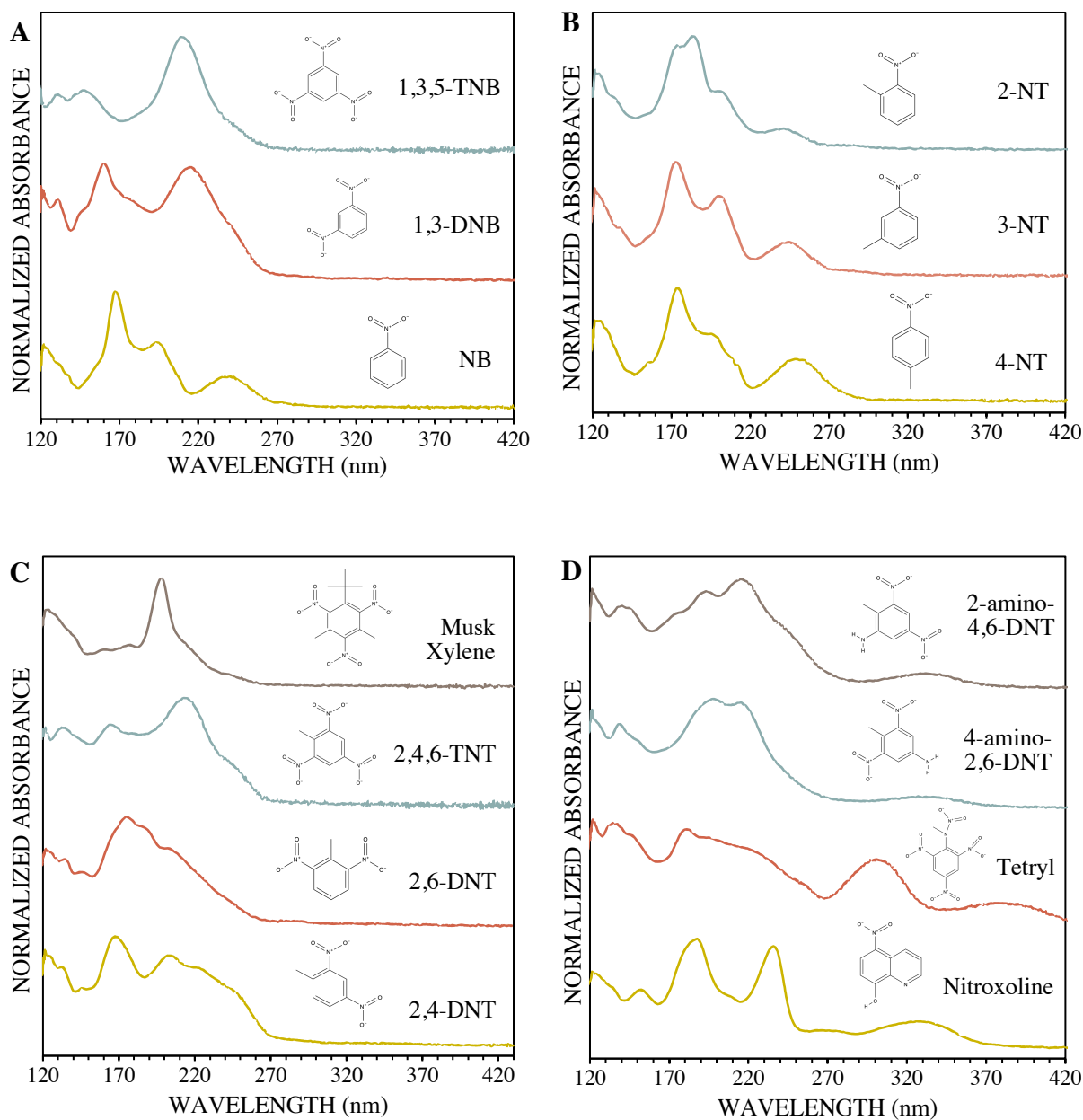


Figure 5.2. VUV spectra at 300 °C of nitroaromatic compounds. Compounds are grouped by parent structure: A) nitrobenzenes, B) mononitrotoluenes, C) di- and tri- nitrotoluenes, and D) more complex nitroaromatics, where TNT = trinitrotoluene, DNT = dinitrotoluene, NT = nitrotoluene, TNB = trinitrobenzene, DNB = dinitrobenzene, and NB = nitrobenzene.

### 5.4.3 Nitrate Esters and Nitramines

Analysis of nitrate ester and nitramine compounds at higher VUV transfer and flow cell temperatures (e.g. >250 °C) result in thermal decomposition.[7, 35] Therefore, these compounds were analyzed at 200 °C to obtain intact spectra to investigate the nitro group absorption band (Fig. 5.3). Compared to the corresponding alkanes for the nitrate ester explosives (EGDN, NG, and PETN), an absorption band was observed between 170 nm and 210 nm that was attributed to the nitro groups. Relative absorbance increased with increase in percent nitrogen content ( $r = 0.86$ ). Additionally, a blue shift is observed with the increase in nitro groups, except for isosorbide mononitrate. Isosorbide mononitrate has the lowest wavelength maximum for the nitro group absorbance, but has the lowest number of nitro groups (one nitro group). This could be due to differences in the chemical structure compared to the other nitrate esters (presence of a hydroxyl group), which could be investigated further in future work.

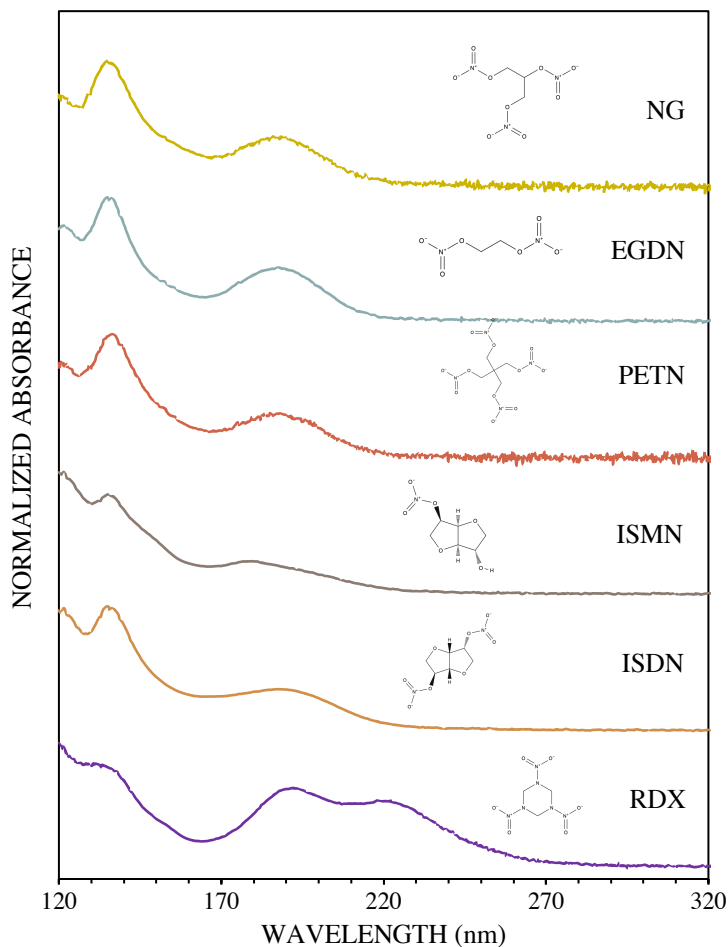


Figure 5.3. Nitrate ester and nitramine VUV intact spectra analyzed at 200 °C.

#### 5.4.4 PCA and DA

Compounds analyzed for PCA and LDA were analyzed at 300 °C to represent a realistic temperature encountered in realistic analyses (typical temperatures in literature are 275 °C). The first four principal components captured >90% of the total variance (the cumulative percent variance for the first four principal components were 68.75%, 81.25%, 88.23%, and 92.64%, respectively). Therefore, these four principal components were selected for LDA analysis.

Investigation of the factor loadings of the variables (the wavelength range from 125 nm to 240 nm) was utilized to understand the chemical differences of the compounds analyzed. Nitroaromatic compounds were distinguished from nitrate esters and nitramine compounds along principal component 1 (Fig. 5.4A). This also distinguished between intact compounds

(nitroaromatics) and decomposed compounds (nitrate esters and nitramine). Principal component 2 discriminated within functional groups in which it is observed that nitroaromatics di- and tri-nitrotoluene have an absorbance at ~220 nm while this is absent for mono-nitrotoluenes. This is due to an overlapping of absorption bands in the di- and tri- nitrotoluenes as the nitro group absorption band shifted to lower wavelengths. Additionally, separation of EGDN, NG, and PETN from RDX, ISMN, and ISDN is apparent along principal component 2 due to presence of formaldehyde in the decomposition spectra as well as a broader absorption band observed at <170 nm in the spectra of RDX, ISMN, and ISDN.

Utilizing an 80:20 validation, zero misclassifications were observed. Demonstrating clear discrimination between nitro compounds with similar chemical structures and the discriminating power of VUV (Fig. 5.4B).

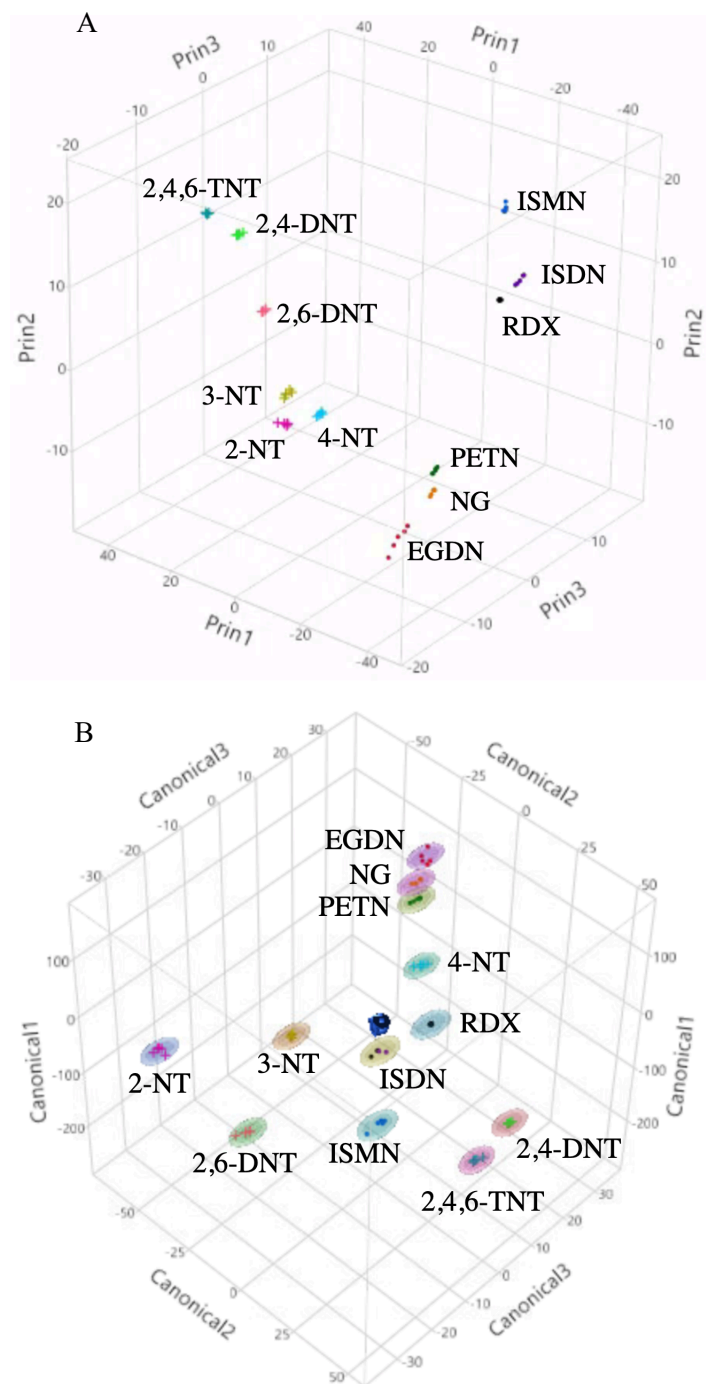


Figure 5.4. A. Three-dimensional factor score plot for five replicates of nitroaromatic, nitrate ester, and nitramine compounds. Cross markers denote nitroaromatic compounds while circle markers denote nitrate ester and nitramine compounds. B. Three-dimensional canonical plot for LDA based upon the first four principal components with 80:20 training:validation.

### 5.4.5 Nitro Group Absorption Classification

The nitro group absorption bands were investigated by structural class to establish structural information and potential for structural elucidation of unknown compounds (Figure 5). Nitrobenzenes and nitrotoluenes have nitro absorption band regions that are distinct from nitroalkanes and nitrate esters. However, nitrate esters and nitroalkanes overlap with nitroalkanes being slightly red shifted compared to the nitrate esters. Additionally, nitrobenzenes and nitrotoluenes overlap (to form a larger nitroaromatic group) with nitrobenzenes having a blue shift and narrower absorption band.

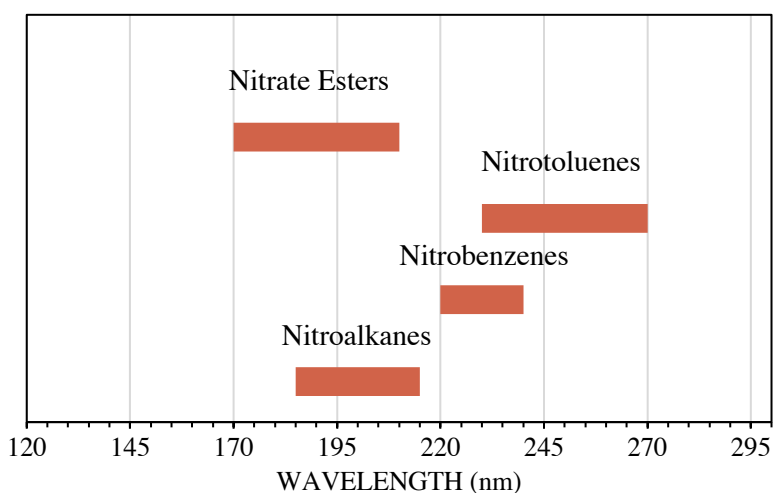


Figure 5.5. Absorption bands of the nitro group characterized by chemical structure.

## 5.5 Conclusions

Nitrated compounds were analyzed by GC/VUV to investigate the characteristic absorption of the nitro group in the wavelength region from 120 nm to 430 nm. Addition of nitro functional groups on benzene or toluene resulted in an increase in intensity and blue shift from approximately 240 nm to 210 nm for the nitro group absorption band. Nitroalkanes exhibited a trend in that the ratio of the relative absorption intensity between these two absorption features between the alkyl group (< 150 nm) and the nitro group (200 nm) increases as the molecular weight increases. In addition, the nitrate ester nitro group absorbs from 170 nm to 210 nm with an increased absorbance, relative to the primary absorption band, with the increase in percent nitrogen content. Analysis of the loading plots from PCA revealed differences based on the chemical structure of the compounds

with principal component 1 differentiating between nitroaromatics and nitrate ester and nitramine compounds, and principal component 2 differentiating EGDN, NG, and PETN from RDX, ISMN, and ISDN. Utilizing the first four principal components, LDA with an 80:20 validation resulted in successful discrimination of all compounds. Thus, further establishing the discriminating power of VUV to differentiate between nitrated compounds

## 5.6 Acknowledgements

This work was supported via a National Institute of Justice Award 2017-R2-CX- 0018 and 2018-R2-CX-0015. Opinions or points of view expressed here represent a consensus of the authors and do not necessarily represent the official position or policies of the U.S. Department of Justice.

The authors would like to acknowledge Robert E. Minto for insightful discussions and Payton West for contribution during sample preparation.

## 5.7 References

1. Schug, K.A., et al., *Vacuum Ultraviolet Detector for Gas Chromatography*. Anal. Chem. (Washington, DC, U. S.), 2014. **86**(16): p. 8329-8335.
2. Roberson, Z.R. and J.V. Goodpaster, *Differentiation of Structurally Similar Phenethylamines Via Gas Chromatography – Vacuum Ultraviolet Spectroscopy (Gc – Vuv)*. Forensic Chemistry, 2019: p. 100172.
3. Kranenburg, R.F., et al., *Distinguishing Drug Isomers in the Forensic Laboratory: Gc–Vuv in Addition to Gc–Ms for Orthogonal Selectivity and the Use of Library Match Scores as a New Source of Information*. Forensic Science International, 2019. **302**: p. 109900.
4. Hodgson, A. and J. Cochran, *Vacuum Ultraviolet Spectroscopy as a New Tool for Gc Analysis of Terpenes in Flavors and Fragrances*. Journal of AOAC International, 2019. **102**(2): p. 655-658.
5. Weber, B.M., P. Walsh, and J.J. Harynuk, *Determination of Hydrocarbon Group-Type of Diesel Fuels by Gas Chromatography with Vacuum Ultraviolet Detection*. Analytical Chemistry, 2016. **88**(11): p. 5809-5817.
6. Fan, H., et al., *Gas Chromatography-Vacuum Ultraviolet Spectroscopy for Analysis of Fatty Acid Methyl Esters*. Food Chem., 2016. **194**: p. 265-271.

7. Cruse, C.A. and J.V. Goodpaster, *Generating Highly Specific Spectra and Identifying Thermal Decomposition Products Via Gas Chromatography/Vacuum Ultraviolet Spectroscopy (Gc/Vuv): Application to Nitrate Ester Explosives*. *Talanta*, 2019. **195**: p. 580-586.
8. Fan, H., et al., *Gas Chromatography-Vacuum Ultraviolet Spectroscopy for Multiclass Pesticide Identification*. *J Chromatogr A*, 2015. **1389**: p. 120-7.
9. Fan, H., et al., *Gas Chromatography-Vacuum Ultraviolet Spectroscopy for Analysis of Fatty Acid Methyl Esters*. *Food Chem*, 2016. **194**: p. 265-71.
10. Qiu, C., et al., *Gas Chromatography-Vacuum Ultraviolet Detection for Classification and Speciation of Polychlorinated Biphenyls in Industrial Mixtures*. *J Chromatogr A*, 2017. **1490**: p. 191-200.
11. Buchalter, S., et al., *Gas Chromatography with Tandem Cold Electron Ionization Mass Spectrometric Detection and Vacuum Ultraviolet Detection for the Comprehensive Analysis of Fentanyl Analogues*. *Journal of Chromatography A*, 2019.
12. Kranenburg, R.F., et al., *Distinguishing Drug Isomers in the Forensic Laboratory: Gc-Vuv in Addition to Gc-Ms for Orthogonal Selectivity and the Use of Library Match Scores as a New Source of Information*. *Forensic Sci Int*, 2019. **302**: p. 109900.
13. Roberson, Z.R. and J.V. Goodpaster, *Differentiation of Structurally Similar Phenethylamines Via Gas Chromatography-Vacuum Ultraviolet Spectroscopy (Gc-Vuv)*. *Forensic Chemistry*, 2019. **15**: p. 100172.
14. Qiu, C., J. Smuts, and K.A. Schug, *Analysis of Terpenes and Turpentine Using Gas Chromatography with Vacuum Ultraviolet Detection*. *J Sep Sci*, 2017. **40**(4): p. 869-877.
15. Schenk, J., et al., *Analysis and Deconvolution of Dimethylnaphthalene Isomers Using Gas Chromatography Vacuum Ultraviolet Spectroscopy and Theoretical Computations*. *Anal Chim Acta*, 2016. **945**: p. 1-8.
16. Groger, T., et al., *A Vacuum Ultraviolet Absorption Array Spectrometer as a Selective Detector for Comprehensive Two-Dimensional Gas Chromatography: Concept and First Results*. *Anal Chem*, 2016. **88**(6): p. 3031-9.
17. Tanen, J.L., I.S. Lurie, and I. Marginean, *Gas Chromatography with Dual Cold Electron Ionization Mass Spectrometry and Vacuum Ultraviolet Detection for the Analysis of Phenylethylamine Analogues*. *Forensic Chemistry*, 2020. **21**: p. 100281.
18. Dunkle, M.N., et al., *Quantification of the Composition of Liquid Hydrocarbon Streams: Comparing the Gc-Vuv to Dha and Gcxgc*. *Journal of Chromatography A*, 2019. **1587**: p. 239-246.

19. Walsh, P., M. Garbalena, and K.A. Schug, *Rapid Analysis and Time Interval Deconvolution for Comprehensive Fuel Compound Group Classification and Speciation Using Gas Chromatography-Vacuum Ultraviolet Spectroscopy*. Anal. Chem. (Washington, DC, U. S.), 2016. **88**(22): p. 11130-11138.
20. Mao, J.X., et al., *Simulation of Vacuum Ultraviolet Absorption Spectra: Paraffin, Isoparaffin, Olefin, Naphthene, and Aromatic Hydrocarbon Class Compounds*. Appl Spectrosc, 2020. **74**(1): p. 72-80.
21. Bai, L., et al., *Comparison of Gc-Vuv, Gc-Fid, and Comprehensive Two-Dimensional Gc-Ms for the Characterization of Weathered and Unweathered Diesel Fuels*. Fuel, 2018. **214**: p. 521-527.
22. Qiu, C., et al., *Gas Chromatography-Vacuum Ultraviolet Spectroscopic Analysis of Organosilanes*. Talanta, 2021. **223**(Pt 2): p. 121781.
23. Garcia-Cicourel, A.R. and H.G. Janssen, *Direct Analysis of Aromatic Hydrocarbons in Purified Mineral Oils for Foods and Cosmetics Applications Using Gas Chromatography with Vacuum Ultraviolet Detection*. J Chromatogr A, 2019. **1590**: p. 113-120.
24. Garcia-Cicourel, A.R. and H.-G. Janssen, *Direct Analysis of Aromatic Hydrocarbons in Purified Mineral Oils for Foods and Cosmetics Applications Using Gas Chromatography with Vacuum Ultraviolet Detection*. J Chromatogr A, 2019. **1590**: p. 113-120.
25. Mao, J.X., P. Kroll, and K.A. Schug, *Vacuum Ultraviolet Absorbance of Alkanes: An Experimental and Theoretical Investigation*. Structural Chemistry, 2019.
26. Qiu, C., K.A. Schug, and J. Smuts, *Analysis of Terpenes and Turpentine Using Gas Chromatography with Vacuum Ultraviolet Detection*. J Sep Sci, 2017. **40**(4): p. 869-877.
27. Leghissa, A., et al., *Detection of Cannabinoids and Cannabinoid Metabolites Using Gas Chromatography with Vacuum Ultraviolet Spectroscopy*. Separation Science Plus, 2018. **1**(1): p. 37-42.
28. Lagesson, V., et al., *Identification of Compounds and Specific Functional Groups in the Wavelength Region 168-330 Nm Using Gas Chromatography with Uv Detection*. Journal of Chromatography A, 2000. **867**(1-2): p. 187-206.
29. Lagesson-Andrasko, L., V. Lagesson, and J. Andrasko, *The Use of Gas-Phase Uv Spectra in the 168-330 Nm Wavelength Region for Analytical Purposes. 1. Qualitative Measurements*. Analytical Chemistry, 1998. **70**(5): p. 819-826.
30. Zanella, D., et al., *Comparison of Headspace Solid-Phase Microextraction High Capacity Fiber Coatings Based on Dual Mass Spectrometric and Broadband Vacuum Ultraviolet Absorption Detection for Untargeted Analysis of Beer Volatiles Using Gas Chromatography*. Anal Chim Acta, 2021. **1141**: p. 91-99.

31. Reiss, R., et al., *Evaluation and Application of Gas Chromatography - Vacuum Ultraviolet Spectroscopy for Drug- and Explosive Precursors and Examination of Non-Negative Matrix Factorization for Deconvolution*. Spectrochim. Acta, Part A, 2019. **219**: p. 129-134.
32. Reiss, R., et al., *Supplementary Material: Evaluation and Application of Gas Chromatography - Vacuum Ultraviolet Spectroscopy for Drug- and Explosive Precursors and Examination of Non-Negative Matrix Factorization for Deconvolution*. Spectrochim Acta A Mol Biomol Spectrosc, 2019. **219**: p. 129-134.
33. Weston, C., et al., *Investigation of Gas Phase Absorption Spectral Similarity for Stable-Isotopically Labeled Compounds in the 125-240nm Wavelength Range*. Talanta, 2018. **177**: p. 41-46.
34. Cruse, C.A. and J.V. Goodpaster, *Thermal and Spectroscopic Analysis of Nitrated Compounds and Their Break-Down Products Using Gas Chromatography/Vacuum Uv Spectroscopy (Gc/Vuv)*. Anal Chim Acta, 2021. **1143**: p. 117-123.
35. Cruse, C.A., J. Pu, and J.V. Goodpaster, *Identifying Thermal Decomposition Products of Nitrate Ester Explosives Using Gas Chromatography-Vacuum Ultraviolet Spectroscopy: An Experimental and Computational Study*. Appl Spectrosc, 2020: p. 3702820915506.
36. Walker, I.C. and M.A.D. Fluendy, *Spectroscopy and Dynamics of Nitromethane (Ch3no2) and Its Anionic States*. International Journal of Mass Spectrometry, 2001. **205**(1-3): p. 171-182.
37. Flicker, W.M., O.A. Mosher, and A. Kuppermann, *Investigation of Low-Lying Electronic States in Nitromethane by Electron-Impact Spectroscopy*. Chemical Physics Letters, 1979. **60**(3): p. 518-522.
38. Bazin, M., et al., *Electron Induced Dissociation in the Condensed-Phase Nitromethane: Ii. Desorption of Neutral Fragments*. J Phys Condens Matter, 2010. **22**(8): p. 084003.
39. Krishnakumar, S., et al., *Experimental and Computational Studies on the Electronic Excited States of Nitrobenzene*. Journal of Quantitative Spectroscopy & Radiative Transfer, 2016. **184**: p. 89-99.
40. Kröhl, O., K. Malsch, and P. Swiderek, *The Electronic States of Nitrobenzene: Electron-Energy-Loss Spectroscopy and Caspt2 Calculations*. Physical Chemistry Chemical Physics, 2000. **2**(5): p. 947-953.
41. Nagakura, S., M. Kojima, and Y. Maruyama, *Electronic Spectra and Electronic Structures of Nitrobenzene and Nitromesitylene*. Journal of Molecular Spectroscopy, 1964. **13**(1-4): p. 174-192.
42. Ari, T., H. Guven, and N. Ecevit, *Electron-Energy-Loss Spectroscopy in Monosubstituted Benzenes*. Journal of Electron Spectroscopy and Related Phenomena, 1995. **73**(1): p. 13-23.

43. Brown, W.G. and H. Reagan, *Steric Effects in the Ultraviolet Absorption Spectra of Aromatic Nitro Compounds*. Journal of the American Chemical Society, 1947. **69**(5): p. 1032-1033.
44. Remington, W.R., *The Effects of Steric Inhibition of Resonance on Ultraviolet Absorption Spectra*. Journal of the American Chemical Society, 1945. **67**(10): p. 1838-1842.
45. Sherwood, D.W. and M. Calvin, *Resonance in Substituted Biphenyls*. Journal of the American Chemical Society, 1942. **64**(6): p. 1350-1353.
46. Clarkson, J., et al., *A Theoretical Study of the Structure and Vibrations of 2,4,6-Trinitrotoluene*. Journal of Molecular Structure, 2003. **648**(3): p. 203-214.
47. VUVAnalytics, *Vuv Spectral Database*. 2018: Austin, TX.

# CHAPTER 6. OPTIMIZATION OF GAS CHROMATOGRAPHY/VACUUM ULTRAVIOLET (GC/VUV) SPECTROSCOPY FOR EXPLOSIVE COMPOUNDS AND APPLICATION TO POST-BLAST DEBRIS

Courtney A. Cruse, John V. Goodpaster\*

Department of Chemistry and Chemical Biology, Indiana University - Purdue University Indianapolis (IUPUI), 402 North Blackford Street LD326, Indianapolis, Indiana 46202, United States

## 6.1 Abstract

A statistical optimization of gas chromatography/vacuum ultraviolet spectroscopy (GC/VUV) for the analysis of explosives has yet to be presented. In this work, a central composite design of experiments was utilized to optimize GC/VUV parameters for explosive and explosive related compounds such as triacetone triperoxide (TATP), dimethyldinitrobutane (DMNB), nitroglycerine (NG), diphenylamine (DPA), 2,4,6-trinitrotoluene (TNT), pentaerythritol tetranitrate (PETN), and cyclonite (RDX). Parameters optimized include the final temperature of a ramped multimode inlet program (200 °C), GC carrier gas flow rate (1.9 mL/min), and VUV make-up gas pressure (0.00 psi). The impact of transfer line/flow cell temperature was determined not to be statistically significant. Post-blast debris was successfully analyzed to illustrate applicability to forensic analysis of explosives. Relevant compounds in single- and double-base smokeless powders were successfully identified in post-blast fragments originating from PVC and steel pipes.

## 6.2 Introduction

The current “gold standard” for forensic analysis of post-blast residues of explosives is gas chromatography/mass spectrometry (GC/MS).[1] A vacuum ultraviolet (VUV) spectrometer for GC was developed in 2014.[2] Since then, research utilizing GC/VUV for explosives has demonstrated increased specificity of VUV, compared to MS, for distinguishing nitrate ester

explosives.[3] However, optimization of the GC/VUV system for explosive analysis has yet to be completed.

GC/VUV has been utilized to study a wide variety of compounds, such as hydrocarbons[4-7], drugs[8-13], explosives[3, 14-16], and pesticides [17]. However, full systematic optimization of both GC and VUV parameters is lacking. Previous GC/VUV optimization has been completed for analysis of ink photoinitiators in food packages[18] and illicit drugs[9]. Parameters optimized in these manuscripts include transfer line/flow cell temperature, make-up gas pressure, acquisition rate, and carrier gas flow rate. Transfer line/flow cell optimizations were investigated for impact on the VUV spectra and on peak areas, respectively. Both studies state an increase in peak area or intensity with lower make-up gas pressures. Furthermore, Roberson and Goodpaster (2020) utilized a response surface methodology (RSM) for optimization of the GC/VUV system.[9]

RSM is a statistical and mathematical approach to optimization that aims to optimize a response dependent on multiple parameters or variables.[19] When there are multiple responses, it becomes important to find the best compromise of the variables so that all responses are optimized.[20] In this work, a central composite design (CCD) was utilized for RSM optimization of multiple factors at three levels (high, medium, low) to obtain the ideal method for a variety of explosive compounds encountered in forensic science applications (*i.e.* triacetone triperoxide (TATP), 2,3-dimethyl-2,3-dinitrobutane (DMNB), nitroglycerine (NG), diphenylamine, 2,4,6-trinitrotoluene (TNT), pentaerythritol tetranitrate (PETN), and RDX). The response optimized was the chromatographic peak area to increase sensitivity and thus decrease the limits of detection. Parameters optimized include the final temperature of a ramped multimode inlet program (200 °C, 250 °C, and 300 °C), GC carrier gas flow rate (1.9 mL/min, 3.2 mL/min, and 4.5 mL/min), and VUV make-up gas pressure(0.00 psi, 0.15 psi, and 0.30 psi). Additionally, a “vary-one-parameter-at-a-time” approach was used to optimize the transfer line/flow cell temperature.

To date, this is the first reported optimization of GC/VUV for explosive analysis and subsequent application to post-blast debris.

## 6.3 Materials and Methods

### 6.3.1 Chemicals

Nitroglycerine (1 mg/ml in methanol), pentaerythritol tetranitrate (1 mg/ml in methanol) and RDX (1 mg/ml in methanol) were purchased from Restek as single component explosive standards. 2,4,6-trinitrotoluene was purchased from Omni Explosives and triacetone triperoxide (0.1 mg/ml in acetonitrile) was purchased from Accustandard. Diphenylamine was purchased from Acros Organic, 2,3-dimethyl-2,3-dinitrobutane from Sigma Aldrich, and methanol (GC Resolv®) and acetone (certified ACS) from Fisher Scientific. Smokeless powders (Alliant Red Dot and IMR 4046) were purchased locally.

### 6.3.2 Sample Preparation

Stock solutions of 10 ppm triacetone triperoxide (TATP) and 100 ppm 2,3-dimethyl-2,3-dinitrobutane (DMNB), nitroglycerine (NG), diphenylamine, 2,4,6-trinitrotoluene (TNT), pentaerythritol tetranitrate (PETN), and RDX were prepared in methanol. The final concentration of TATP was limited by the analytical standard concentration.

Seven calibrant concentrations from 5 ppm to 1000 ppm run were prepared in triplicate for the LOD study for DMNB, NG, diphenylamine, TNT, PETN and RDX. For TATP, the concentration ranged from 5 ppm to 100 ppm.

Four post-blast fragments were analyzed: PVC IMR 4064 (0.7 g), PVC Red Dot (1.1 g), steel IMR 4064 (1.2 g), and steel Red Dot (48.3 g). Post-blast PVC fragments were extracted with 1 mL of acetone and filtered with a PTFE 0.45 µL syringe filter prior to analysis by GC/VUV. Steel fragments were extracted with 1 mL of acetone, blown down to near dryness via Nitrogen and reconstituted in 100 µL acetone before filtered and analyzed.

### 6.3.3 Gas Chromatography/Vacuum Ultraviolet Spectroscopy

An Agilent 7890B series GC equipped with a multimode inlet and Agilent 7390 autosampler was utilized. The carrier gas was hydrogen and a spitless ramped inlet temperature program (50 °C ramped at 900 °C/min to various final temperatures) was used. A Restek Rtx®-5MS column (15

m x 0.32 mm x 0.25  $\mu$ m) was utilized for the design of experiments optimization study. The oven program utilized was 50 °C held for 0.5 min, ramped 20 °C/min to 200 °C.

A VUV Analytics VGA-101 VUV detector was utilized. All experiments were run with a spectral range of 125 nm to 430 nm with a 4.5 Hz scan rate, nitrogen make-up gas and a deuterium lamp as the light source. Make-up gas pressure and flow cell temperature were varied for the optimization.

#### **6.3.4 DOE**

JMP software was utilized to design a three factor, three level face-centered central composite design (FC-CCD) with five replicates and six center points. The three factors analyzed include flow cell make-up gas pressure (0.00 psi, 0.15 psi, and 0.30 psi), ramped multimode final inlet temperature (200 °C, 250 °C, and 300 °C), and GC flow rate (1.9 mL/min, 3.2 mL/min, and 4.5 mL/min). A randomized design was utilized. As the flow cell temperature is not controlled by the VUV or GC software, optimization of the VUV flow cell temperature was completed independently. Randomized triplicate measurements were taken for flow cell temperatures 200 °C, 220 °C, 240 °C, 260 °C, 280 °C, and 300 °C.

### **6.4 Results and Discussion**

#### **6.4.1 GC/VUV Analysis of Explosives**

Seven explosive and explosive related compounds with a variety of chemical structures were utilized for the optimization: nitrate esters, nitramines, nitroaromatics, nitroalkanes, and peroxide-based (Fig. 6.1). NG, PETN, and RDX thermally decompose in the transfer line/flow cell as indicated by fine structure of the VUV spectra at higher temperatures that is attributed to decomposition products.[3, 14, 15] TATP has been reported to also decompose utilizing GC/UV into acetone at elevated temperatures.[21] Fine structure in the TATP VUV spectrum at 140 nm, 153 nm, and 195 nm are consistent with that of acetone indicating thermal decomposition of TATP by GC/VUV.

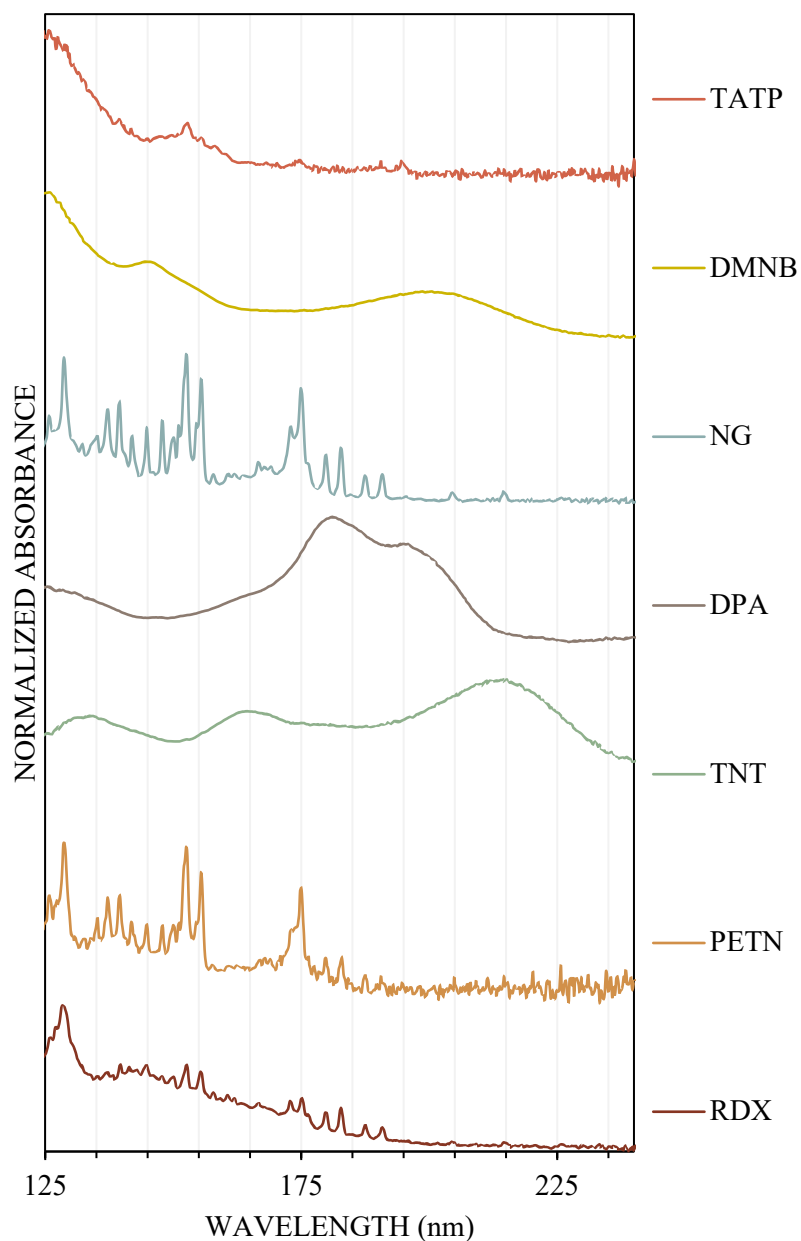


Figure 6.1. VUV spectra of seven explosive and explosive related compounds (TATP, DMNB, NG, diphenylamine (DPA), TNT, PETN, RDX) analyzed in DOE optimization with the following parameters: final ramped inlet temperature 200 °C, flow rate 1.9 mL/min, VUV make-up gas pressure 0.00 psi, and flow cell temperature 300 °C.

Chromatographic separation was achieved for all compounds (Fig. 6.2). Diphenylamine was observed to have the highest sensitivity with TATP and PETN having the lowest.

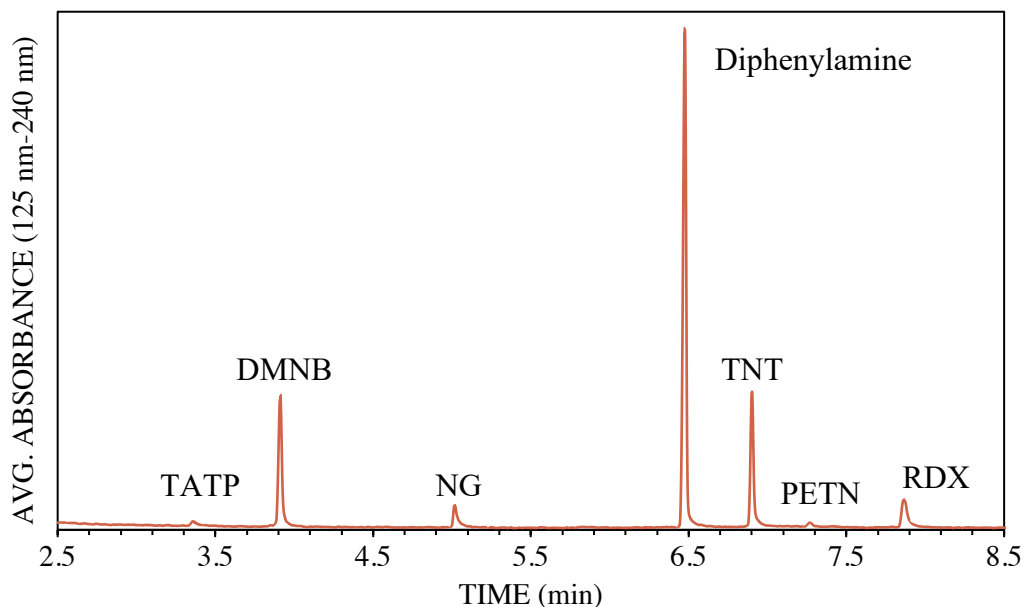


Figure 6.2. Chromatogram of stock solution with the following parameters: final ramped inlet temperature 200 °C, flow rate 1.9 mL/min, VUV make-up gas pressure 0.00 psi, and flow cell temperature 300 °C.

#### 6.4.2 Optimization Results

Utilizing JMP, the optimization parameters were obtained when considering increasing the peak area for all compounds and for each compound individually. The reported p values for variable and variable interactions are displayed in Table 6.1. Values that are not statistically significant are underlined. Example response surface plots for DMNB for variable interactions with statistical significance in Figure 6.3.

Table 6.1 JMP summary of variables and variable interaction p-values for all compounds and for each individual compound where flow rate=FR, make-up gas pressure=MGP. Underlined values are p-values >0.05, indicating variable/variable interactions are not statistically significant.

COMPOUND	FR	MGP	FINAL RAMPED INLET TEMP	FR * MGP	FR * INLET TEMP	MGP * INLET TEMP	FR * MGP * INLET TEMP
All	0.000	0.000	0.000	0.000	0.000	<u>0.061</u>	0.014
TATP	0.003	0.001	0.000	<u>0.416</u>	0.047	<u>0.138</u>	0.034
DMNB	0.000	0.000	0.000	0.000	0.000	<u>0.061</u>	0.014
NG	0.017	0.001	<u>0.264</u>	<u>0.124</u>	<u>0.527</u>	<u>0.371</u>	<u>0.452</u>
Diphenylamine	0.000	0.000	0.000	0.000	<u>0.882</u>	<u>0.910</u>	<u>0.504</u>
TNT	0.000	0.000	<u>0.072</u>	0.000	<u>0.076</u>	<u>0.148</u>	<u>0.390</u>
PETN	0.000	0.032	<u>0.588</u>	<u>0.663</u>	<u>0.696</u>	<u>0.702</u>	<u>0.912</u>
RDX	<u>0.287</u>	0.000	0.002	0.025	0.033	<u>0.270</u>	<u>0.255</u>

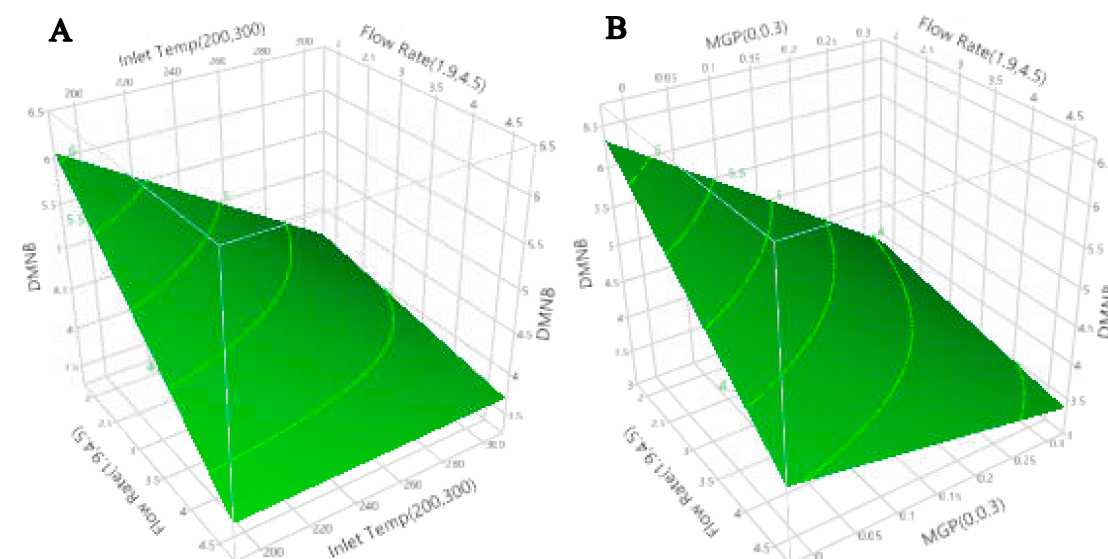


Figure 6.3. DMNB response surface plots for A) final ramped inlet temperature \* flow rate and B) make-up gas pressure \* flow rate.

A summary of the optimized parameters values is listed in Table 6.2. Utilizing the optimized parameters for all the compounds is advantageous if numerous explosive compounds are encountered. The individual parameters could be used to further improve sensitivity if a particular explosive compound is targeted. It was observed that, compounds that exhibit extensive thermal

decomposition in the transfer line/flow cell (NG and PETN) optimize to faster flow rates (4.5 mL/min). All other compounds optimize to the lower flow rate limit in the optimization.

Additionally, all compounds optimized to the lower instrumental limit of 0.00 psi make-up gas pressure. A previous VUV optimization study discouraged the use of 0.00 psi and recommended a make-up gas pressure of 0.10 psi to avoid contamination of the make-up gas line.[18] Of the statistically significant values, an optimized lower final ramped inlet temperature of 200 °C was determined for all compounds apart from diphenylamine which optimized to 300 °C.

Table 6.2 DOE Optimized parameters for all compounds and for each individual compound.  
\*Parameter is not statistically significant.

COMPOUND	FLOW RATE (ML/MIN)	MAKE-UP GAS PRESSURE (PSI)	FINAL RAMPED INLET TEMP (°C)	DESIRABILITY	SUMMARY OF FIT R <sup>2</sup>
All	2.4	0.00	200	0.566	-
TATP	1.9	0.00	200	0.426	0.719
DMNB	1.9	0.00	200	0.904	0.121
NG	4.5	0.00	200*	0.504	0.825
Diphenylamine	1.9	0.00	300	0.746	0.345
TNT	1.9	0.00	200*	0.701	0.520
PETN	4.5	0.00	300*	0.695	0.209
RDX	1.9*	0.00	200	0.737	0.232

Transfer line/flow cell temperature optimization results did not have statistical significance for varying temperatures. As higher temperatures provide increased specificity for thermally labile compounds, a transfer line/flow cell temperature of 300 °C was utilized for the optimized parameters.

### 6.4.3 Figures of Merit

A calibration curve was constructed for each compound with the optimized method (Table 3). The LOD, linear range, linearity, and sensitivity were determined utilizing the 125 nm to 240 nm wavelength range with a previously published method.[3] All compounds analyzed have a calculated LOD in the low ppm concentration range with NG and PETN having the higher LODs

(21.0 ppm and 12.3 ppm, respectively) and lower sensitivities (slopes of 0.4 ppm<sup>-1</sup> and 0.1 ppm<sup>-1</sup>, respectively).

Table 6.3 LOD, linear range, linearity (R<sup>2</sup>), and sensitivity (slope) of GC/VUV for all compounds utilizing the optimized method.

<b>Compound</b>	<b>Calculated LOD (ppm)</b>	<b>Linear Range (ppm)</b>	<b>R<sup>2</sup></b>	<b>Slope (ppm<sup>-1</sup>) x 1,000</b>
<b>TATP</b>	0.10	5-50	0.9943	0.7
<b>DMNB</b>	0.42	5-500	0.9916	1.1
<b>NG</b>	21.0	100-1000	0.9957	0.4
<b>Diphenylamine</b>	1.21	10-100	0.9899	5.4
<b>TNT</b>	1.66	10-250	0.9914	2.1
<b>PETN</b>	12.3	50-1000	0.9927	0.1
<b>RDX</b>	3.29	10-1000	0.9955	1.2

#### 6.4.4 Application to Post-Blast Debris

Post-blast debris were collected with the assistance of the Indiana State Police (ISP) Bomb Squad for realistic analysis of pipe bombs (PVC and steel) containing smokeless powders (SBSP and DBSP). Pipes were assembled and initiation by the ISP Bomb Squad in a 2 ft<sup>3</sup> perforated steel cube to contain the debris for more efficient collection.

GC/VUV analysis of PVC and steel post-blast fragments containing IMR 4046 SBSP (Fig. 6.4 A and B) detected 2,4-dinitrotoluene and diphenylamine (5.7 min and 6.1 min, respectively). The compound that eluted at 5.0 min in the PVC SBSP chromatogram was not identified in the VUV library but is not a relevant compound to this study. Analysis of Red Dot DBSP (Fig. 6.4 C and D) detected nitroglycerine and diphenylamine (4.7 min and 6.1 min, respectively). The DBSP PVC analysis also identified ethyl centralite (7.4 min) as the other relevant compound in Red Dot. The unlabeled compounds in the Steel DBSP chromatogram were identified as hydrocarbons originating from the petroleum jelly used on the endcap threads prior to initiation.

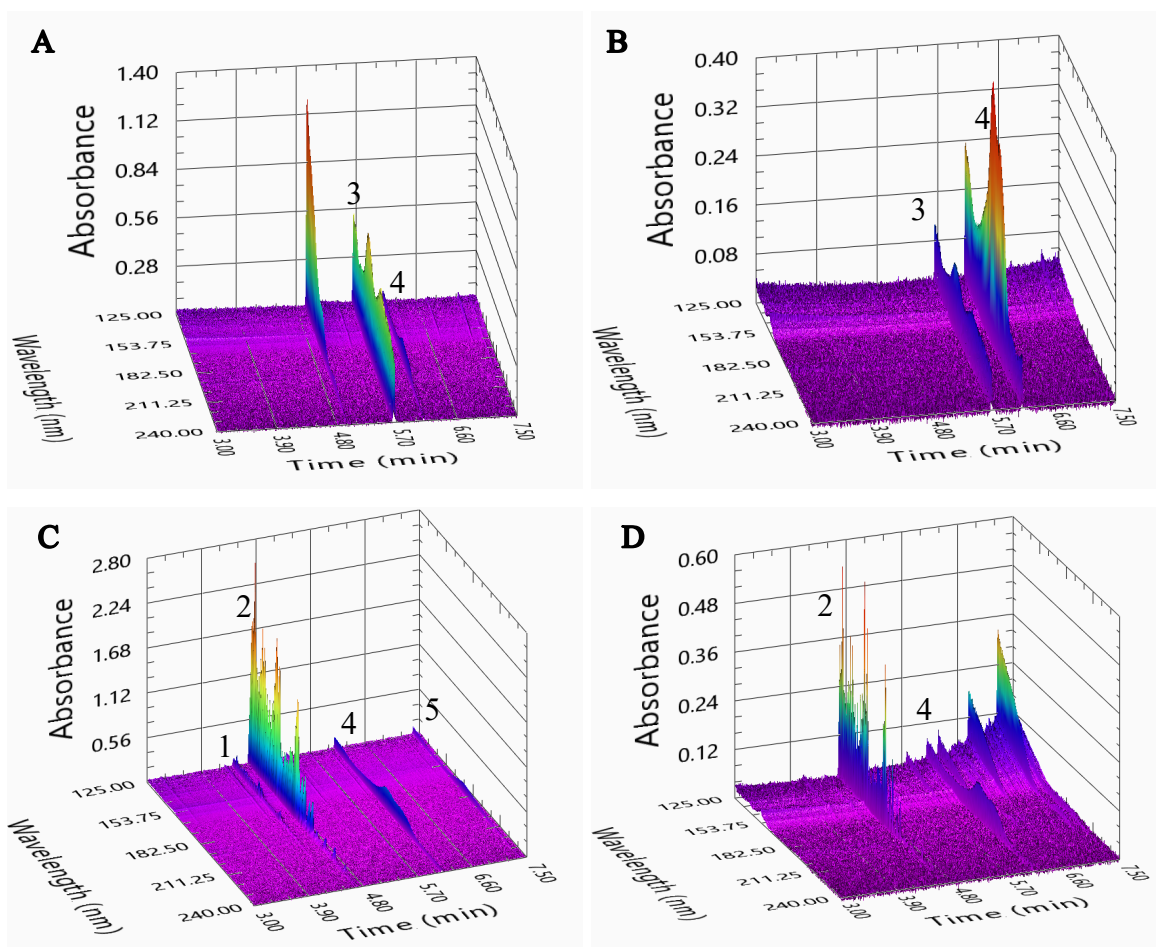


Figure 6.4. 3D chromatograms of post blast debris A) SBSP in PVC, B) SBSP in steel, C) DBSP in PVC, and D) DBSP in steel. 1) NG decomposition product, 2) NG, 3) 2,4-dinitrotoluene, 4) diphenylamine, and 5) ethyl centralite.

## 6.5 Conclusions

A CCD design of experiments was utilized to optimize GC/VUV parameters for analysis of explosives. Explosive and explosive related compounds included in the optimization include TATP, DMNB, NG, diphenylamine, TNT, PETN, and RDX. The optimized parameters were a GC flow rate of 1.9 mL/min, make-up gas pressure of 0.00 psi, and final ramped inlet temperature of 200 °C. Transfer line/flow cell temperature was determined not to be statistically significant, thus 300 °C was utilized as the optimized temperature for increased specificity.

Additionally, the optimized method was applied to post-blast debris to illustrate realistic application of GC/VUV for post-blast debris analysis. Relevant compounds in SBSP and DBSP were successfully identified in fragments originating from PVC and steel pipes.

## 6.6 Acknowledgements

This work was supported via a National Institute of Justice Award 2017-R2-CX- 0018 and 2018-R2-CX-0015. Opinions or points of view expressed here represent a consensus of the authors and do not necessarily represent the official position or policies of the U.S. Department of Justice.

## 6.7 References

1. Beveridge, A., *Forensic Investigation of Explosions. Chapter 11 Investigation of Pipe Bombs*. 2011, Taylor & Francis. p. 429-491.
2. Schug, K.A., et al., *Vacuum Ultraviolet Detector for Gas Chromatography*. *Anal Chem*, 2014. **86**(16): p. 8329-35.
3. Cruse, C.A. and J.V. Goodpaster, *Generating Highly Specific Spectra and Identifying Thermal Decomposition Products Via Gas Chromatography / Vacuum Ultraviolet Spectroscopy (Gc/Vuv): Application to Nitrate Ester Explosives*. *Talanta*, 2019. **195**: p. 580-586.
4. Hodgson, A. and J. Cochran, *Vacuum Ultraviolet Spectroscopy as a New Tool for Gc Analysis of Terpenes in Flavors and Fragrances*. *J AOAC Int*, 2019. **102**(2): p. 655-658.
5. Qiu, C., J. Smuts, and K.A. Schug, *Analysis of Terpenes and Turpentine Using Gas Chromatography with Vacuum Ultraviolet Detection*. *J Sep Sci*, 2017. **40**(4): p. 869-877.
6. Weber, B.M., P. Walsh, and J.J. Harynuk, *Determination of Hydrocarbon Group-Type of Diesel Fuels by Gas Chromatography with Vacuum Ultraviolet Detection*. *Anal Chem*, 2016. **88**(11): p. 5809-17.
7. Schenk, J., et al., *Analysis and Deconvolution of Dimethylnaphthalene Isomers Using Gas Chromatography Vacuum Ultraviolet Spectroscopy and Theoretical Computations*. *Anal Chim Acta*, 2016. **945**: p. 1-8.
8. Roberson, Z.R. and J.V. Goodpaster, *Differentiation of Structurally Similar Phenethylamines Via Gas Chromatography-Vacuum Ultraviolet Spectroscopy (Gc-Vuv)*. *Forensic Chemistry*, 2019. **15**: p. 100172.
9. Roberson, Z.R. and J.V. Goodpaster, *Optimization of the Qualitative and Quantitative Analysis of Cocaine and Other Drugs of Abuse Via Gas Chromatography - Vacuum Ultraviolet Spectrophotometry (Gc - Vuv)*. *Talanta*, 2021. **222**: p. 121461.
10. Roberson, Z.R., H.C. Gordon, and J.V. Goodpaster, *Instrumental and Chemometric Analysis of Opiates Via Gas Chromatography-Vacuum Ultraviolet Spectrophotometry (Gc-Vuv)*. *Anal Bioanal Chem*, 2020. **412**(5): p. 1123-1128.

11. Kranenburg, R.F., et al., *Distinguishing Drug Isomers in the Forensic Laboratory: Gc-Vuv in Addition to Gc-Ms for Orthogonal Selectivity and the Use of Library Match Scores as a New Source of Information*. Forensic Sci Int, 2019. **302**: p. 109900.
12. Buchalter, S., et al., *Gas Chromatography with Tandem Cold Electron Ionization Mass Spectrometric Detection and Vacuum Ultraviolet Detection for the Comprehensive Analysis of Fentanyl Analogues*. J Chromatogr A, 2019. **1596**: p. 183-193.
13. Tanen, J.L., I.S. Lurie, and I. Marginean, *Gas Chromatography with Dual Cold Electron Ionization Mass Spectrometry and Vacuum Ultraviolet Detection for the Analysis of Phenylethylamine Analogues*. Forensic Chemistry, 2020. **21**: p. 100281.
14. Cruse, C.A. and J.V. Goodpaster, *Thermal and Spectroscopic Analysis of Nitrated Compounds and Their Break-Down Products Using Gas Chromatography/Vacuum Uv Spectroscopy (Gc/Vuv)*. Anal Chim Acta, 2021. **1143**: p. 117-123.
15. Cruse, C.A., J. Pu, and J.V. Goodpaster, *Identifying Thermal Decomposition Products of Nitrate Ester Explosives Using Gas Chromatography-Vacuum Ultraviolet Spectroscopy: An Experimental and Computational Study*. Appl Spectrosc, 2020. **74**(12): p. 1486-1495.
16. Reiss, R., et al., *Evaluation and Application of Gas Chromatography - Vacuum Ultraviolet Spectroscopy for Drug- and Explosive Precursors and Examination of Non-Negative Matrix Factorization for Deconvolution*. Spectrochim Acta A Mol Biomol Spectrosc, 2019. **219**: p. 129-134.
17. Fan, H., et al., *Gas Chromatography-Vacuum Ultraviolet Spectroscopy for Multiclass Pesticide Identification*. J Chromatogr A, 2015. **1389**: p. 120-7.
18. Pechancova, R., et al., *Comparative Study of Ink Photoinitiators in Food Packages Using Gas Chromatography with Vacuum Ultraviolet Detection and Gas Chromatography with Mass Spectrometry*. J Sep Sci, 2019. **42**(2): p. 556-565.
19. Montgomery, D., *Design and Analysis of Experiments*. 6 ed. 2005: John Wiley & Sons, Inc.
20. Bradley, N., *The Response Surface Methodology*, in *Department of Mathematical Sciences*. 2007, Indiana University.
21. Andrasko, J., et al., *Analysis of Explosives by Gc-Uv*. J Forensic Sci, 2017. **62**(4): p. 1022-1027.

## CHAPTER 7. FUTURE DIRECTIONS

### 7.1 Solid Phase Microextraction (SPME) GC/VUV

Solid phase microextraction (SPME) is a sample introduction technique for GC that allows for automated sample preconcentration and introduction onto the GC column. SPME uses a fiber coated in a sorption phase to adsorb analytes from the sample vial (through headspace or direct immersion) which reduces the use of solvents and matrix effects. The analytes are then eluted onto the column by thermal desorption.[1, 2] This results in simplified sample preparation, reduced analysis times, reduced cost from the elimination of solvents, and lower detection limits which are advantageous to trace analysis of post-blast debris.[3] Fiber chemistries studied for explosive analysis include polydimethylsiloxane (PDMS) [4, 5], PDMS-divinylbenzene (DVB) [6], Carbowax-DVB (CW-DVB) [3, 7], Polyethylene glycol (PEG),[8, 9] and polyacrylate resin [10].

A more recent development is a high capacity SPME fiber known as the SPME Arrow. The SPME Arrow is a large volume SPME fiber that has improved robustness and sensitivity.[1, 11] The SPME Arrow design has a stabilizing stainless steel rod coated in the sorption phase and a tip that improves that improves the robustness (Fig. 6.1).[2] Additionally, the larger stationary phase volumes compared to traditional SPME fibers translates to an increase in analyte mass on column and lower limits of detection.[1] Marketed as having an approximately 4x increase in response for volatile compounds and approximately 2x increase for semi-volatile compounds.[1]

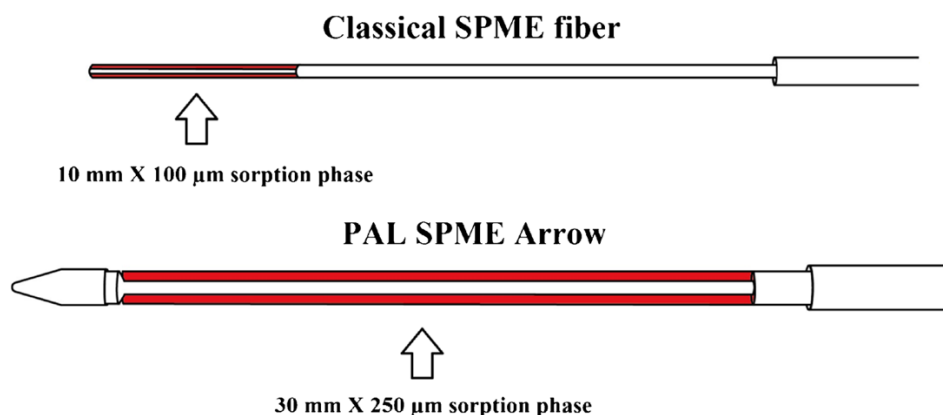


Figure 7.1. Comparison of traditional SPME fiber and SPME Arrow fiber.[2]

To date, research in GC/VUV has been limited in utilization of SPME with only one published manuscript using SPME Arrow for the analysis of volatile organic compounds in beer.[12] An interesting research direction would be to explore the utilization of SPME and/or SPME Arrow for the analysis of explosives and their post-blast debris by GC/VUV. Of interest is comparison of liquid injection and SPME to determine the technique that achieves superior limits of detection. This would involve investigation of the ideal fiber chemistry for explosive analysis by GC/VUV. Previous research by GC/MS suggests a PDMS or PDMS-DVB fibers provide improved sample extraction for explosive compounds. A limitation to SPME Arrow is the lack of fiber chemistry variety compared to traditional fibers. Therefore, investigation of CW-DVB would be limited to traditional fibers only. Furthermore, optimization of the adsorption time, adsorption temperature, desorption time, and desorption temperature could further improve sensitivity.

## **7.2 Total Vaporization-SPME GC/VUV**

Compared to traditional SPME methods (headspace and direct immersion SPME), total vaporization (TV)-SPME completely vaporizes the sample (Fig. 6.2).[13] TV-SPME eliminates the partitioning of the analyte between the liquid sample and headspace resulting in only a two-phase system (the analyte vapor phase and SPME fiber).[13-16] With TV-SPME, the extraction temperature and sample volume are of most importance in optimizing the method.[13] Previous research has applied TV-SPME as a sampling method for post-blast debris analysis of smokeless powders in steel and PVC pipes.[8, 9, 17] TV-SPME was compared to liquid injection for these pipe bomb studies analysis with the conclusion that TV-SPME was an order of magnitude more sensitive than liquid injection.[8, 9] However, TV-SPME was not compared to headspace SPME to determine if one is more sensitive for the analysis of explosive compounds. The only published comparison between these techniques found TV-SPME as more sensitive when compared to headspace SPME and direct immersion SPME for gamma-butyrolactone (GBL) in water.[18] Therefore, it would be advantageous to determine how TV-SPME compares to headspace and/or direct immersion SPME for analysis of explosive compounds. Additionally, TV-SPME has yet to be investigated with GC/VUV. It is anticipated that the higher sensitivity of TV-SPME sample introduction method and the higher specificity observed with GC/VUV will be ideal for analysing extraction of post-blast debris originating from pipe bombs.

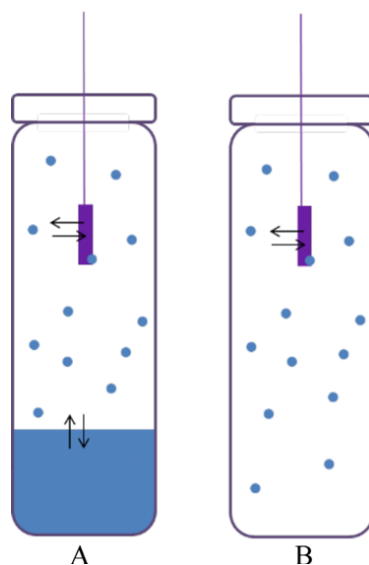


Figure 7.2. Comparison of (A) headspace SPME and (B) total vaporization SPME. [13]

It would also be of interest to investigate how SPME Arrow behaves with total vaporization and how it compares to headspace SPME Arrow, TV-SPME, and headspace SPME. To date, there are no manuscripts detailing TV-SPME Arrow. It is anticipated that the optimization parameters for the SPME Arrows for total vaporization would differ than those optimized for traditional SPME fibers. Optimization parameters would be the sample volume, fiber chemistry, adsorption time, adsorption temperature, desorption time, and desorption temperature.

Based on preliminary data, adsorption temperature and desorption time are significant. Adsorption temperatures investigated include 100 °C, 125 °C, and 150 °C. At 100 °C early eluting explosives (e.g., EGDN, DMNB, NG, DNT) are present in the chromatogram but PETN and RDX were not. However, increasing the temperature to 125 °C and 150 °C allowed detection of PETN and RDX; however, at 150 °C EGDN and DMNB peak area began to decrease significantly. Additionally, decreasing desorption time (from 60 s to 6 s) improved chromatographic performance. Tailing was reduced and peaks were more symmetrical allowing for improved quantification.

### 7.3 Analysis of High Explosives in Soil

Research encompassed in this dissertation includes analysis of low and high explosives by GC/VUV. However, application to post-blast debris of high explosives has not been investigated. Further research into this is of interest to establish GC/VUV as a viable forensic science laboratory

instrument for both low and high explosives in post-blast debris. Unlike low explosives, high explosives do not require containment for detonation to occur. Therefore, it is forensically relevant to detect and identify trace explosive material in soils.

Analysis of soil can be analyzed by liquid injection or by SPME. Liquid injection require sample preparation steps prior to analysis: extraction (with acetonitrile, acetonitrile/dichloromethane, or acetonitrile/methanol), sonication, and filtration.[19-22] This is time consuming and has the potential for loss of analyte in the extraction.[21, 23] SPME methods previously published require converting the soil sample into an aqueous solution.[23, 24] To overcome drawbacks from each of these methods, a solid sample placed in the vial can be analyzed by headspace SPME. Previous research studied SPME analysis of solid soil sample with the addition of water to aid in extraction.[23] However, varying the volume of water added had little impact on extraction. Analysis without the addition of water was not conducted. This would be of interest to investigate if soil samples could be analyzed “as is.” This would eliminate the need for sample preparation and use of solvent making it an ideal sample introduction technique for soil analysis.

Using SPME GC/VUV, a variety of soil types should be investigated with concentrations of explosive compounds down to low ng/g level to establish the ability of GC/VUV to detect and identify analytes at levels encountered in post-blast soil samples. Optimization of extraction temperature/time and desorption temperature/time.

#### **7.4 Analysis of Inorganic Explosives by GC/VUV**

All explosive compounds discussed thus far are organic compounds. However, inorganic explosives, such as ammonium nitrate and black powder, are of interest as they are used in improvised explosive devices (IEDs). The sensitivity and selectivity of GC/MS and its routine use in forensic science laboratories analysis of complex mixtures and trace analysis makes this technique ideal for inorganic explosive analysis.[25] In order to analyse inorganic explosives by GC, compounds must be derivatized to form more volatile compounds. This has been investigated in literature for analysis of several inorganic compounds (ammonium nitrate, black powder/black powder substitutes, and chlorate/sugar mixtures).

However, analysis by GC/VUV is of interest as it has been predicted that derivatization can decrease the LOD of drugs.[26] Upon derivatization, the resulting change in chemical structure

changes the excitation energy of the molecule and impacts the observed VUV spectra.[26] A future direction would be to investigate how the derivatization of inorganic explosives impacts analysis by GC/VUV and how it compares to GC/MS.

**Ammonium Nitrate.** Ammonium nitrate is a fertilizer explosive that has two main approaches for derivatization: derivatization of ammonia and derivatization of nitrate ions. Derivatization agents for ammonia include butyl chloroformate,[27-30] ethyl chloroformate,[30] and methyl chloroformate[30]. Conversely, inorganic anions can be derivatized to form pentafluorobenzyl derivatives with several derivatizing agents to be analyzed by GC. Derivatization of the nitrate ion has previously been accomplished with *t*-butylbenzene to form mono- or dinitro derivatives.[31]. The drawback of derivatization of the nitrate ion is there is not a way to discriminate ammonium nitrate and urea nitrate due to formation of the same anion derivatives. This lends itself to derivatization of ammonia and urea for differentiation.

**Black Powder and Black Powder Substitutes.** Black powder and black powder substitutes are low explosives used in IEDs. Black powder mainly consists of sulfur, potassium nitrate and charcoal.[32] Black powder substitutes differ in that they contain less or no sulfur and other components such as potassium perchlorate, sodium benzoate, dicyandiamide (DCDA), benzoic acid, and 3-nitrobenzoic acid.[25] Nitrate ions, sulfur, and thiocyanate ( $\text{SCN}^-$ ) ions (products of black powder combustion) have been identified by derivatization with 2,3,4,5,6-pentafluorobenzyl bromide PFB-Br in black powder residues.[32] Additionally, components of black powder substitutes have been derivatized with N,O-bis(trimethylsilyl)trifluoroacetamide (BSTFA) with 1% trimethylchlorosilane (TMCS) derivatization agent for form TMCS derivatives and with N,O-bis(trimethylsilyl)acetamide (BSA) used to form trimethylsilyl (TMS) derivatives.[25, 33]

**Chlorates and Perchlorates.** Chlorate/sugar mixtures are a homemade explosive used in IEDs in which the sugar acts as the fuel and the chlorate as the oxidizer (potassium or sodium chlorates). Potassium chlorate/sucrose mixture has been analyzed by GC/MS by forming the TMS derivative.[34] Additionally, identification of potassium chlorate has been accomplished by derivatizing chloride in the headspace by derivatization with propylene oxide.[35]

In conclusion, by analysis of inorganic explosives by GC/VUV, the limits of detection for sensitivity compared to GC/MS and spectral differentiation for specificity the VUV spectra could be a future direction of research. Additionally, optimization of derivatizing agents and SPME derivatization could be investigated. It would be of interest to investigate a variety of derivatizing

agents and the resulting impact on the VUV spectra and limits of detection. On fiber derivatization using SPME would also be an avenue to investigate as this would aid in further decreasing the limits of detection and simplifying the sample preparation.[28, 30]

## 7.5 References

1. Herrington, J.S., et al., *Hunting Molecules in Complex Matrices with Spme Arrows: A Review*. Separations, 2020. **7**(1): p. 12.
2. Kremser, A., M.A. Jochmann, and T.C. Schmidt, *Pal Spme Arrow--Evaluation of a Novel Solid-Phase Microextraction Device for Freely Dissolved Pahs in Water*. Anal Bioanal Chem, 2016. **408**(3): p. 943-52.
3. Furton, K.G., et al., *Application of Solid-Phase Microextraction to the Recovery of Explosives and Ignitable Liquid Residues from Forensic Specimens*. J Chromatogr A, 2000. **885**(1-2): p. 419-32.
4. Huang, S.D., C.P. Cheng, and Y.H. Sung, *Determination of Benzene Derivatives in Water by Solid-Phase Microextraction*. Analytica Chimica Acta, 1997. **343**(1-2): p. 101-108.
5. Harper, R., J. Almirall, and K. Furton, *Discrimination of Smokeless Powders by Headspace Spme-Gc-Ms and Spme-Gc-Ecd, and the Potential Implications Upon Training Canine Detection of Explosives*. Defense and Security. Vol. 5778. 2005: SPIE.
6. Darrach, M.R., A. Chutjian, and G.A. Plett, *Trace Explosives Signatures from World War Ii Unexploded Undersea Ordnance*. Environmental Science & Technology, 1998. **32**(9): p. 1354-1358.
7. Barshick, S.A. and W.H. Griest, *Trace Analysis of Explosives in Seawater Using Solid-Phase Microextraction and Gas Chromatography Ion Trap Mass Spectrometry*. Analytical Chemistry, 1998. **70**(14): p. 3015-3020.
8. Bors, D. and J. Goodpaster, *Mapping Smokeless Powder Residue on Pvc Pipe Bomb Fragments Using Total Vaporization Solid Phase Microextraction*. Forensic Sci Int, 2017. **276**: p. 71-76.
9. Bors, D. and J. Goodpaster, *Mapping Explosive Residues on Galvanized Pipe Bomb Fragments Using Total Vaporization Solid Phase Microextraction (Tv-Spme)*. Analytical Methods, 2015. **7**(23): p. 9756-9762.
10. Kirkbride, K.P., G. Klass, and P.E. Pigou, *Application of Solid-Phase Microextraction to the Recovery of Organic Explosives*. J Forensic Sci, 1998. **43**(1): p. 76-81.
11. Helin, A., et al., *Solid Phase Microextraction Arrow for the Sampling of Volatile Amines in Wastewater and Atmosphere*. J Chromatogr A, 2015. **1426**: p. 56-63.

12. Zanella, D., et al., *Comparison of Headspace Solid-Phase Microextraction High Capacity Fiber Coatings Based on Dual Mass Spectrometric and Broadband Vacuum Ultraviolet Absorption Detection for Untargeted Analysis of Beer Volatiles Using Gas Chromatography*. Anal Chim Acta, 2021. **1141**: p. 91-99.
13. Rainey, C.L., D.E. Bors, and J.V. Goodpaster, *Design and Optimization of a Total Vaporization Technique Coupled to Solid-Phase Microextraction*. Anal Chem, 2014. **86**(22): p. 11319-25.
14. Li, H., et al., *Rapid Determination of Ethanol in Fermentation Liquor by Full Evaporation Headspace Gas Chromatography*. J Chromatogr A, 2009. **1216**(1): p. 169-72.
15. Schuberth, J., *A Full Evaporation Headspace Technique with Capillary Gc and Itd: A Means for Quantitating Volatile Organic Compounds in Biological Samples*. J Chromatogr Sci, 1996. **34**(7): p. 314-9.
16. Ochiai, N., et al., *Full Evaporation Dynamic Headspace and Gas Chromatography-Mass Spectrometry for Uniform Enrichment of Odor Compounds in Aqueous Samples*. J Chromatogr A, 2012. **1240**: p. 59-68.
17. Sauzier, G., et al., *Optimisation of Recovery Protocols for Double-Base Smokeless Powder Residues Analysed by Total Vaporisation (Tv) Spme/Gc-Ms*. Talanta, 2016. **158**: p. 368-374.
18. Davis, K.E. and J.V. Goodpaster, *Gas Chromatography-Mass Spectrometry Paired with Total Vaporization Solid-Phase Microextraction as a Forensic Tool*. Jove-Journal of Visualized Experiments, 2021(171).
19. Walsh, M.E., *Determination of Nitroaromatic, Nitramine, and Nitrate Ester Explosives in Soil by Gas Chromatography and an Electron Capture Detector*. Talanta, 2001. **54**(3): p. 427-38.
20. Jenkins, T.F. and C.L. Grant, *Comparison of Extraction Techniques for Munitions Residues in Soil*. Analytical Chemistry, 1987. **59**(9): p. 1326-1331.
21. Holmgren, E., S. Ek, and A. Colmsjo, *Extraction of Explosives from Soil Followed by Gas Chromatography-Mass Spectrometry Analysis with Negative Chemical Ionization*. J Chromatogr A, 2012. **1222**: p. 109-15.
22. Campbell, S., et al., *Trace Analysis of Explosives in Soil: Pressurized Fluid Extraction and Gas and Liquid Chromatography-Mass Spectrometry*. J Chromatogr Sci, 2003. **41**(6): p. 284-8.
23. Mayfield, H.T., E. Burr, and M. Cantrell, *Analysis of Explosives in Soil Using Solid Phase Microextraction and Gas Chromatography*. Analytical letters, 2006. **39**(7): p. 1463-1474.
24. Halasz, A., et al., *Detection of Explosives and Their Degradation Products in Soil Environments*. Journal of Chromatography A, 2002. **963**(1-2): p. 411-418.

25. Routon, B.J., B.B. Kocher, and J.V. Goodpaster, *Discriminating Hodgdon Pyrodex((R)) and Triple Seven((R)) Using Gas Chromatography-Mass Spectrometry*. J Forensic Sci, 2011. **56**(1): p. 194-9.
26. Roberson, Z.R., H.C. Gordon, and J.V. Goodpaster, *Instrumental and Chemometric Analysis of Opiates Via Gas Chromatography-Vacuum Ultraviolet Spectrophotometry (Gc-Vuv)*. Anal Bioanal Chem, 2020. **412**(5): p. 1123-1128.
27. Katilie, C.J., A.G. Simon, and L.E. DeGreeff, *Quantitative Analysis of Vaporous Ammonia by Online Derivatization with Gas Chromatography - Mass Spectrometry with Applications to Ammonium Nitrate-Based Explosives*. Talanta, 2019. **193**: p. 87-92.
28. Lubrano, A.L., et al., *Analysis of Ammonium Nitrate Headspace by on-Fiber Solid Phase Microextraction Derivatization with Gas Chromatography Mass Spectrometry*. J Chromatogr A, 2016. **1429**: p. 8-12.
29. DeGreeff, L.E. and K. Peranich, *Headspace Analysis of Ammonium Nitrate Variants and the Effects of Differing Vapor Profiles on Canine Detection*. Forensic Chemistry, 2021. **25**: p. 100342.
30. Brown, H., et al., *New Developments in Spme Part 2: Analysis of Ammonium Nitrate-Based Explosives*. J Forensic Sci, 2004. **49**(2): p. 215-21.
31. Beveridge, A., *Forensic Investigation of Explosions*. 2 ed. 2011: Taylor & Francis. 696.
32. Chajistamatiou, A.S. and E.B. Bakeas, *Identification of Thiocyanates by Gas Chromatography - Mass Spectrometry in Explosive Residues Used as a Possible Marker to Indicate Black Powder Usage*. Talanta, 2019. **195**: p. 456-462.
33. Goodpaster, J.V. and R.O. Keto, *Identification of Ascorbic Acid and Its Degradation Products in Black Powder Substitutes*. J Forensic Sci, 2004. **49**(3): p. 523-8.
34. Nowicki, J. and S. Pauling, *Identification of Sugars in Explosive Residues by Gas Chromatography-Mass Spectrometry*. Journal of Forensic Sciences, 1988. **33**(5): p. 1254-1261.
35. Cajigas, J.M.C., L. Perez-Almodovar, and L.E. DeGreeff, *Headspace Analysis of Potassium Chlorate Using on-Fiber Spme Derivatization Coupled with Gc/Ms*. Talanta, 2019. **205**: p. 120127.

## VITA

### EDUCATION

#### **Indiana University-Purdue University Indianapolis (Indianapolis, IN)**

**August 2017 to December 2021**

- PhD Analytical Chemistry.
- National Institute of Justice (NIJ) Graduate Research Fellow: Jan. 2019-Dec. 2021.
- IUPUI University Fellow: Aug. 2017- July 2018.
- GPA 3.953

#### **Honors College at Western Kentucky University (Bowling Green, KY)**

**August 2013 to May 2017**

- Bachelor of Science in Chemistry, American Chemical Society Certified
- Bachelor of Arts in Criminology
- Summa cum laude; GPA 3.97
- Honors Thesis: Detection of Tetracyclines in an Anaerobic Waste Digester Using Solid Phase Extraction and High- Performance Liquid Chromatography Mass Spectrometry.

### RESEARCH

#### **Indiana University Purdue University Indianapolis (Indianapolis, IN)**

**August 2017 to December 2021**

- PhD research under P.I. Dr. John V. Goodpaster.
- Analyzing nitrated explosives and their thermal decomposition products by gas chromatography/vacuum ultraviolet spectroscopic (GC/VUV) and gas chromatography/mass spectrometric (GC/MS) analysis.
- Investigating specificity of VUV and the key factors underlying fine structure in VUV spectra.
- Investigating thermal and spectroscopic analysis of nitrated compounds and their break-down products.

- Developing optimized GC/VUV methods for nitrated explosives via central composite design of experiments.
- Investigating discriminating power of VUV for nitrated explosives via chemometric methods.
- Calculating computational excited states (TD-DFT and CIS) of nitrated explosives, their decomposition products, and ignitable liquids.
- Developing methods of separation of nitrated explosives by GC-MS.
- Assessing cross-contamination of explosive canine training aids by gas chromatography/negative ion chemical ionization/mass spectrometry (solid phase microextraction and liquid injection) for establishing ideal storage in collaboration with the U.S. Army Combat Capabilities Development Command-Chemical Biological Center and the Indianapolis Metropolitan Police Department.

**Western Kentucky University: (Bowling Green, KY)**

**February 2015 to May 2017**

- Research Assistant under Dr. Eric Conte.
- Conducted research on detecting tetracycline in swine waste by HPLC and LC/MS and assessing photodegradation in anaerobic digesters for antibiotic resistance. Collaboration with Bowling Green U.S. Department of Agriculture laboratory.
- Developed solid phase extraction and HPLC methods.

**Department of Homeland Security Customs and Border Protection (Springfield, VA)**

**May 2016 to July 2016**

- Interned 5 days per week, 40 hours per week.
- Developed a searchable library of 200 known man-made reference fibers using FT/IR spectroscopy, with and without ATR, to be used for trade enforcement and forensic investigations.

**Food and Drug Administration: Center for Devices and Radiological Health, Division of Biology, Chemistry and Material Sciences (Silver Spring, MD)**

**June 2015 to August 2015**

- Interned 4 days per week, 36 hours per week.
- Developed chemical database for toxicity of color additives and chemicals released from medical device using quantitative structure–activity relationship (QSAR) models.

-Validated Danish QSAR model's ability to accurately predict TD<sub>50</sub> values.

## **PUBLICATIONS**

-Cruse, C.A.; Goodpaster J.V. Optimization of Gas Chromatography/Vacuum Ultraviolet (GC/VUV) Spectroscopy for Explosive Compounds and Application to Post-Blast Debris. Forensic Chemistry 2021.

-Cruse, C.A.; Goodpaster J.V. A systematic study of the absorbance of the nitro functional group in the vacuum UV region. Analytica Chimica Acta 2021.

-Rael, A.; Cruse, C.A.; Rydberg, M.; Goodpaster J.V. A critical comparison of vacuum UV (VUV) spectrometer and electron ionization single quadrupole mass spectrometer detectors for the analysis of alkylbenzenes in gasoline by gas chromatography: Experimental and statistical aspects. Talanta 2021.

-Cruse, C.A.; Goodpaster J.V. Thermal and spectroscopic analysis of nitrated compounds and their break-down products using gas chromatography/vacuum UV spectroscopy (GC/VUV). Analytica Chimica Acta 2020.

-Cruse, C.A.; Pu, J.; Goodpaster J.V. Identifying Thermal Decomposition Products of Nitrate Ester Explosives Using Gas Chromatography–Vacuum Ultraviolet Spectroscopy: An Experimental and Computational Study. Applied Spectroscopy 2020.

-Cruse, C.A.; Goodpaster, J.V. Generating Highly Specific Spectra and Elucidation of Thermal Decomposition Products via Gas Chromatography/Vacuum Ultraviolet Spectroscopy (GC/VUV): Application to Nitrate Ester Explosives. Talanta 2018.

## **ORAL PRESENTATIONS**

-Beyond Boundaries Indiana Academies Symposium 2021. ACS Indiana Local Section Selected Graduate Student Symposium. April 2021. The Optimization of Gas Chromatography/Vacuum Ultraviolet (GC/VUV) Spectroscopy for the Analysis of Explosives and Their Post-Blast Residues.

- American Academy of Forensic Sciences 72nd Annual Scientific Meeting. February 2021. The Optimization of Gas Chromatography/Vacuum Ultraviolet (GC/VUV) Spectroscopy for the Analysis of Explosives and Their Post-Blast Residues.
- International Symposium on the Analysis and Detection of Explosives. April 2021. Analysis of Explosive Compounds and their Decomposition Products via Gas Chromatography/Vacuum Ultraviolet Spectrometry (GC/VUV).
- American Academy of Forensic Sciences 72nd Annual Scientific Meeting. February 2020. Study Of The Thermal Decomposition Of Nitrate Ester Explosives by Gas Chromatography/Vacuum Ultraviolet Spectroscopy (GC/VUV) and Its Application to Post-Blast Debris.
- Pittcon: Pittsburgh Conference on Analytical Chemistry and Applied Spectroscopy. Presented by Dr. John V. Goodpaster. March 2019. Identification of Nitrate Ester Explosives and Their Thermal Decomposition Products by Gas Chromatography/Vacuum Ultraviolet Spectroscopy.
- Indiana University-Purdue University Indianapolis Department of Chemistry and Chemical Biology. Chemistry Research Day 2018. Identification of Explosives and their Post-Blast Residues via Gas Chromatography (GC) Coupled with Vacuum Ultraviolet Spectroscopy.

## **POSTER PRESENTATIONS**

- Indiana University-Purdue University Indianapolis Department of Chemistry and Chemical Biology. Chemistry Research Day 2021. A systematic study of the absorbance of the nitro functional group in the vacuum UV region.
- Beyond Boundaries Indiana Academies Symposium 2021. ACS Indiana Local Section Think Like a Molecule Poster Symposium. April 2021. The Optimization of Gas Chromatography-Vacuum Ultraviolet (GC-VUV) Spectroscopy for the Analysis of Explosives and Their Post-Blast Residues.
- Pittcon: Pittsburgh Conference on Analytical Chemistry and Applied Spectroscopy. NIJ Poster Session. March 2020. Vacuum Ultraviolet (VUV) Spectroscopy and Computational Analysis of the Thermal Decomposition of Nitro Compounds.

- Turkey Run Analytical Chemistry Conference 2019. Identification of Nitrate Ester Explosives and their Thermal Decomposition Products by Gas Chromatography / Vacuum Ultraviolet Spectroscopy.
- Pittcon: Pittsburgh Conference on Analytical Chemistry and Applied Spectroscopy. NIJ Poster Session. Presented by Ashur Rael. March 2019. Gas Chromatography / Vacuum Ultraviolet Spectroscopic Analysis of Intact and Burned Smokeless Powders and Their Post-Blast Residues.
- Midwestern Universities Analytical Chemistry Conference 2018. Computational Analysis of Electronic and Vibrational Transitions of Thermal Decomposition Products of Nitrate Ester Explosives in the Vacuum Ultraviolet Region.
- Turkey Run Analytical Chemistry Conference 2018. Gas Chromatography/Vacuum Ultraviolet Spectroscopic and Computational Analysis of the Thermal Decomposition Products of Nitrate Ester Explosives.
- Midwestern Association of Forensic Scientists 47th Annual Fall Meeting 2018. Application of Gas Chromatography / Vacuum Ultraviolet Spectroscopy to Intact Smokeless Powders and Their Post-Blast Residues.
- Midwestern Association of Forensic Scientists 47th Annual Fall Meeting 2018. Co-author. Specificity of Gas Chromatography/Vacuum Ultraviolet Spectroscopy (GC/VUV) Versus Gas Chromatography/Mass Spectrometry (GC/MS) for Alkylbenzenes Common Ignitable Liquids.
- ACS Indiana Annual Poster Session 2018. UV/vis spectroscopic and gas chromatography/mass spectrometric analysis of nitrated explosives in preparation for gas chromatography-vacuum ultraviolet analysis.
- University of Louisville Graduate Student Regional Research Conference 2018. UV-Visible Spectroscopy and Gas Chromatography-Mass Spectrometry Analysis of Nitrated Explosives as a Prelude to Gas Chromatography-Vacuum Ultraviolet (VUV) Detection.
- Chemistry and Chemical Biology Departmental Poster Session 2017. Vacuum ultraviolet and UV-vis spectroscopic analysis of  $\pi$  to  $\pi^*$ ,  $n$  to  $\pi^*$ , and  $\sigma$  to  $\sigma^*$  transitions of nitrated explosives.

- Indiana University-Purdue University Indianapolis Department of Chemistry and Chemical Biology Departmental Poster Session 2017. Vacuum ultraviolet and UV-vis spectroscopic analysis of  $\pi$  to  $\pi^*$ ,  $n$  to  $\pi^*$ , and  $\sigma$  to  $\sigma^*$  transitions of nitrated explosives.
- 253<sup>rd</sup> American Chemical Society National Meeting 2017. Degradation of tetracyclines in anaerobic digestion using solid phase extraction and HPLC.
- U.S. Food and Drug Administration Intern Poster Session 2015. Validation of a QSAR Model to Predict Carcinogenic Potency of Chemical Compounds.
- Society of Toxicology Meeting 2016. Co-author. Inhalation TTC Values for Compounds Released into the Breathing Circuit of Respiratory Devices.

## **AWARDS**

- International Symposium on the Analysis and Detection of Explosives (ISADE) Graduate Student Travel Fellowship 2020.
- American Society of Trace Evidence Examiner (ASTEE) 2019 Scholarship Award.
- IUPUI Elite 50 2019.
- National Institute of Justice Graduate Research Fellowship in STEM Jan. 2019-Aug. 2021.
- IUPUI University Fellowship 2017.
- American Institute of Chemists: Outstanding Graduating Senior in Chemistry Award (WKU) 2017.
- WKU Presidential Scholar- Eight consecutive semesters.
- Golden Key International Honour Society Member since 2014.
- WKU 1906 Founder's Scholarship- Competitively awarded- min. 3.80 GPA and ACT composite of 31.
- Honors Travel Abroad Grant- 2014.
- Student Government Association Study Abroad Grant- 2014.
- World Topper Abroad Scholarship- 2014.

## **TEACHING**

### **Undergraduate Laboratory Teaching Assistant at Western Kentucky University**

**September 2015 to May 2017**

- Primary TA General Chemistry II (Fall 2016, Spring 2017); 8 hours per week.
- Secondary TA Quantitative Analysis (Spring 2016); 8 hours per week.
- Secondary TA General Chemistry I and II (Fall 2015); 5 hours per week.
- Prepared materials for lab, ensured safety measures are followed, answered student questions concerning experiments.

### **Chemistry Tutor**

**September 2014 to May 2017**

- Private tutor for high school and college students.
- Western Kentucky University chemistry department tutor, 5 hours per week.

## **ADDITIONAL EDUCATION**

### **Fundamentals of Explosives Training (Kingston, RI)**

**April 30 to May 3, 2019**

- Completed short course on the fundamentals of explosives: chemical and physical principles with applications from the University of Rhode Island and Hazards & Explosives Research and Education (HERE), LLC. Taught by Maurice Marshall (O.B.E., Ph.D.), Jimmie Oxley (Ph.D. URI), Blaine W. Asay (Ph.D., Spring Hill Energetics), and James E. Kennedy (Ph.D., HERE, LLC)

### **The Washington Center for Internships and Academic Seminars (Washington, DC)**

**May 2015 to August 2015**

- Participated in Forensic Psychology course; Leadership, Engagement, Achievement and Development Colloquium
- Attended panels from the Marshals Service, Drug Enforcement Administration, Federal Bureau of Investigation, and DC Metropolitan Police Department.

-Attended The Simpson-Mineta Leaders Series: engaged with leaders and explored issues of contemporary public concern.

**Cooperative Center for Study Abroad (London, England)**

**December 2014 to January 2015**

-Completed “Rediscovering Chemistry’s British Roots” course: explored the 18th through 20th century advances in science by visiting museums and learning from the perspective of Britain’s history.

**PROFESSIONAL MEMBERSHIP**

-Member: American Chemical Society (March 2016 – present).

-Student Affiliate: American Academy of Forensic Sciences (Jan. 2017 – present).